ELSEVIER

Catalysis Today 58 (2000) 1–53

CATALYSIS TODAY

www.elsevier.com/locate/cattod

Solid state aspects of oxidation catalysis

Paul J. Gellings *, Henny J.M. Bouwmeester

Laboratory for Inorganic Materials Science, University of Twente, PO Box 217, NL-7500 AE Enschede, The Netherlands

Abstract

The main subject of this review is the consideration of catalytic oxidation reactions, which are greatly influenced by solid state effects in the catalyst material. Emphasis is laid upon the correlation between the presence of mobile ionic defects, together with the associated ionic conductivity, and the catalytic performance. Both total and selective oxidation reactions and oxidative conversion reactions are considered. Well-known examples of such behaviour include oxidative methane conversion with lanthanide oxides, carbon monoxide oxidation on fluorite type catalysts, selective olefin oxidation using vanadia based catalysts, etc. Furthermore, because oxygen exchange between gas and solid is always part of the oxidation process, this is considered too.

The discussion of the application of the solid oxides under consideration to practically important oxidation processes, together with the influence thereon of their solid state properties, forms a major part of this review. Computational modelling and simulation of catalyst structure and behaviour is also considered.

Special attention is given to the potentialities offered by using ionic and mixed conducting oxides either as the electrode material in a solid electrolyte fuel cell (SOFC) or as a separating, dense membrane in a ceramic membrane reactor. The use of porous membranes in such reactors is also taken into consideration. On the one hand these may be used to study the above relationship between catalytic behaviour and solid state properties, on the other hand to obtain a reactor configuration allowing better use of reactants and/or catalysts. Besides the controlled supply of (or removal) of oxygen to (or from) the side where the catalyst and the reactants are located, a promising feature of both experimental approaches is that the oxygen flux may alter the relative presence of different oxygen species (O_2, O, O_2^-, O_2^{2-}, O_3^-, O^-, etc.) on the catalyst surface. In this way species are provided having a strong influence on the selectivity for partial oxidation reactions and oxidative conversion reactions.

Keywords: Oxidation catalysis; Oxygen ion and proton conductors; Computational modelling; Oxygen surface exchange; Membranes

1. Introduction

This review is a sequel to that on ion and mixed conducting oxides as catalysts by Gellings and Bouwmeester [1]. First a very brief survey is given of some important solid state properties and phenomena, but the major part of this review is devoted to detailed discussions of a number of catalysts and catalytic reactions in which these solid state properties are considered to play an important role.

The catalytic reactions discussed in this review are not only those which are used in production processes in the chemical industry, but also those taking place at electrodes, in particular in solid electrolyte fuel cells (SOFCs), reactions at membrane surfaces and in electrochemical processes using solid oxides as electrolyte and electrode.

Recent reviews giving a more comprehensive discussion of the fundamentals and the applications of

* Corresponding author.

0920-5861/00/$ – see front matter
PII: S0920-5861(00)00240-6

solid state phenomena are collected in a recent handbook [2].

A new type of conducting oxides to be discussed in this paper, which was not yet considered in the previous review [1], is that of proton conducting oxides which have become of increased importance.

It is important to remark that originally the use of solid state chemistry in catalysis was mainly limited to the study of the influence of the crystal structure on catalytic reactions, as is seen, e.g., in many of the papers in the 'Proceedings of the 1985 Symposium on Solid State Chemistry in Catalysis' [3]. Quite separate from these were the considerations on the influence of semi-conducting properties of catalyst materials on their catalytic properties, see, e.g. [4,5]. Although the main emphasis in this review is on the influence of solid state effects related to ionic and mixed ionic–electronic conduction, structural considerations are also given some attention. An important phenomenon sometimes observed in multi-phase catalysts is that active species formed on one of the phases move during the reaction to the surface of another phase. This is usually called *spill-over* and has been discussed, e.g., by Delmon [6], but is not treated further in this paper. Of great importance in many catalytic reactions are the acid–base properties of solids. These also fall mainly outside the subject matter of this review but some special subjects in this field are mentioned.

Important contributions to the interpretation of the relation between solid state properties and catalytic behaviour have been obtained by computational modelling and simulation, including quantum mechanical calculations. Therefore these subjects are also covered in this review.

Apart from the interpretation of catalytic behaviour of catalysts in terms of solid state properties, attention is also given to new possibilities where ion or mixed conducting oxides are used as membranes separating reactants and reactant products. This gives exciting new possibilities for reactor configurations leading in particular to higher selectivities.

2. Structures of compounds used as catalysts

For the most important structures of oxides used as catalysts, in particular the sodium chloride structure, the fluorite and the pyrochlore structures and the perovskite structure, we refer to the previous review [1] and to a recent paper by Abrahams and Bruce [7]. A structure not treated in the previous review is that of hexagonal lanthanum sesquioxide, which is also that of several other lanthanide oxides, e.g., Ce_2O_3, Nd_2O_3 and Pr_2O_3. The lattice parameters are a=3.9373 Å, c=6.1299 Å. Lanthanum positions are $\pm(\frac{1}{3}, \frac{2}{3}, u)$ with u=0.245, oxygen positions (0 0 0) and $\pm(\frac{1}{3}, \frac{2}{3}, u)$ with u=0.645 [8]. A (1 1 0)-cross-section of this structure is shown in Fig. 1.

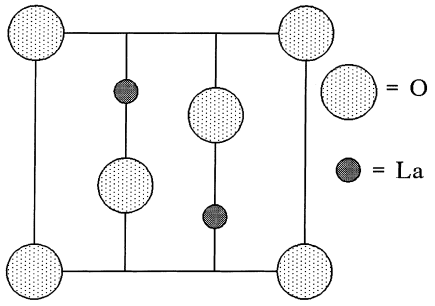

Fig. 1. (1 1 0)-cross-section through hexagonal La_2O_3-structure.

In this structure there are two, nearly close-packed, slightly buckled La–O planes between close-packed oxygen planes. The lanthanum ions are surrounded by a distorted oxygen polyhedron with three oxygens at a distance of 2.37 Å, one at 2.45 Å and three others at 2.72 Å, so that the lanthanum ions have a seven-co-ordination. Caro and Less [9] have described this structure as a succession of $(LaO)_2^{2+}$ and O^{2-} layers which is easily cleaved between these layers.

3. Point defects

3.1. Notation for point defects

The defects under consideration here may, e.g., be vacant lattice sites (called *vacancies*), ions placed at normally unoccupied sites (called *interstitial ions*), foreign ions present as impurity or dopant and ions with charges different from those expected from the overall stoichiometry. Electron defects may arise either in the form of ions present with charges deviating from the normal lattice ions, or as a consequence of the transition of electrons from normally filled energy

Table 1
Kröger–Vink notation for point defects in crystals. Divalent ions are chosen as example with MX as a compound formula with M^{2+}, X^{2-} as cation and anion, respectively

Symbol	Type of defect
V_M''	Metal ion vacancy: vacant metal site with effective charge −2 (with respect to the ideal lattice)
$V_X^{\bullet\bullet}$	X ion vacancy: vacant X site with effective charge +2 (with respect to the ideal lattice)
M_M^x, X_X^x	Metal, respectively, X ion on their normal lattice position (neutral)
L_M'	L^+ dopant ion on metal site with effective charge −1 (with respect to the ideal lattice)
$N_M^{\bullet}$	N^{3+} dopant ion on metal site with effective charge +1 (with respect to the ideal lattice)
e'	(Quasi)-free electron in conduction band
$h^{\bullet}$	(Quasi)-free electron hole in valence band
$M_i^{\bullet\bullet}$	Interstitial metal ion with effective charge +2 (with respect to the ideal lattice)
X_i''	Interstitial X ion with effective charge −2 (with respect to the ideal lattice)
M_M'	Monovalent metal ion on M^{2+}-position (localised electron, only possible if the metal M has multiple valencies)
$M_M^{\bullet}$	Trivalent metal ion on M^{2+}-position (localised electron hole, only possible if the metal M has multiple valencies)

levels, usually the valence band, to normally empty levels, the conduction band. In those cases where an electron is missing, i.e. when there is an electron deficiency, this is usually called an *electron hole* (often abbreviated to *hole*). Usually it is convenient to consider point defects, such as vacancies or electron holes, to be the moving entities in a lattice even though in reality of course the ions or electrons move through the lattice in the opposite direction.

In the absence of macroscopic electric fields ionic lattices must be electrically neutral everywhere. This requires that a charged defect must be compensated by the presence of a number of defects, together having a joint charge of opposite sign. This is called the *electroneutrality* condition. This means that these charged defects are always present as a combination of two (or more) types of defects. The charges of defects and of the regular lattice particles are defined with respect to the neutral, unperturbed (ideal) lattice and are called *effective charges*. These are indicated by a dot ($^{\bullet}$) for a positive excess charge, by a prime ($'$) for a negative excess charge and by an x (^{x}) for effectively neutral defects (i.e. ions having their normal charges corresponding with the stoichiometry of the compound).

The notation used for defects is from Kröger and Vink [10] and are shown for a number of examples in Table 1. Only fully ionised defects are indicated in this table. For example, considering anion vacancies we could also have, besides doubly ionised anion vacancies: $V_x^{\bullet\bullet}$, singly ionised or uncharged anion vacancies: $V_x^{\bullet}$ or V_x^x, respectively.

Unfortunately in many papers concerned with the interpretation of catalytic results in terms of defects present in the solid catalyst this notation is not yet used. On the one hand this makes comparison between the results of different authors often very difficult. On the other hand the defects are in many cases insufficiently defined and one speaks only of "vacancies" (sometimes indicated only as) without indicating what the missing atom or ion is or what its charge is. Also in the case of redox reactions incorporating electron transfer the electron is only indicated as e^-, with no description of where the electron comes from: conduction band, valence band, leaving an electron hole, from a metal or oxide ion, etc. In a number of cases the indications of the involved defects is such that it is not even possible to write a complete catalytic cycle involving these defects. In fact this led a participant in a recent conference on catalysis to state that he was often puzzled about the exact meaning of the terms used in published papers or in lectures at conferences [11]. It is certainly to be hoped that the Kröger–Vink notation, which is already used widely in solid state chemistry, is going to find more widespread use in catalysis as well.

It is also necessary to realise that the Kröger–Vink notation as defined for bulk defects above has to be extended to cover surface defects too. Some of the problems connected with this extension can be illustrated with a very simple example, considering the (1 0 0) surface of a crystal with the NaCl-structure and composition MO. When an oxygen atom is present as an O^{2-}-ion on top of a M^{2+}-ion in the surface it can be

designated as O_s'' indicating the surface with subscript s and the effective charge in the same way as done for an interstitial ion. However, when the surface contains oxygen vacancies, these can be indicated as $V_{O,s}^{\bullet\bullet}$, where the subscript s indicates that the vacancy is a surface vacancy. Such a vacancy can be filled with an O^{2-}-ion, which then has to be indicated as $O_{O,s}{}^{x}$, because now it resides on a (surface)-oxygen position and has an effective charge zero. This of course means that a much more precise description of what is meant by "adsorbed oxygen" is necessary than that usually given.

3.2. Protons in oxides

The presence of defects, which contain hydrogen, sometimes has a great influence on chemical and catalytic properties of oxidic materials. One of these types of properties, the Brønsted acidity, is not considered further here. The property we consider here is proton conduction in the solid state, as discussed, e.g., by Iwahara [12]. A review of the nature of these defects and their reactions and the computational techniques used in investigating these has recently been published by Catlow et al. [13]. The energy of water dissolution in several oxides has been calculated by Wright et al. [14] and Wright and Catlow [15,16]. Baram and Parker [17] also discussed the atomistic simulation of hydroxide ions in inorganic solids.

For the protonic defects in oxides the most important formation reaction is that between water molecules and oxygen vacancies

$$O_O{}^{x} + V_O{}^{\bullet\bullet} + H_2O(g) \rightarrow 2OH_O{}^{\bullet} \tag{1}$$

in which two effectively positive hydroxyl-groups on regular oxygen positions are formed. The consequences of this defect formation are discussed later in connection with the catalytic reactions in which they are supposed to play a role.

There are also some important defect reactions where protonic defects are formed by reaction with hydrogen. The first is the reaction with electron holes according to

$$2h^{\bullet} + 2O_O{}^{x} + H_2 \rightarrow 2OH_O{}^{\bullet} \tag{2}$$

for which the presence of excess holes is obviously necessary. An alternative possibility is the oxidation of hydrogen under formation of free electrons according to

$$2O_O{}^{x} + H_2 \rightarrow 2OH_O{}^{\bullet} + 2e' \tag{3}$$

where the electrons are assumed to be donated to the conduction band in the case of band conductors.

There are two mechanisms for proton conduction. The first is that of *proton hopping*, also called the Grotthus-mechanism, in which the proton hops between adjacent oxygen ions. The other conduction mechanism is *hydroxyl-ion migration*, also called the "vehicle" mechanism. One possibility to distinguish these mechanisms is by measurement of the isotope effect, e.g., by comparing the magnitudes of H^+- and D^+-ion conduction. In the first mechanism a significant isotope effect is expected, whereas in the second, due to the large mass of the oxygen atom, this is almost absent.

Schober et al. [18] discussed the defect model of proton insertion into oxides in detail, in particular for perovskite type oxides showing proton conductivity. In all cases vacancies in the oxygen sublattice are essential for the uptake of protons. They considered especially the compound $SrCe_{0.95}Yb_{0.05}O_{3-\alpha}$ and proposed the following series of coupled equilibria

$$\begin{array}{ll} \frac{1}{2}O_2(g) + V_O{}^{\bullet\bullet} = O_O{}^{x} + 2h^{\bullet} & K_1 \\ O_O{}^{x} + V_O{}^{\bullet\bullet} + H_2O(g) = 2OH_O{}^{\bullet} & K_3 \\ O_O{}^{x} = \frac{1}{2}O_2(g) + V_O{}^{\bullet\bullet} + e' & K_O \\ H_2(g) + \frac{1}{2}O_2(g) = H_2O(g) & K_W \\ 0 = e' + h^{\bullet} & K_e \end{array} \tag{4}$$

where the K's are the equilibrium constants of these reactions.

As one of the results they calculated the predominance diagram of the different defects in the p_{H_2O}–p_{O_2}-plane shown in Fig. 2 using the different limiting regions of the electroneutrality condition, written for the case of Yb as dopant, using the majority defect as the criterion

$$2[V_O{}^{\bullet\bullet}] + [OH_O{}^{\bullet}] + [h^{\bullet}] = [e'] + [Yb_{Ce}'] \tag{5}$$

In Fig. 2 some critical pressures of water, oxygen and hydrogen are indicated, which are defined by the following relations, again written for Yb as dopant:

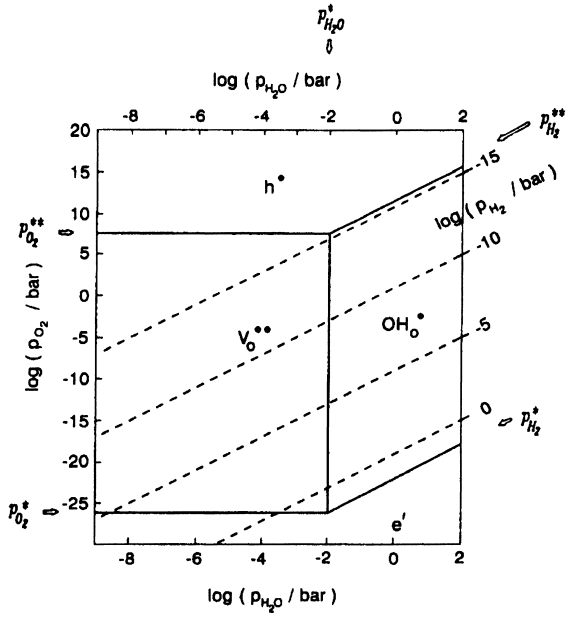

Fig. 2. Predominance diagram in the p_{H_2O}–p_{O_2}-plane showing the regions in which the different defects predominate (reproduced from Fig. 1 of [18], copyright 1996, with permission from Elsevier Science).

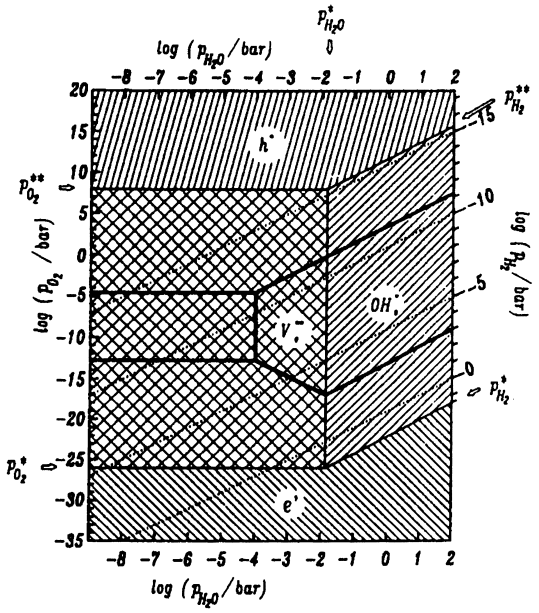

Fig. 3. Predominance diagram as that of Fig. 2, where the thick lines give the boundaries of the regions with predominating (a) proton (central right); (b) oxygen ion (central left); (c) electron hole (upper); and (d) electron (lower) conductivity (reproduced from Fig. 3 of [18], copyright 1996, with permission from Elsevier Science).

$$p_{H_2O}{}^{*} = \frac{[Yb'_{Ce}]}{K_3}, \quad p_{O_2}{}^{*} = \frac{K_O{}^2}{[Yb'_{Ce}]^6},$$

$$p_{O_2}{}^{**} = \frac{[Yb'_{Ce}]^2}{K_1{}^2},$$

$$p_{H_2}{}^{*} = \frac{[Yb'_{Ce}]^4}{K_W}, \quad p_{H_2}{}^{**} = \frac{K_1/K_W}{K_3} \tag{6}$$

Taking into account the mobilities of the different defects this diagram can also be used to calculate the regions where these dominate the conductivity, as shown in Fig. 3.

Brouwer or Kröger–Vink diagrams, discussed, e.g., in [1,19,20] for systems with proton defects are also calculated by Schober et al. [18] and one example is shown in Fig. 4. These diagrams, combined with the values of the mobility of the different effects, give more insight into the relative importance and significance of proton contributions to the conductivity.

Stevenson et al. [21] reported an investigation of the proton conduction of Gd, Yb and Nd doped barium cerates. All investigated samples showed the incorporation of water under wet-annealing conditions.

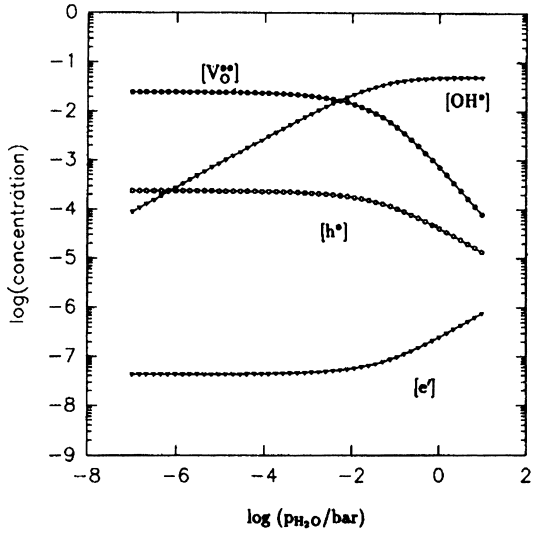

Fig. 4. Calculated Kröger–Vink diagram at T=700°C and p_{O_2} = 0.2 bar for $SrCe_{0.95}Yb_{0.05}O_{3-\alpha}$ showing the dependence of the concentrations of the four dominant defect types on p_{H_2O} (reproduced from Fig. 5 of [18], copyright 1996, with permission from Elsevier Science).

Table 2
Activation energy for bulk (proton) conductivity (data from Stevenson et al. [21])

Dopant	Wet: H_2O ($kJ\,mol^{-1}$)	Wet: D_2O ($kJ\,mol^{-1}$)	Dry ($kJ\,mol^{-1}$)
5% Nd	55.0	56.0	58.9
10% Nd	56.9	–	–
15% Gd	56.0	59.8	–
20% Gd	56.0	56.9	58.8
10% Yb	52.1	53.1	56.0
15% Yb	48.2	49.2	–

This water uptake was observed to have a maximum at about 500°C and it became nearly zero above 800°C. The water uptake in Gd- and Yb-doped materials was about 55–70% of theoretical, but in the Nd-doped materials it was lower than about 30% at 15 at.% Nd and 6% at 5 at.% Nd. The activation energies for the bulk conductivities are given in Table 2.

The data in this table show a clear H/D-isotope effect, supporting the conclusion that these materials are proton conductors with the Grotthus-mechanism for proton movement. Aside from the bulk conductivity the authors also observed a clear effect of grain boundary conductivity.

Schober et al. [22] studied Yb^{3+}-substituted strontium cerate and strontium zirconate. They found that the effective chemical diffusivities of protons in these compounds are of the same order of magnitude as in other similar high-temperature proton conductors.

Iwahara et al. [23] investigated the protonic conduction of calcium, strontium and barium zirconates, all having the perovskite structure. These authors observed that in all these compounds partial replacement of zirconium by a trivalent element like In, Sc, Y, etc. led to proton conduction in hydrogen containing atmospheres at high temperature. They also observed clear isotope effects, both in IR spectra and in the conductivity of $SrZr_{0.95}Y_{0.05}O_{3-\alpha}$ between protonated and deuterated samples. The authors suggest, upon the basis of these observations, that protonic conduction in these materials occurs via a Grotthus-type mechanism.

Labrincha et al. [24] investigated the defect structure of $SrZrO_3$. Undoped and Y-doped $SrZrO_3$ showed mixed p-type and oxygen conduction in dry air in the temperature range 800–1100°C. However, La-doped material showed n-type conduction at low p_{O_2} (below 10^{-10} Pa at 1000°C) and is a nearly pure ionic conductor for higher p_{O_2}. In the presence of H_2O or D_2O vapour the Y-doped strontium zirconate in particular shows protonic conduction. The authors propose a defect structure similar to that proposed by Schober et al. [18], shown in Eq. (4), which is consistent with the observations. A defect diagram for this material proposed by Labrincha et al. [24] is shown in Fig. 5.

Liang et al. [25] studied the non-stoichiometric perovskites $Sr_2(Sc_{1+x}Nb_{1-x})O_{6-\delta}$ (with x=0.05, 0.1) and $Ba_3(Ca_{1.18}Nb_{1.82})O_{9-\delta}$. These compounds become good proton conductors upon exposure to H_2O and D_2O in the temperature range 300–550 K. Their conductivities fall in the same range as those for M^{3+}-doped $SrCeO_3$ and $BaCeO_3$. However, they have the advantage that they do not show electronic conduction in highly reducing atmospheres.

Iwahara et al. [26] studied $BaCeO_3$ which behaves as an electron hole conductor in dry atmospheres but as a protonic conductor in wet or hydrogen containing atmospheres. Doping with Nd_2O_3 led to an increased proton conductivity, which in fact was larger than that of $SrCeO_3$. The exact mechanism of the proton conduction was probably more complex than in $SrCeO_3$, but further studies were needed to establish this.

Münch et al. [27] performed a quantum molecular dynamics study of proton conduction in $BaCeO_3$.

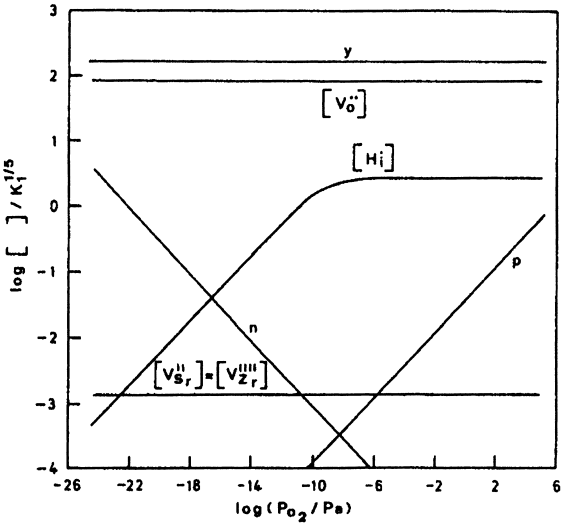

Fig. 5. Proposed defect diagram for $SrZr_{0.95}Yb_{0.05}O_{3-\alpha}$, with y=[Y'_{Zr}] (reproduced from Fig. 5 of [24], copyright 1993, with permission from Elsevier Science).

They conclude that the motion consists of two components: a relatively slow jump of a proton from one oxygen to another, followed by a fast rotation of the hydroxyl-group formed. This process then repeats during continuous proton motion. Matzke et al. [28], using quasi-elastic thermal neutron scattering experimentally determined this same mechanism of proton movement in $SrCe_{0.95}Yb_{0.05}H_{0.02}O_{2.985}$.

Kreuer et al. [29] used pulsed magnetic field gradient NMR and conductivity measurements to study the diffusivity of protons and of oxygen vacancies in acceptor doped $BaCeO_3$. They also performed thermodynamic measurements and calculations for the water solubility in this material. The results show that defect interactions are small. Also evidence has been found for strong oxygen ion relaxation around oxygen vacancies, which may explain the small defect interactions. The hydration enthalpy is rather high, which is considered to reflect the high basicity of this oxide. The results agree well with those of Krug et al. [30] for $SrCeO_3$.

The IR spectrum of hydroxyl-ion defects in MgO and CaO was studied by Freund and Wengeler [31]. The observed OH-IR bands correspond with three types of defect associates, involving cation vacancies, denoted as V''_{cat}: doubly compensated $[OH_O^{\bullet}V''_{cat}OH_O^{\bullet}]^x$, singly compensated $[OH_O^{\bullet}V''_{cat}]'$ and overcompensated cation vacancies $[OH_O^{\bullet}OH_O^{\bullet}V''_{cat}OH_O^{\bullet}]^{\bullet}$.

In perovskites of the type $LaMO_3$, where M=Cr, Mn, Fe, Co, which have been studied by Islam and Cherry [32] proton hopping is also observed. Calculation of the activation energy of the conductivity and comparing with the experimental activation energy has shown that the main contribution to the activation energy is not the tunnelling barrier energy for the proton movement but the energy needed for rearranging the lattice in such a way that an equivalent environment is obtained for the oxygen atoms between which the proton jumps.

The mechanism of proton conductivity in perovskites like $BaCeO_3$ has been shown by Kreuer et al. [33] to be the Grotthus-mechanism because the ^{18}O-tracer diffusion coefficient is more than three orders of magnitude smaller than is necessary to explain the protonic conductivity via the migration of hydroxyl ions. Similarly Norby et al. [34] have shown that in several lanthanide sesquioxides the experimental e.m.f. values in concentration gradients of oxygen, hydrogen and water are only consistent with the movement of protons. Some general considerations on the proton conduction mechanism of proton conduction and the H/D isotope effect on proton conductivity have been presented by Kreuer et al. [35]. In agreement with the work of Islam et al. [32] mentioned previously, they also find that the configuration change necessary to admit hopping of protons between oxygen atoms contributes significantly to the activation energy of the proton conductivity and at the same time this diminishes the H/D isotope effect. Other aspects of the isotope effect and proton hopping in perovskite type materials are discussed by Nowick and Vaysleyb [36] and a theoretical investigation of proton conduction in these materials has been presented by Matsushita and Tanase [37]. Numerical simulations of the diffusion of protons, oxygen vacancies, electrons and holes in $SrCe_{0.95}Yb_{0.05}O_{3-\delta}$ were performed and reported by Condon and Schober [38]. These authors find that due to the high overall concentration of charged particles, leading to very short Debye length, the diffusion is nearly always linked into chemical diffusion. The interactions between the charged particles in a number of cases leads to the formation of concentration profiles of unusual form.

Kreuer [39] has given a survey of the requirements for developing proton conducting materials for technological applications. He pointed out that often there are conflicting requirements, such as, e.g., the basicity should be high to give a sufficiently high proton solubility, but this also means that such an oxide is less stable in acid gases such as CO_2, SO_2, etc. Detailed knowledge of the stability and other properties of the oxide systems proposed for use is necessary to prevent the disappointments resulting from trial-and-error investigations of groups of compounds.

3.3. Oxide properties

The properties, in particular the ionic and/or electronic conductivity, of a number of oxides of the types under consideration have recently been discussed for ionically conducting materials by Kudo [40] and for mixed ionic–electronic conductors by Riess [41].

The thermodynamics and transport of ionic and electronic defects in crystalline oxides has been treated in detail by Lankhorst et al. [42] who derived

equations which enable comparison of thermodynamic data with calculated or measured defect formation energies. Also expressions were derived, starting from irreversible thermodynamics, for the thermally activated transport of localised electronic and ionic defects.

Norby and Andersen [43] have studied the electrical conductivity and defect structure of lithium-doped magnesium oxide. The main conclusion of this work is that at near-atmospheric oxygen pressure and high-temperature p-type bulk conductivity predominates. At lower temperature (typically below 700°C) surface and/or grain boundary conductivity paths become important, probably also mainly with p-type electronic conduction. Lithium is proposed to dissolve as Li'_{Mg}-ions according to the reaction

$$\text{“}Li_2O(s)\text{”} + \tfrac{1}{2}O_2(g) \rightarrow 2Li'_{Mg} + 2h^{\bullet} + 2O_O{}^{x} \qquad (7)$$

in which the electron holes are directly formed. This can be compared with the discussion about the defect structure of Li/MgO in Section 5.5, from which it follows that reaction (7) can also be obtained from the summation of the reactions

$$\text{“}Li_2O\text{”} + 2Mg_{Mg}{}^{x} + O_O{}^{x} \rightarrow 2Li'_{Mg} + V_O{}^{\bullet\bullet} + 2\text{“}MgO\text{”}$$

$$V_O{}^{\bullet\bullet} + \tfrac{1}{2}O_2 \rightarrow O_O{}^{x} + 2h^{\bullet}$$

Balint and Aika [44,45] investigated the conductivity both of pure and of lithium-doped magnesium oxide as influenced by oxygen and water in the gas phase at temperatures between 673 and 1173 K. They observe a strong influence of water on this conductivity at temperatures below about 773 K, while oxygen has a significant influence only at temperatures above 873 K. They propose that at low temperatures the dissolution of water in the Li/MgO catalyst occurs through reaction with oxygen, or with oxygen vacancies, as shown in the following equations:

$$2O_O{}^{x} + H_2O \rightarrow V''_{Mg} + 2OH_O{}^{\bullet} \qquad (8)$$

$$V_O{}^{\bullet\bullet} + O_O{}^{x} + H_2O \rightarrow 2OH_O{}^{\bullet} \qquad (9)$$

At low temperatures (673 K) the conductivity is found to be caused by $OH_O{}^{\bullet}$-ions as the main charge carriers. One of the arguments for this is the absence of an isotope effect when D_2O is used instead of H_2O. As discussed in Section 3.2 such an effect would be expected for movement of protons, but for $OH_O{}^{\bullet}$-ions it is expected to be negligible due to the large mass of the oxygen atom. With increasing temperature there is clear evidence of conduction by movement of protons and proton holes. Simultaneously there is an increasing contribution of electron hole conductivity due to the creation of oxygen vacancies as part of the water and hydrogen are removed from the lattice. At high temperatures (above 1073 K) the conductivity becomes independent of the water partial pressure. However, oxygen incorporation into the free oxygen vacancies, whose concentration depends on the level of doping, leads to an increase of the hole concentration and thus of the p-type conductivity.

The associated pair of one Li^{+}-ion and one O^{-}-ion, denoted as $[Li^{+}O^{-}]$, is thought to be responsible for the catalytic activity, by the hydrogen abstraction from methane. In terms of defects we prefer the notation $[Li'_{Mg}O_O{}^{\bullet}]$ (=$[Li^{+}O^{-}]$). These defect associates cannot be formed at low temperature because then the oxygen vacancies are filled with proton defects like $OH_O{}^{\bullet}$-ions. Only at temperatures above about 743 K significant amounts of the $[Li'_{Mg}O_O{}^{\bullet}]$-pairs are formed.

One of the methods for determining oxygen transport in electronically conducting materials like perovskites is the solid state potentiostatic technique, which was recently used and critically analysed by Sunde et al. [46]. These authors studied the conduction of $SrFe_{1-x}Fe_xO_{3-\delta}$ and found that in this material there are high-diffusivity paths in the sample. The overall transport was found to be controlled by an oxygen exchange reaction at the grain boundaries. This complication prevented the determination of the oxygen diffusion coefficient for these materials. The authors propose that the large differences in diffusion data for similar materials reported in the literature may be due to the application of experimental methods which do not give detailed information about the mechanism of the transport.

Yokokawa et al. [47] discussed the thermodynamic stabilities of perovskites, including the energetics of the formation of point defects in perovskites and the effect of dopants thereon. They observed that oxygen vacancies are more easily formed upon doping with strontium and barium than with calcium. Depending on the desired direction of the formation

of defects this gives a guideline for the choice of dopant.

Finally the acid–base properties of solid oxides must be mentioned briefly. From a descriptive and theoretical point of view the so-called "optical basicity" is of interest in finding correlations, also in catalytic oxidation. Recent developments in this subject have been discussed by Duffy [48], Portier et al. [49] and more in particular in connection with catalysis by Lebouteiller and Courtine [50]. Of the many papers concerned with the experimental determination of acid–base properties, using adsorption measurements of compounds such as NH_3 and SO_2, only one is mentioned here as a typical example [51].

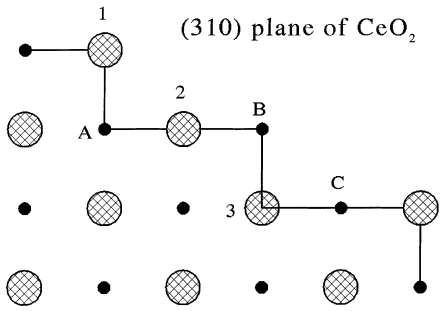

Fig. 6. Cross-section through (3 1 0) plane of CeO_2. 1, 2, 3: three different surface oxygen sites; A, B, C: three different surface cerium sites.

3.4. Surface phenomena and defects

In principle most of the defects mentioned in Section 3.1 can also be present at free surfaces of a crystal, but their energies are certainly different from those of the defects in the bulk. This means that the defect concentrations at the surface also differ from those in the bulk. Depending on the sign of the energy difference this can either lead to an increased concentration, also called positive defect segregation to the surface, or the reverse which is called negative (or reverse) segregation. Due to the changes in band energies near the surface in semi-conducting oxides, the so-called *band-bending* or *band curvature*, the electron or electron hole concentrations in the conduction or valence bands, respectively, are different close to the surface from those in the bulk.

Recently a review devoted in particular to interface phenomena in oxidic materials has been published by Nowotny [52].

Even on "stoichiometric" surfaces there are non-idealities, which should not be called defects in the strict sense. These are, e.g., the ledges shown in the cross-section of the (3 1 0) surface of CeO_2 in Fig. 6. This leads to the presence of sites of the same type of ion with different properties as discussed further in Section 5.1.

At the interfaces between different oxides, such as in supported or mixed oxide catalysts, similar effects occur. As shown by Sayle et al. [53] the energy of formation of oxygen vacancies near the boundary between BaO and MgO is decreased by about 385 kJ mol^{-1} with respect to that in bulk BaO and increased by about 100 kJ mol^{-1} in MgO near the interface as shown in Fig. 7.

These results mean that in BaO the vacancy concentration near the interface is expected to be higher and in MgO lower than in the bulk.

Another example of segregation effects is shown in the study of Scanlon et al. [54] of the surface composition of ceramic CeGd-oxide. Using low energy ion scattering (LEIS) the atomic composition of the outermost layers of a mixed oxide of composition $Ce_{0.8}Gd_{0.2}O_{1.9}$ was determined. It was possible to determine that the outer five atomic layers are enriched in Gd, the Ce/Gd ratio changing from 1 at the outer surface to 4.2 deeper in the oxide. This means that the ionic conductivity in the first few atomic layers is significantly lower than in the bulk, which is expected to have a significant effect on surface sensitive reactions such as occur in catalysis and in electrode processes.

Palladium, rhodium or platinum added to ceria have been shown to improve the effectiveness of three-way catalysts in automotive exhaust catalysis. A study of surface segregation of Rh^{3+}-, Pd^{2+}- and Pt^{2+}-ions in cerium dioxide has therefore been performed by Sayle et al. [55]. It was shown that these ions segregate, together with oxygen vacancies, to the surface of the CeO_2, indicating an explanation of the influence these metals have on the catalytic activity.

The influence of the co-ordination of vanadium ions at the surface of V_2O_5/SiO_2 catalysts was studied by Sokolovskii et al. [56] by studying H_2- and CO-TPR and photoluminescence spectra for low- and high-loaded V_2O_5/SiO_2 catalysts. These authors

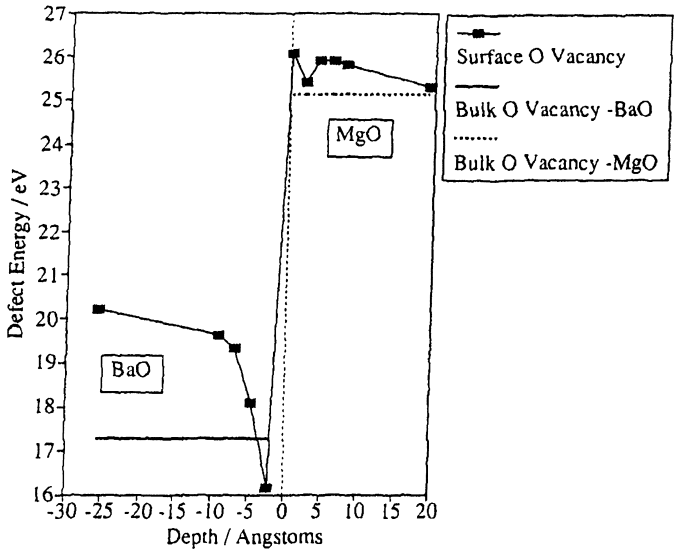

Fig. 7. Oxygen vacancy formation energies as a function of depth in the near interface region of the BaO (1 0 0)/MgO (1 0 0) interface (reproduced with permission from Fig. 2 of [53]).

conclude that for tetrahedrally co-ordinated vanadium ions partial reduction is possible without oxygen abstraction. This makes it possible for oxygen to be adsorbed in a form which is sufficiently long-lived to participate in the catalytic reaction. On octahedrally co-ordinated vanadium, reduction is only possible by oxygen abstraction, so that adsorbed oxygen is very quickly transformed into lattice oxygen and is thus unable to participate in the catalytic reaction.

4. Types of adsorbed and surface oxygen

There are a number of oxygen species: O_2 (adsorbed molecule), O (adsorbed neutral atom), O_2^- (superoxide), O_2^{2-} (peroxide), O_3^- (ozonide), O^-, etc. which may be present on the catalyst surface. Bielanski and Haber [57] (also cited in [1]) presented a scheme of the different types of oxygen of importance in catalysis, shown in Fig. 8, which is not further discussed here.

Using electron paramagnetic resonance (EPR) Louis et al. [58] studied the formation, stability and other properties of the O_2^--ion on La_2O_3 and its role in the oxidative coupling of methane. Upon admitting oxygen at room temperature to La_2O_3, after evacuation of the oxide at 650°C, O_2^--ions are adsorbed on the surface. As shown by the hyperfine-structure of the EPR-spectrum, they are situated in the immediate neighbourhood of the La^{3+}-ion. Upon adsorption at 650°C both surface-O_2^- (85%) and bulk-O_2^-

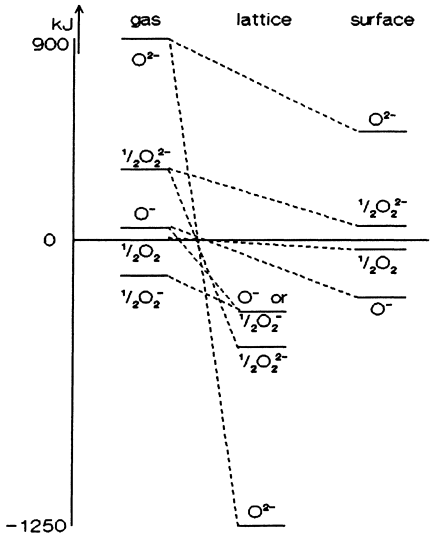

Fig. 8. Survey of oxygen species (reproduced from Fig. 20 of [1], copyright 1992, with permission from Elsevier Science).

(15%) are formed. The latter is situated between the $(LaO_2)^{2+}$ and O^{2-} layers of the La_2O_3 lattice (see Section 2). The authors suggest that the surface O_2^--ions are formed by insertion of O_2 into the surface oxygen vacancies formed during the vacuum pre-treatment at 650°C combined with electron donation to the oxygen molecule. The bulk O_2^--ions are supposed to be inserted by migration between the relatively loosely bound $(LaO_2)^{2+}$ and O^{2-} layers, similar to the insertion of molecules like H_2O and CO_2 in this structure. However, no satisfactory explanation could be given for the origin of the electron. The most probable origin of the electron is the donation of an electron from lattice oxygen: O_O^x under the formation of an electron hole, present as an $O_O^\bullet$-ion. Admission of CH_4 or CO_2 to the adsorbed O_2^- leads to its desorption upon heating as shown by the disappearance of the EPR-signal. This also means that the superoxide species O_2^- is not present after the methane coupling reaction and thus probably is not the active species for this reaction.

Dubois et al. [59] suggested that peroxycarbonate-ions are formed in the reaction between superoxide ions and carbonate ions, formed from the CO_2 produced by methane oxidation and that these give rise to the formation of peroxide, i.e. O_2^{2-}-ions according to

$$CO_3^{2-} + O_2^- \rightarrow CO_4^{2-} + O^- \quad (10)$$

which is followed by

$$2O^- \rightarrow O_2^{2-} \quad (11)$$

These authors then suggest that the peroxide ion could be the active species for the methane coupling reaction. For further information on the possible role of peroxide species in this reaction see also the work by Islam et al. [60]. This is discussed in more detail in Section 5.4.

It is unfortunate that similar measurements have not been performed with doped La_2O_3, which would give the possibility for a better comparison with some other investigations of La_2O_3 discussed in this review.

The formation of O^- ($=O_O^\bullet$) in MgO was considered by Kathrein et al. [61] and studied by EPR. They showed that it can be formed by heating above about 900 K by decomposition of water or CO_2 present as impurities in the MgO, e.g.

$$2O_O^x + H_2O(ads) \rightarrow V''_{Mg} + 2O_O^\bullet \quad (12)$$

where the magnesium vacancy may form a neutral associate with the two oxygen ions: $[O_O^\bullet V''_{Mg} O_O^\bullet]^x$. Furthermore the two oxygen ions may dimerise to the peroxide ion, remaining in close association with the magnesium vacancy: $[(O_2)_O^\bullet V''_{Mg}]^x$. Heating may then lead to the formation of an unbound $O_O^\bullet$-ion and an effectively negative associate of a magnesium vacancy with one $O_O^\bullet$-ion

$$[(O_2)_O^{\bullet\bullet} V''_{Mg}]^x \rightarrow [V''_{Mg} O_O^\bullet]' + O_O^\bullet \quad (13)$$

The unbound $O_O^\bullet$-ion may then move through the lattice to the surface and either take part in a catalytic reaction or be exchanged with gaseous oxygen molecules.

The role of cerium oxide on the reducibility and the oxygen species in $CeO_2/MgAl_2O_4$ catalysts was studied by Wang et al. [62] using temperature programmed reduction. Three different oxygen species were observed to exist on the surface of these catalysts. The reduction of the lattice oxygen of CeO_2 monolayers was observed to be easier than that of pure ceria and this is ascribed to the interaction with the $MgAl_2O_4$ support. Furthermore there is a form of adsorbed oxygen which is reduced at a lower temperature than the lattice oxygen. The authors propose this to be a O^- ($=O_O^\bullet$)-ion, which can either react further to form a lattice oxygen ion or be reduced by hydrogen. An important conclusion is that the lattice oxygen on $CeO_2/MgAl_2O_4$ is very active and has a high recoverability. The authors studied this material for its de-SO_2-activity, which is shown to be high. No other catalytic reactions were studied, but it would indeed be interesting to study this material for its behaviour in selective oxidation reactions.

5. Computational modelling of catalysts and catalytic reactions

In our previous review [1] we mentioned the possibility to relate the catalytic behaviour of oxides to the electrostatic potential of the oxygen ion in the oxide lattice. In the mean time there has been much progress in the field of computational modelling of catalytic phenomena. Recent reviews of this field have been published, e.g., by Catlow et al. [63–65] who considers both the classical ionic bonding methods of computational modelling and quantum mechanical

calculation methods. As stated in these papers computer modelling can make some important contributions to the solution of the following fundamental problems in the science of catalysis:

1. Development of models of the structures at the atomic level of catalysts, including both bulk and surface structures.
2. Elucidation of the structure of *local* states which provide the active sites on the catalyst surface.
3. Determination of the mechanisms of molecular diffusion to and adsorption at active sites.
4. Understanding the detailed reaction mechanisms of adsorbed molecules.

The principles of the methods employed for ionic solids are discussed, e.g., by Lidiard [66] for the calculation of defect energies, entropies and mobilities, by Mackrodt [67] for the calculation and simulation of oxide surfaces and more in general by Harding [68].

5.1. Calculations of surface phenomena

It has been shown to be possible to calculate the relative stability of different lattice planes [68–72], which means that in this way it is possible to predict which lattice planes are expected to be present and also in what proportion on a catalyst surface. Of the two examples treated in the review [63], the activation of oxygen is discussed later in this paper in connection with methane coupling on Li/MgO catalysts. A survey of early applications of computer modelling to catalysts, together with the background of the necessary computations, has been given by Catlow et al. [73]. Attention is focused in this paper on oxides with the NaCl (rock-salt), the perovskite, the fluorite and the pyrochlore structure. Computer simulations of the structures and their surfaces, together with applications to catalysis have also been reviewed by Catlow et al. [74]. Examples of calculations of [75] for the fluorite structure are the variation of the energy of oxygen vacancies and of Y^{3+}-substitutionals as a function of the distance from the (1 1 1) surface in ThO_2, the results of which are shown in Fig. 9. Similar calculations were performed for oxygen vacancies, Y^{3+}-substitutionals and metal ion vacancies in UO_2 and CeO_2.

The oxygen vacancy energy shows a maximum somewhat below the surface, meaning that this forms a barrier for oxygen ion movement to and from the surface, which can be of importance for oxygen transport needed for a catalytic reaction. On the other hand the Y^{3+}-substitutional energy is highest at the outer surface. This means that it will preferentially segregate away from the surface.

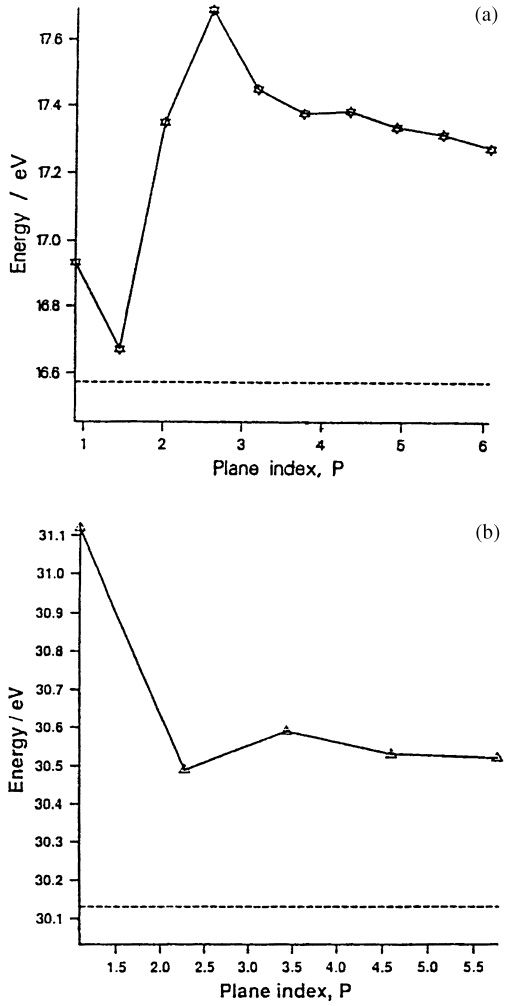

Fig. 9. Variation of dopant and oxygen vacancy energies in ThO_2 with distance from the (1 1 1) surface of the oxide: (a) oxygen vacancy; (b) Y^{3+}-substitutional. The plane index *P* indicates the *p*th plane parallel to the (1 1 1) plane (reproduced from Fig. 4a and b of [73], copyright 1990, with permission from the American Chemical Society).

Purton et al. [76] determined the electronic structure of the ideal and defective structures of rutile using atomic simulations. In agreement with experimental results the (1 1 0) plane is the most stable while (0 0 1) is least stable with (1 0 0) in between. For defective

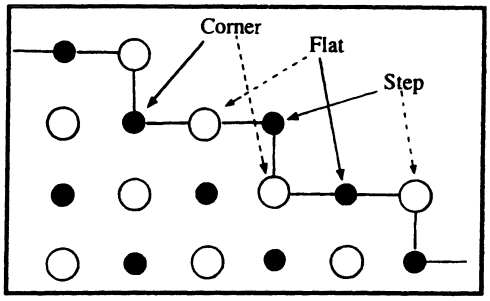

Fig. 10. (3 1 0) surface plane of CeO_2 showing three different sites: step, flat and corner. Oxygen: big, open circles; cerium: small, closed circles (reproduced from Fig. 1 of [77], copyright 1994, with permission from Elsevier Science).

surfaces a surface state, mainly of Ti (3d) character, is observed at the bottom of the conduction band and this is about 1 eV below the Fermi level in XPS experiments.

Sayle et al. [77] studied the surface energies of the (1 1 1), (1 1 0) and (3 1 0) planes of CeO_2, an oxide with the fluorite structure. The (3 1 0) surface was studied in particular because it has different step sites, which might act as active sites in catalytic reactions, as shown in Fig. 10. When calculations of surface energies are performed it is important to take into account the relaxation of the ions, i.e. their displacement from their ideal positions in the undeformed lattice leading to a lower surface energy. In Table 3 the calculated surface energies of the above-mentioned three surfaces are given and it is seen that the order of stability remains unchanged by relaxation, but the absolute values show large changes, in particular for the (3 1 0) plane. The authors suggest that the higher energy of the (3 1 0) plane may result in higher catalytic activity, although it is expected to be present in low proportions, unless it is stabilised by defects. Also because of this, for some reactions, favourable sites on the (3 1 0) surface it is nevertheless expected to play an important role in catalysis.

Table 3
Calculated surface energies of CeO_2 surfaces (data from Sayle et al. [77])

Surface	Energy ($J\,m^{-2}$)[a]	
	Unrelaxed	Relaxed
(1 1 1)	1.7	1.2
(1 1 0)	3.6	1.6
(3 1 0)	11.6	2.5

[a] The energies are given to three decimal places in the original paper, but are rounded to one decimal place here.

Even more important is the possibility to calculate the stability of defects, such as oxygen vacancies, on the different planes forming the external surface of the catalyst particles. Sayle et al. [77,78] performed this type of calculation for the catalytic oxidation of CO on CeO_2. An important conclusion of this work is that for the reaction

$$CO(g)+\text{“}CeO_2\text{”} \rightarrow CO_2(g) + V_O^{\bullet\bullet} + 2Ce'_{Ce} \quad (14)$$

or written in the form of separate consecutive reactions

$$O_O{}^x + 2Ce_{Ce}{}^x \rightarrow \tfrac{1}{2}O_2(g) + V_O^{\bullet\bullet} + 2Ce'_{Ce} \quad (15)$$

$$CO(g)+\tfrac{1}{2}O_2(g) \rightarrow CO_2(g)$$

the reaction enthalpy is positive for bulk CeO_2 ($+294.3\,kJ\,mol^{-1}$) but negative for the (1 1 1), (1 1 0) and (3 1 0) planes (-59.8, -273.1, $-459.3\,kJ\,mol^{-1}$, respectively). Here we see that the special geometry of the (3 1 0) plane leads to lowest energy, so that this surface is expected to play the main role in CO-oxidation. In view of the interesting properties of solid solutions of CeO_2–ZrO_2, Balducci et al. [79,80] investigated the surface and reduction energies of these compounds by computer modelling. They first performed a computer simulation for bulk reduction and oxygen migration in CeO_2–ZrO_2 [79]. It was found that even small additions of ZrO_2 decrease the bulk reduction energy of Ce^{4+} to a value close to that for surface reduction of pure CeO_2. Activation energy calculations show that the mobility of oxygen increases almost monotonically with ZrO_2 content.

For the surface reduction, treated in [80], they found that for the whole range of ceria-contents the order of stability of the (relaxed) surfaces (1 1 0), (1 1 1) and (3 1 0) was the same as that found earlier by Sayle et al. [77]. The redox behaviour of the CeO_2–ZrO_2 surfaces was investigated on the basis of the energy changes of the reaction

$$2Ce_M{}^x + O_O{}^x \rightarrow \tfrac{1}{2}O_2 + 2Ce'_M + V_O^{\bullet\bullet} \quad (16)$$

In the calculation the formation of neutral $[Ce'_M–V_O^{\bullet\bullet}–Ce'_M]$ clusters was taken into account. The results show that for the (1 1 0) and (1 1 1) planes

the reduction of Ce^{4+} to Ce^{3+} at the surface is approximately equal to that in the bulk for pure CeO_2 but becomes more favourable with increasing zirconia content. For the (3 1 0) surface, which shows a much larger reorganisation than the other planes, the results depend very much upon the precise situation of the ions on the surface so that this case is less clear. On the average the behaviour is opposite to that of the other planes: the reduction energy decreases with increasing ceria fraction. Moreover the energy difference becomes negative at higher CeO_2 contents, thus indicating the formation of a low-energy route for the Ce^{4+} to Ce^{3+} reduction on this surface. These results indicate that reconstruction of the outer surfaces, together with the formation of a low-energy route for the Ce^{4+} to Ce^{3+} reduction, may be an important factor in the high storage capacity for oxygen observed in these solid solutions.

An experimental investigation of the redox behaviour of CeO_2 induced by structural doping with ZrO_2 has been reported by Fornasiero et al. [81] by comparing the reduction/oxidation process of CeO_2 and $Ce_{0.5}Zr_{0.5}O_2$. It was shown that the sintering, induced by the reduction, leads to a larger crystal size and a decrease in the reducibility of CeO_2. In the mixed oxide the sintering induced a structural modification. The modified structure shows a high efficiency of the $Ce^{4+} \leftrightarrow Ce^{3+}$-redox cycle at moderate temperatures, which is considered to be of importance for certain catalytic applications.

Cordatos et al. [82] investigated the structure and reducibility of ceria clusters using simulated annealing calculations. The calculated lattice energy increased with the cluster size, in agreement with expectations. Only for the largest cluster consisting of 50 CeO_2 molecule-units was the fluorite structure clearly observed. The reducibility in general decreased with cluster size, but large fluctuations were also observed. These conclusions are in agreement with experimental results indicating that the reducibility of ceria is structure sensitive and that larger crystals are more difficult to reduce (see also the effect of sintering observed by Fornasiero et al. [81]).

Structural modelling of the structure of V_2O_5 was performed by Dietrich et al. [83]. It was shown that the deviations of the observed structure from the ideal model based on regular VO_6 octahedra is correctly reproduced, both using full ionic charges and with partial charges. In view of the important role of vanadia in oxidation catalysis computer modelling of the surface structure, crystal morphology and ethene sorption of V_2O_5 was performed by Sayle et al. [84], again based on an ionic model for the V_2O_5-crystal. In agreement with experimental observations the (0 0 1) face dominates the crystal morphology having the lowest energy. The sorption energy of ethene has been calculated to be $-23\,kJ\,mol^{-1}$ on the (2 0 0) plane, $-33\,kJ\,mol^{-1}$ on the (0 0 1) plane and $-77\,kJ\,mol^{-1}$ on the (3 0 1) plane. Because the number of V=O groups on the (0 0 1) and (3 0 1) planes is high and both planes are expected to play an important role in catalytic oxidation this means that the strong adsorption on the (3 0 1) plane may well outweigh its smaller relative contribution to the surface of the catalyst.

An important field of study is that of the interface between a catalyst and its support or between different components of a catalyst, which was already mentioned in Section 3.4. An example is the calculation of Sayle et al. [85] for the V_2O_5/TiO_2 interface. These authors showed that supported V_2O_5 thin films of TiO_2, anatase exhibit remarkable modifications of their structure compared with unsupported V_2O_5. For example the vanadyl O–O distance ranges from 3.99 to 4.22 Å depending on the thickness of the vanadia layer. This also alters the configuration of adsorbed molecules. Thus the sorption of ethene and ethane on V_2O_5 (0 0 1) both free and supported as a monolayer on TiO_2 (0 0 1) anatase was studied using simulation techniques by Sayle et al. [86]. In Table 4 the results of these calculations are collected. Ethene can approach the (0 0 1) face much closer than ethane which explains its larger adsorption enthalpy.

Sayle et al. [87,88] investigated the energetics of defects near the interface in MgO/MgO and CeO_2/Al_2O_3 and in $BaO/SrTiO_3$ and CeO_2/Al_2O_3. In the CeO_2/Al_2O_3 system it was found that oxygen

Table 4
Adsorption enthalpies of ethene and ethane adsorbed on unsupported and supported V_2O_5 (0 0 1) (data from Sayle et al. [86])

Molecule	Adsorption enthalpy ($kJ\,mol^{-1}$)	
	Pure V_2O_5	Monolayer V_2O_5 on anatase
C_2H_4	−39.7	−79.6
C_2H_6	−25.4	−27.4

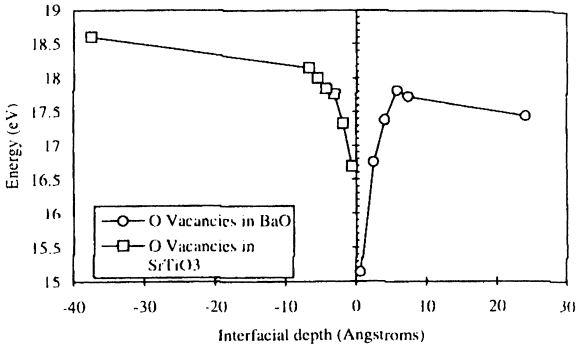

Fig. 11. Oxygen vacancy formation energies (in eV, 1 eV=96.5 kJ mol^{-1}) as a function from the BaO (0 0 1)/$SrTiO_3$ (0 0 1) interface. Depth=0 is the interface, depth<0 is BaO, depth >0 is $SrTiO_3$ (reproduced from Fig. 6 of [88], copyright 1994, with permission from the American Physical Society).

vacancies in a triple CeO_2 layer on Al_2O_3 are more stable than on free CeO_2. Also the energy of oxygen vacancies is more favourable near to the CeO_2/Al_2O_3 interface than on the exterior of CeO_2. This means that movement of oxygen through this layer from the interface to the outside is promoted, which may be important for catalytic reactions.

It is to be expected that the changes in structure of supported V_2O_5 [85] also lead to similar effects because the oxygen atoms of vanadia certainly participate in the catalytic reaction.

For the BaO/$SrTiO_3$ interface [88] the vacancy formation energies are also clearly different from those in the separate oxides and are a function of the distance to the interface. As an example Fig. 11 shows the oxygen vacancy formation energies in this system.

It is seen that close to the interface the formation energy is smallest, meaning that the oxygen vacancies tend to segregate to the interface. Titanium vacancy formation in $SrTiO_3$ and barium vacancy formation in BaO also have minimum energies near the interface, but for strontium vacancies in $SrTiO_3$ the formation energy is maximum near the interface.

5.2. Quantum cluster calculations

In the calculations discussed in the previous section the oxides were supposed to be completely ionic which often is a reasonably good approximation. However, when considering adsorption and/or reaction on their surfaces it becomes necessary to apply quantum chemical calculations.

In these calculations the quantum chemical methods are usually applied to a cluster of atoms and/or ions, taken to be representative for the system under consideration. Without considering catalytic applications as yet, Kuhlenbeck et al. [89] performed quantum cluster calculations of the adsorption of NO on NiO (1 0 0) planes. The cluster consisted of a NiO_5-group together with an NO-molecule bound to the Ni-ion in octahedral co-ordination. Ab initio self consistent field (SCF) calculations showed that the stable configuration has an angle of 45° between the NO bond and the Ni–N bond, with a binding energy of about 16 kJ mol^{-1}. Pöhlchen [90] reported that the bonding energy of NO to the NiO (1 0 0) plane was at most 22 kJ mol^{-1}. Similarly Pöhlchen and Staemmler [91] performed calculations for the adsorption of CO in the same system. They used two types of clusters: bonding of CO to $Ni(H_2O)_3(OH)_2$, where the protons are added to obtain a neutral cluster, and bonding to $Ni^{2+}(O^{2-})_5$ embedded in a lattice of point charges which represent the half-infinite ionic crystal. It was shown that the two types of calculation lead to practically identical results with a binding energy of Ni–CO of about 10 kJ mol^{-1} with the CO molecule perpendicular to the NiO (1 0 0) plane. The small values of the adsorption energies indicate that these correspond both for NO and CO with physisorption.

Van Santen [92] has reviewed the application of the cluster approach to catalysis by metals and to zeolite catalysts. Catlow et al. [63–65] discussed applications to oxidic systems as well. Cluster calculations by Ackermann et al. [93] on the CH_4–O^-–Li^+–[MgO] system are discussed in Section 5.5.

Extensive quantum mechanical cluster calculations of V_2O_5 (0 1 0) were performed by Witko [94], Haber et al. [95], Witko et al. [96], Haber et al. [97] and Witko et al. [98]. The bonding in V_2O_5 is found to be mixed ionic–covalent, where the vanadyl bond is more covalent than the bridging vanadium–oxygen bonds. This is in agreement with the different catalytic properties of the inequivalent oxygen centres. These differences are also shown in the calculations on proton adsorption. In a series of calculations where the proton approached different oxygen atoms perpendicularly the proton was stabilised at all oxygen sites with the bonding being

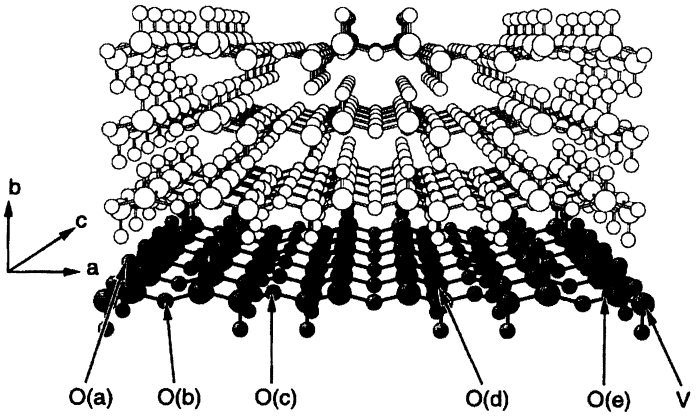

Fig. 12. Perspective view of the orthorhombic lattice of V_2O_5, where the large balls represent V-atoms, the small ones O-atoms. The location of the V-atoms and of the symmetry inequivalent surface O-atoms (O(a)–O(e)) is indicated (reproduced from Fig. 1 of [98], copyright 1997, with permission from Elsevier Science).

strongest for the O(c) site (see Fig. 12 for the notation used), which is in agreement with the result of other calculations which show this oxygen atom to be the most nucleophilic. In a second series of calculations the proton was kept fixed 3 Å above the oxygen site and the corresponding oxygen atom was allowed to relax. Only the oxygen atoms O(c) and O(d) leave their surface positions and form surface-hydroxyl-groups.

Furthermore Witko et al. [98] also performed calculations concerning the adsorption and reaction of propene and toluene on the V_2O_5 (0 1 0) plane. A detailed pathway for the formation of acrolein from propene could be calculated in which first, with the carbon atom of the methyl group, C–O is formed using the O(c) centre, followed by abstraction of two hydrogens from the methyl group. The formation of acrolein is connected with the reduction of the two vanadium atoms bound to the O(c) centre. For the reaction with toluene to benzaldehyde the calculations led to a similar mechanism as that found for propene.

Recently Witko [99] reported on cluster calculations for a number of vanadium compounds which are used in catalysis: V_2O_5 (0 1 0), cluster $V_{10}H_{31}H_{12}$; V_2O_4 (0 1 1), cluster $V_7O_{24}H_{20}$; $VOPO_4$ (0 1 0) cluster $V_4P_5O_{33}H_{21}$; and $(VO)_2P_2O_7$ (1 0 0), cluster $V_{10}P_6O_{50}H_{30}$. It is not yet certain whether the cluster $V_4P_5O_{33}H_{21}$ is large enough for convergence to have been obtained and further calculations are in progress. In Table 5 the calculated bond orders for the different types of oxygen atoms present on the surfaces are given. It is seen that, except for $VOPO_4$, the bond orders are lowest for the triply bridged oxygens, intermediate for the doubly bridged and highest for the vanadyl oxygen.

Density functional cluster calculations and angular resolved photoemission (ARUPS) measurements were performed by Hermann et al. [100] to study the properties of differently co-ordinated oxygen atoms at the V_2O_5 (0 1 0) surface. Calculated total and partial densities of states were used to identify differently co-ordinated oxygen atoms. The shape of the experimental ARUPS curves, obtained using freshly cleaved V_2O_5 (0 1 0) samples, were in good agreement with the calculated cluster density of states. The most prominent peak in the spectrum could be assigned to emission from the terminal (=vanadyl) oxygen, while the peaks at the top and the bottom of the spectrum were proposed to be due to mixtures

Table 5
Calculated total bond orders for oxygen atoms in vanadium compounds according to [99]

Compound	V=O	P=O	V–O–V	V–O–P	V–O–V V	V–O–V P
V_2O_5	2.13	–	1.78	–	1.58	–
V_2O_4	–	–	1.93	–	1.81	–
$VOPO_4$	1.64	1.67	2.05	1.81	–	–
$(VO)_2P_2O_7$	2.36	1.78	–	1.86	–	1.73

of contributions from the bridging oxygens. Differences in the spectra between different V_2O_5 (0 1 0) cleavages were due to surface imperfections, which were concluded to be mainly incompletely occupied bridging oxygen sites. A definitive characterisation of possible imperfection structures fell outside the scope of the investigation. ARUPS measurements for V_2O_5 (0 1 0) exposed to hydrogen showed that adsorbing hydrogen affects bridging oxygen atoms more strongly than terminal oxygens, in agreement with the cluster calculations discussed earlier. It is clearly shown by this study that the combination of electronic structure calculations with photoemission measurements makes detailed molecular understanding of complex oxide surfaces possible. These results also show that these methods can be used to study details of catalytic reactions occurring at the surface of oxides.

Zhanpeisov et al. [101] performed similar calculations using a different calculation method. In all cases the (0 1 0) surface of V_2O_5 was modelled, both without and with hydrogen or proton adsorption. The structural and energetic details were calculated with different cluster sizes and for large enough clusters showed good agreement with experimental data. These authors also calculated the formation energies of oxygen vacancies at the surface. The calculations show that the creation of an oxygen vacancy at the vanadyl oxygens is energetically favourable with respect to the formation of such a vacancy on the bridging oxygen sites. Unfortunately it is not clear what the type of the vacancy is: V_O^x or $V_O^\bullet$ or $V_O^{\bullet\bullet}$, because no localised charges of the calculated vacancy are given.

An important advantage of the calculations considered in this section is that not only structures and energies but also reactivities can be calculated, as shown in particular by those performed by Witko et al. [98]. It is difficult to compare these results with those obtained by Dietrich et al. [83] and of Sayle et al. [84] for V_2O_5, discussed in the previous section, because in the cluster calculations only the (0 1 0) surface was considered while sorption properties were considered for different molecules.

A limitation which is still present in all calculations is that only equilibrium, or at most steady-state, properties can be calculated. The true dynamics and in particular the true rates of the reactions cannot yet be obtained.

5.3. Modelling of diffusion in solids

Because in many cases the transport of ions through a (defect) lattice is of importance for catalytic reactions occurring at the surface, the calculation of transport properties and the mobilities of defects is also of great importance. Similarly the transport through membranes in membrane reactors strongly depends on the transport properties of these materials.

For these calculations models of localised defects are needed as discussed by Grimes and Catlow [102] who performed calculations using the Mott–Littleton method and embedded quantum cluster methods.

An example is the calculation of oxygen transport in yttria-doped ceria by Adler and Smith [103]. An important conclusion is that, at least in this case, long-range forces play an important role. Inclusion of these leads to significant deviations from the results calculated with a simple point-defect model. Furthermore they show that for this material the vacancy-defect association energy is well approximated by considering only Coulombic interactions between point charges in the ceria treated as a dielectric continuum.

A computer simulation study of the defect structure of calcia-stabilised zirconia by Dwivedi and Cormack [104] has shown that, at low dopant concentrations, oxygen vacancies are preferentially situated on next nearest neighbour instead of on nearest neighbour sites. Values of calculated migration activation enthalpies include a contribution from the dissociation energy of vacancy–dopant pairs, which indicates the importance of defect interactions for migration.

Molecular dynamics simulations of diffusion in yttria-stabilised zirconia have been performed by Brinkman et al. [105]. It was found that oxygen ions migrate through a discrete hopping process between neighbouring tetrahedral sites. An important result was that diffusion occurs in a short-time and a long-time regime, meaning that in order to obtain data relevant for macroscopic diffusion the time scale of the calculations must be sufficiently long. The authors obtained a reasonably close agreement between experimental and calculated oxygen tracer diffusion coefficients.

Cherry et al. [106] performed a molecular dynamics study of oxygen diffusion in the perovskites

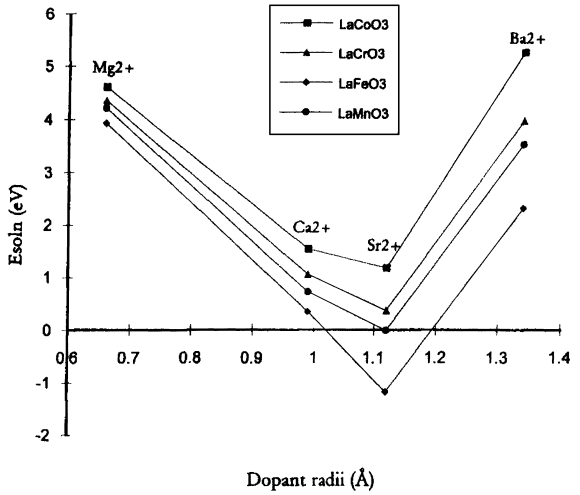

Fig. 13. Calculated energies of solution as a function of ionic radius for alkaline earth dopants in perovskites $LaMO_3$, with M=Co, Cr, Fe and Mn (reproduced from Fig. 9 of [106], copyright 1995, with permission from Academic Press).

$La_{1-x}A_xBO_3$ with A=Mg, Ca, Sr, Ba and B=Cr, Mn, Fe, Co. This investigation showed that diffusion occurs through hopping of oxygen vacancies along the anion tetrahedral edges with migration via a curved path. The calculated migration energies are in agreement with experimental values and the calculations show the importance of including relaxation effects at the migration saddle point. Furthermore it was shown that ion size effects are important for the solution enthalpies, as shown in Fig. 13 with Sr^{2+}-ions being most favourable. This result is somewhat different from that indicated by Yokokawa et al. [47], but as those authors do not give quantitative values direct comparison is not possible.

Also Cherry et al. [106] observed a clear trend towards lower migration energies with smaller A-site cations and larger B-site cations, although there are some irregularities in the lines as shown in Fig. 14.

Islam et al. [107] performed a molecular dynamics study of oxygen diffusion in $La_{1-x}Sr_xBO_3$, with B=Mn, Co. No sign of oxygen diffusion was found in the stoichiometric compounds (x=0) and it was shown that acceptor doping is essential to obtain high ionic conductivity. The calculated activation energies are higher for the manganates than for the cobaltates and are in good agreement with experimentally observed values.

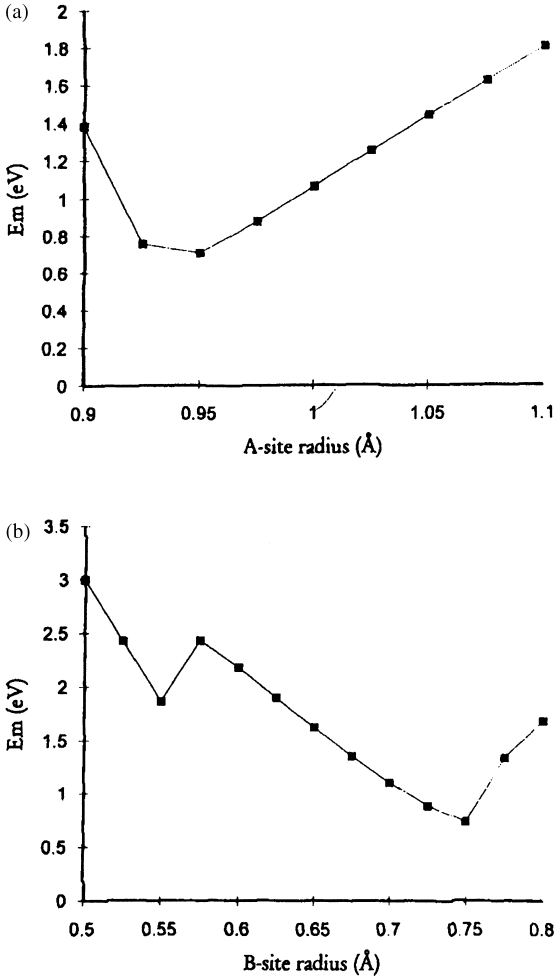

Fig. 14. Calculated migration energy as a function of cation size (a) at the A-site, (b) at the B-site (reproduced from Fig. 7 of [106], copyright 1995, with permission from Academic Press).

5.4. Lanthanide oxide catalysts

Islam et al. [60] have studied methane oxidation on La_2O_3 as catalyst. They investigated in particular the formation of O^- and O_2^{2-}-peroxide species as these are supposed to be responsible for methane activation on this material [108,109]. The most important results of this study are in the first place that the (0 0 1) and (0 1 1) surfaces are the most stable external crystal planes and are therefore expected to play an important role in catalytic reactions. The calculated binding energies, as shown in Table 6, indicate the possibility of

Table 6
Energies of peroxide ion formation (data from Islam et al. [60], negative value indicates bound configuration)

Position	O^-–O^--separation (Å)	Binding energy (kJ mol^{-1})
Bulk	3.92	9.6
(0 0 1) surface	3.92	34.7
(0 1 1) surface	3.93	−61.8

the formation of O_2^{2-}-peroxide ions in particular on the (0 1 1) face. The authors suggest that the catalytic activity of doped La_2O_3 is correlated with its ability to (re)generate reactive oxygen hole centres ($O^-=O_O^\bullet$ and $O_2^{2-} = (O_2)_O^{\bullet\bullet}$) by reaction between gaseous oxygen and oxygen vacancies at the surface.

The authors propose that the active oxygen centre is generated by the reaction of gaseous oxygen with the solid. This occurs by the filling of oxygen vacancies by molecular oxygen to form a hole species. This reaction can be written as

$$V_O^{\bullet\bullet} + \tfrac{1}{2}O_2 \rightarrow O_O^{x} + 2h^\bullet \quad (17)$$

where $2h^\bullet$ is a small polaron species, i.e. either $2(O^-=O_O^\bullet)$ or $O_2^{2-} = (O_2)_O^{\bullet\bullet}$. The oxidation energies for this reaction are given in Table 7.

These results show three main points. The oxidation energies are more favourable on the surface than in the bulk, which means that incorporation of oxygen at the surface is easier than in the bulk. Secondly the lowest oxidation energy is that for the formation of peroxide ions on the (0 1 1) surface implying that this is the most active. Finally the authors suggest that the relatively small values of the oxidation energy indicate that the partial pressure of oxygen may be an important factor in the relative rates of formation of peroxide ions in the total catalytic process. These results are also in agreement with oxygen exchange experiments by Kalenik and Wolf [110–112] and Anshits et al. [113] which are discussed more fully in Section 7.

Table 7
Energies of the oxidation reaction (17) (data from Islam et al. [60])

Position	E_{ox} (kJ mol^{-1})	
	O^-	O_2^{2-}
Bulk	138.9	143.8
(0 0 1) surface	56.0	62.7
(0 1 1) surface	40.5	9.65

5.5. Alkali-metal doped earth-alkali oxide catalysts

Catlow et al. [73] discussed the computer modelling of the defect properties of Li/MgO which is a promising catalyst for methane coupling, of which oxygen exchange properties are discussed in Section 7 and catalytic properties in Section 8.1.3. The most straightforward mode of incorporation van Li^+-ions in the MgO lattice is as substitutional ions on magnesium sites, with oxygen vacancies for charge compensation. In the Kröger–Vink notation this can be written as

$$\text{“}Li_2O\text{”} + 2Mg_{Mg}{}^{x} + O_O{}^{x} \rightarrow 2Li'_{Mg} + V_O{}^{\bullet\bullet} + 2\text{“}MgO\text{”} \quad (18)$$

where “Li_2O” and “MgO” represent the incoming lithium oxide and the displaced magnesium oxide, respectively. The calculated dissolution energies corresponding to this reaction are given for different similar systems in Table 8.

The solution energies are endothermic and are particularly high for the Li/MgO system, so that the solubility of Li_2O in MgO is expected to be much lower than, e.g., that of Na_2O in CaO or K_2O in BaO, which is considered to be of interest in connection with their catalytic properties (Fig. 15).

In order to make Li/MgO catalytically active the presence of oxygen is necessary. In terms of defect chemistry this means that in the oxidation of the vacancies hole states are formed according to the reaction equation

$$V_O^{\bullet\bullet} + \tfrac{1}{2}O_2 \rightarrow O_O{}^{x} + 2h^\bullet \quad (19)$$

Since the valence band of this type of oxide is obtained from O (2p) orbitals, localised hole states may be de-

Table 8
Energies of solution of alkali-metal oxides into alkaline earth oxides, with oxygen vacancy formation (column 3) and energies of oxidation of vacancy to hole (column 4) (data from Catlow et al. [73], positive energies correspond with endothermic reaction)

Alkali-metal oxide	Alkaline earth oxide	Solution energy (kJ mol^{-1} M_2O)	Oxidation energy (kJ mol^{-1} vacancy)
Li_2O	MgO	525.8	−220.0
Na_2O	CaO	294.3	−166.0
K_2O	SrO	300.8	−284.6
K_2O	BaO	142.8	−167.9

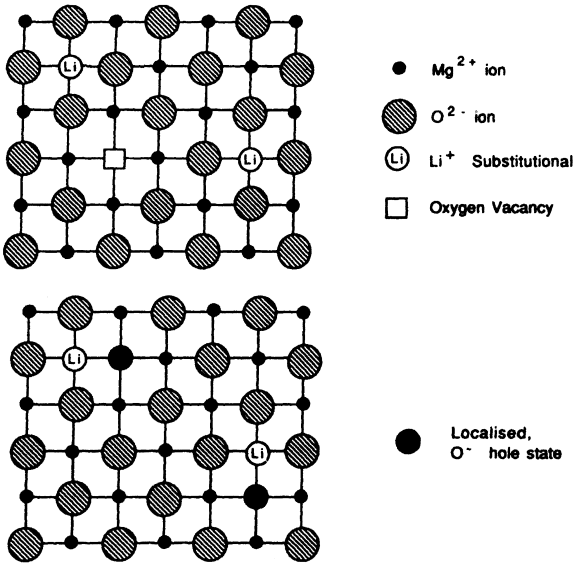

Fig. 15. Defect structures of Li/MgO (reproduced, with some corrections, from Fig. 2 of [73], copyright 1994 with permission from the American Chemical Society).

scribed as $O^- = O_O^\bullet$ ions. The calculated energies for this reaction are given in the fourth column of Table 8. These energies are exothermic, so that at not too low oxygen partial pressures it is expected that holes are predominant over oxygen vacancies and also that oxidation increases the solubility of the alkali-metal oxide in the alkaline earth substrate. In fact for BaO the total energy is exothermic which indicates that the use of BaO instead of MgO as solid solvent is probably advantageous to obtain an improved catalyst.

Of course what is needed also is knowledge of the behaviour of these defects at the surface of the catalyst. From the catalytic and EPR experiments described in Section 8.1.3 it follows that the $[Li'_{Mg}O_O^\bullet]$ is expected to be the active site for proton-abstraction from CH_4. In Table 9 the calculated segregation energies, i.e. the energy difference between the defect at the surface, minus that in the bulk, for the different defects in the Li/MgO system are given, showing that the segregation of the combined defects is the most advantageous.

Table 9
Calculated segregation energies in Li^+-doped MgO (data from Catlow et al. [73])

Defect	Segregation energy ($kJ\,mol^{-1}$)
Li'_{Mg}	−17.4
$O_O^\bullet$	−91.7
$[Li'_{Mg}O_O^\bullet]$	−164.0

More complete data and background information can be found in the paper by Foot et al. [114] in which the original calculations are described. In a recent paper of Catlow et al. [64] quantum chemical calculations of the CH_4–$[Li'_{Mg}O_O^\bullet]$ cluster as performed by Ackermann et al. [115] are also discussed. In the first instance a very simple cluster: CH_4–O^-–Li^+–[MgO] was used, which was embedded in an array of point charges to take into account the effect of the MgO lattice. Although this already gave useful results a more exact calculation was performed using a much larger cluster: CH_4–O^-–Li^+–$[Mg_{29}O_{13}]^{32+}$. This cluster was then embedded in an array of 750 point charges which represent the MgO lattice (note: the charge of the cluster as given in the original paper, $[Mg_{29}O_{13}]^{32-}$, is not in agreement with the stoichiometry, but the surrounding lattice of course had the charge −32). Various quantum mechanical methods were applied: Hartree–Fock, with different approximations and wave function sets and density functional theory. In these calculations it was shown that it is important to include extensive relaxation of atoms in and near the surface in order to obtain accurate defect geometries of the surface defect sites. For further details we refer to the original paper.

6. Surface science of oxides

There have been many studies of the surface science of metals and its application to catalysis and several reviews [116,117] indicate the great progress made in this field. Oxide surfaces are at present receiving increasing attention as shown by the review of Freund [118] and although of course many questions are not yet answered there are indications that in the (near) future experiments are going to provide the same kind of detailed information about complex, e.g., oxide, surfaces as is available now for metals. The state of present knowledge is described in the books by Henrich and Cox [119] and Noguera [120]. Both books are mainly devoted to the discussion of properties of and processes on single crystal surfaces of oxides at very low pressures. One chapter in the

second book is wholly dedicated to a discussion of the acid–base properties of metal oxide surfaces. It is stressed, however, that much more work on the model systems, together with quantum mechanical considerations, is necessary to allow a detailed understanding to be reached. Being devoted especially to surfaces it is a pity that these books do not discuss defects in the sense of Section 3 of this review and insofar as defects are mentioned the Kröger–Vink notation is not used.

From the point of view of surface science there is a need for better and more accurate definition both of surface structure in general and of surface defects and in this respect close co-operation with computational modelling is desirable.

An example of investigations of this type is that of the adsorption of NO and CO on the NiO (1 0 0) plane for which the corresponding quantum cluster calculations have been briefly considered in Section 5.2. Kuhlenbeck et al. [89] used different types of electron spectroscopy and were able to show that NO is adsorbed on the nickel-ions and that the NO bond is at the angle of about 45° with respect to the Ni–NO bond, in agreement with the calculations. Wichtendahl et al. [121] performed a thermal desorption spectroscopy method to study the bonding of CO and NO to vacuum-cleaved NiO (1 0 0). They found a bonding energy of about 29 kJ mol^{-1} for CO, desorption temperature 30 K, and of about 55 kJ mol^{-1} for NO, desorption temperature about 56 K. This is significantly larger than the values obtained from the cluster calculations. The authors propose this to be due to the influence of the Ni (3d) electrons because the calculated value for the adsorption energy of CO on vacuum-cleaved MgO (1 0 0) is in much better agreement with the experimental value. The TDS-experiments show a broad desorption feature for CO at about 115 K and for NO at about 220 K which are probably due to adsorption to surface defects, because it is more intense on thin film samples, which contain more defects than vacuum-cleaved surfaces, and after ion bombardment. Summarising the conclusion is that both NO and CO show only physisorption on NiO (1 0 0) at low temperatures, but that at higher temperatures chemisorption occurs on defects in this surface. From a catalytic point of view the latter are probably of large interest but up to now have not been investigated in more detail.

In many surface investigations the time needed for the measurements is so long that only equilibrium states can be studied. However, recently there has been progress in the study of dynamic processes as well, as exemplified by the study of laser induced desorption of NO from NiO (1 0 0) by Baumeister and Freund [122] and Klüner et al. [123,124].

In the paper by Freund [118] several other examples of studies of this kind are reported, together with extensive references to the relevant literature. This shows the increasing attention given to surface science investigations of oxides. But it is also clear that much work still has to be done before direct applications to catalytically interesting systems become possible.

7. Kinetics of oxygen exchange between gas and oxide

In Section 8 of [1] a discussion of the mechanism and kinetics of oxygen exchange and its relation with oxidation catalysis has been given.

Anshits et al. [113] and Kalenik and Wolf [110–112] studied oxygen exchange of Sr promoted La_2O_3 in connection with the use of this oxide as a catalyst for oxidative methane coupling. In this investigation the authors used direct isotopic exchange of oxygen as well as a new technique: temperature programmed isotopic exchange (TPIE) of lattice oxygen during oxidative methane coupling.

A typical result of the isotopic exchange between $^{16}O_2$ and a 1 at.% SrO/$La_2{}^{18}O_3$ catalyst is shown in

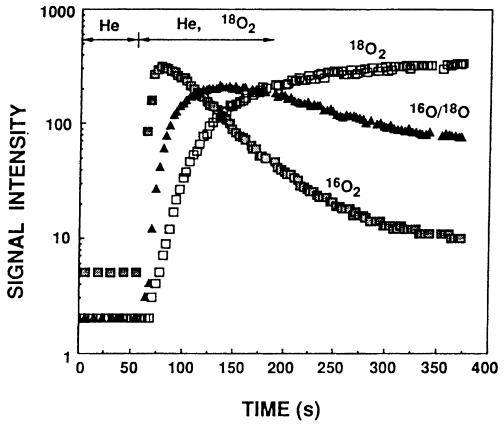

Fig. 16. $^{18}O/^{16}O$-exchange on 1 at.% SrO/La_2O_3 catalyst at 750°C (reproduced from Fig. 2 of [110], copyright 1991, with permission from Baltzer Science Publishers).

Table 10
Exchange parameters $^{18}O/^{16}O$-exchange on La_2O_3 based catalysts at 750°C (D_0=oxygen tracer diffusion coefficient. Data from Kalenik and Wolf [110])

Catalyst	BET area (m^2)	$\%O_2$ exchanged	$D_0 \times 10^{15}$ ($cm^2\ s^{-1}$)
La_2O_3	5.03	68.9	9.83
1 at.% SrO/La_2O_3	6.86	79.0	18.86
2 at.% SrO/La_2O_3	7.64	72.0	11.18

Fig. 16. After a time delay corresponding with the reactor dead volume a large amount of $^{16}O_2$ is released from the catalyst, which corresponds with the oxygen adsorbed on and just below the surface. The $^{16}O^{18}O$-signal behaves differently: it stays constant much longer due to the slow release of ^{18}O from the bulk of the catalyst. Steady flow of the $^{18}O_2$ is regained after about 5 min. For undoped and for 2 at.% SrO/La_2O_3 similar results were obtained.

Some numerical results are collected in Table 10. It is seen that doping with 1 at.% SrO increases the amount of exchanged oxygen by about 10% and doubles the oxygen self-diffusion coefficients, which can be obtained from these observations. Further increasing the doping percentage decreases both the amount of oxygen, which can be exchanged, and the self-diffusion coefficient.

The increase in the self-diffusion coefficient with doping percentage is clearly due to the increased oxygen vacancy concentration caused by the strontium addition. The improvement in the catalytic activity with increasing number of oxygen vacancies suggests that in the oxidative coupling methane is activated by oxygen trapped in an anion vacancy.

The accelerating effect of doping with strontium oxide is even more clearly seen by the TPIE experiments as shown in Fig. 17 where the $^{16}O^{18}O$-signal is plotted for both catalysts as a function of the increasing temperature during the experiment. The oxygen exchange starts at a temperature of about 100°C lower for the 1 at.% SrO/La_2O_3 catalyst than for the undoped La_2O_3. Also this start lies about 350°C lower than the usual temperatures used in the oxidative coupling of methane. The results indicate that doping with Sr enables a much faster exchange of lattice oxygen with oxygen from the gas phase, which probably explains the improved activity of the doped catalyst.

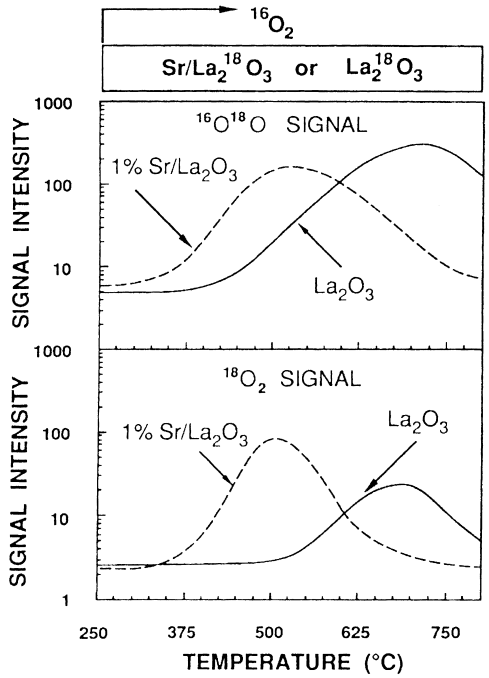

Fig. 17. The effect of Sr-promotion on the starting exchange temperature, during a TPIE-experiment (reproduced from Fig. 5 of [112], copyright 1992, with permission from Elsevier Science).

Gayko et al. [125] studied the influence of strontium doping of Nd_2O_3 on its electrical conductivity and on oxygen exchange. They observed an increase of the conductivity by two orders of magnitude upon doping Nd_2O_3 with 1 at.% SrO. The conductivity increased with oxygen partial pressure which indicates the presence of positive holes as dominating charge carriers. Experimentally σ was found to be proportional to $p_{O_2}{}^{1/4}$, which is in agreement with the following defect formation reactions:

$$\tfrac{1}{2}O_2 + V_O^{\bullet\bullet} \rightarrow O_O{}^{x} + 2h^{\bullet} \quad (20)$$

$$2\text{“SrO”} \rightarrow 2Sr'_{Nd} + V_O^{\bullet\bullet} + 2O_O{}^{x} \quad (21)$$

Their results obtained for the influence of doping of Nd_2O_3 with SrO on oxygen exchange are shown in Fig. 18. In agreement with the measurements on La_2O_3 discussed above here also both the amount exchanged isothermally and the rate of exchange as a function of temperature increase upon doping.

Oxygen exchange of lithium-promoted magnesium oxide catalysts has been studied by Peil et al.

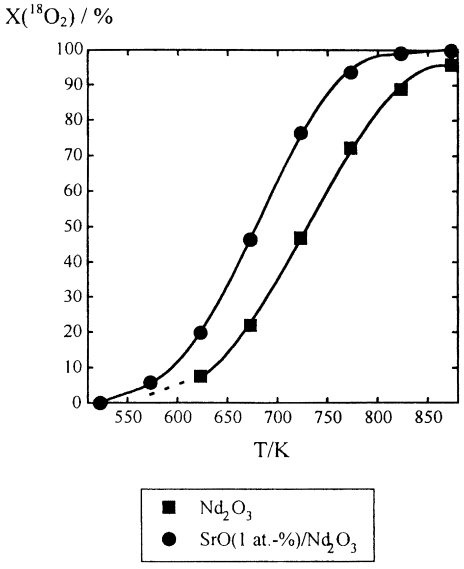

Fig. 18. Conversion of $^{18}O_2$ in $^{18}O^{16}O$ by oxygen exchange on Nd_2O_3 and SrO (1 at.%)/Nd_2O_3 as a function of temperature (reproduced from Fig. 8 of [125], copyright 1998, with permission from Academic Press).

[126,127]. In this investigation it was observed that the catalyst has three regions: (1) the physical surface at which very fast exchange between the gas phase and the solid occurs; (2) a number of subsurface atomic layers with which exchange is rapid; (3) the bulk oxide with which exchange is very slow or even absent. The number of layers mentioned under (2) is about 8–12. An important observation was further that the oxygen diffusivity was, at the same temperature, about an order of magnitude larger in lithium-doped MgO than in pure MgO. The activation energy of diffusion decreased from 266 kJ mol^{-1} for pure MgO to 61 kJ mol^{-1} for lithium-doped MgO. This change of the activation energy, together with the increased number of oxygen vacancies, discussed in Section 5.5, is proposed to explain these observations.

An investigation of the isotopic oxygen exchange between dioxygen and MgO catalysts was also performed by Karasuda and Aika [128]. These authors consider the $O_O^{\bullet}$-ion to be the active species both in oxygen exchange and in the methane coupling reaction and also the formation of these ions to occur through decomposition of water as discussed in Section 10 (see also reference [61]). In agreement with

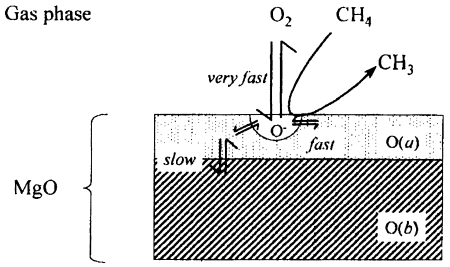

Fig. 19. Model of oxygen atom flux in MgO-based catalysts (reproduced from Fig. 14 of [128], copyright 1997, with permission from Academic Press).

Peil et al. [126,127] they find two steps in the oxygen exchange: a fast step which they suppose to occur between the $O_O^{\bullet}$-ion and directly surrounding oxygen atoms or ions in or on the surface of the oxide and a much slower step which is proposed to be due to exchange with oxygen ions present in the bulk. However, they observed the methane coupling reaction to be much faster even than the fast exchange reaction. This leads them to propose that the exchange between gaseous oxygen molecules and the $O_O^{\bullet}$-ions on the surface is even faster than that with the surface oxygens. This leads them to propose the model of oxygen atom flux as shown in Fig. 19.

Apart from pure MgO the influence of addition of 1 mol% Li_2O and 1 mol% ZrO_2 was also studied. The addition of Li_2O leads to the formation of $[Li'_{Mg}O_O^{\bullet}]$ associates which increase the activity for the methane

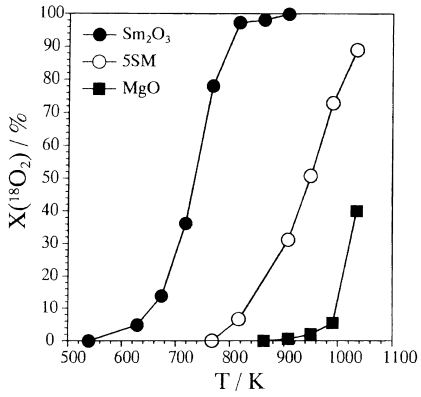

Fig. 20. Dependence of the conversion of $^{18}O_2$ in the isotopic exchange reaction on temperature (reproduced from Fig. 1 of [129], copyright 1994, with permission from Academic Press).

coupling reaction. The addition of ZrO_2 causes the production of additional active oxygen which plays a role in the oxidation of CH_4 to CO_2. The oxygen exchange showed the same features as those found for pure MgO with only some quantitative differences.

Buyevskaya et al. [129] investigated oxygen exchange over Sm_2O_3, Sm_2O_3/MgO and MgO. Characteristic results are given in Fig. 20.

In agreement with the results discussed above the exchange with MgO is very slow and limited in amount, while Sm_2O_3 shows the fastest and most extensive exchange. Because no mixed phases of MgO and Sm_2O_3 are known it is suggested by the authors that a layer of Sm_2O_3 present on the surface of the MgO particles is responsible for the increase in exchange rate.

Electrical conductivity relaxation and high- temperature calorimetric titration experiments were used by ten Elshof et al. [130,131] to study chemical diffusion and oxygen exchange of $La_{1-x}Sr_xFeO_{3-\delta}$ (x=0.1, 0.4) and $La_{0.6}Sr_{0.4}Co_{0.6}Fe_{0.4}O_{3-\delta}$. For samples of a thickness of 0.36–0.5 mm it was found that at oxygen pressures between 0.1 and 1 bar the oxygen exchange was diffusion controlled, while at oxygen pressures below about 0.03 bar it was controlled by surface reaction. In the high pressure region the chemical diffusion coefficients were 6.5×10^{-6} cm^2 s^{-1} for x=0.1 and 5×10^{-5} cm^2 s^{-1} for x=0.4 for the first compound while they were of the same order of magnitude for the second compound. At low pressures, where the oxygen exchange is controlled by the surface reaction, it is first order in O_2 which suggests the involvement of molecular oxygen reacting with a surface oxygen vacancy in the rate determining step.

8. Oxidation catalysis with transition metal oxides

In this section some important catalytic reactions catalysed by solid oxides are reviewed. Even if this is not always stated explicitly in many cases the basic mechanism of the catalytic oxidation reaction is supposed to be the Mars–van Krevelen mechanism [132]. In its simplest terms this consists of two consecutive steps: (1) the oxidation of the substrate by the catalyst, which thus is reduced; (2) the reoxidation of the catalyst, usually by gas phase oxygen. In many practical cases these steps are not simple, elementary reactions, but consist of a number of parallel or consecutive partial reactions and it is often the purpose of the investigations to be discussed below to unravel the complete mechanism.

8.1. Oxidative conversion of methane

Under this heading there are two main types of oxidative conversion. The first is often denoted as oxidative coupling of methane, i.e. a reaction in which it is tried to convert methane selectively to C_2-hydrocarbons by oxidation. The C_2-yield of this reaction can be strongly influenced by the mode of reactor operation, as shown, e.g., by Jiang et al. [133], but this falls outside the subject of this paper.

This particular type of reaction and the influence of the solid state properties of the catalysts has recently also been reviewed by Zhang et al. [134] and Voskresenskaya et al. [135]. Dubois and Cameron [136] examined a large number of oxides which had been used as catalysts for the oxidative conversion of methane. Their main conclusions are that active and selective catalysts consist of basic oxides, which are p-type conductors at high temperature under normal oxygen pressure. This reaction has also been discussed by a number of authors in a book edited by Wolff [137] and in a review by Martin and Mirodatos [138] who concentrate on the surface chemistry in the oxidative coupling of methane.

In this reaction an important problem is to find catalysts or modes of operation of reactors making it possible to obtain high selectivities at high methane conversions. At low methane conversion very high selectivities to C_2-products of up to 97% have been obtained. However, because ethane and ethene are much more reactive towards oxygen than methane, these are oxidised preferentially at high methane conversions, leading to total combustion and decreasing C_2-selectivities (see, e.g. [139,140]) at these higher conversions, in many cases leading to decreased yields. The application of alternative reactor designs, e.g., using membrane or electrochemical reactors are discussed later (see Section 9). In the following sections in particular the influence of catalyst composition and type on the course of this reaction is discussed in more detail.

Another type of process is the formation of synthesis gas, i.e. $CO+H_2$ by partial oxidation of methane as

discussed, e.g., by Lercher et al. [141]. Finally there are some other processes which could be lumped together as selective oxidation of methane and in these the formation of products like methanol and formaldehyde are studied.

8.1.1. Lithium/magnesium oxide based catalysts

In this reaction Driscoll et al. [142] suggested already in 1985 that there are strong indications that surface O^--ions are responsible for hydrogen abstraction from CH_4 by Li/MgO catalysts and that these are present in the form of $[Li^+O^-]$ centres. Ito et al. [143] and Wang and Lunsford [144] confirmed these conclusions and presented further data. The formation of these centres and the energies involved in their creation has been discussed already in Section 5.5. Similarly Lin et al. [145] found that in the oxidative dimerisation of methane over sodium-promoted calcium oxide $[Na^+O^-]$ centres perform the same role as the $[Li^+O^-]$ centres in the lithium-promoted magnesium oxide catalysts. These centres are proposed to be the active sites for hydrogen abstraction from CH_4 under the formation of a methyl radical

$$CH_4 + O_O^\bullet \rightarrow {}^\bullet CH_3 + (OH)_O^\bullet \quad (22)$$

where the Kröger–Vink formulation has been used and, in order to prevent confusion with the Kröger–Vink indication of the effective positive charge, the dot indicating a free radical has been placed on the left-hand side of the corresponding formula. The $^\bullet CH_3$-radicals dimerise in the gas phase to form C_2H_6, which is further oxidised to C_2H_4. The formation of carbon oxides (the non-selective pathway) in the presence of gaseous O_2 is suggested to be formed by a gas phase free radical reaction, starting with the formation of $^\bullet CH_3O_2$ radicals which then react further to CO and CO_2. At higher temperature the equilibrium of the $^\bullet CH_3O_2$ formation reaction lies more to the left so that the selectivity increases with temperature.

Aside from the oxygen exchange measurements of [126,127] mentioned in Section 7, these authors also investigated isotope exchange phenomena during reaction of the oxide with methane. Typical results of oxygen transient measurements during the reaction methane on a Li/MgO catalyst are shown in Fig. 21.

Similarly carbon transients, obtained by switching from $^{12}CH_4$ to $^{13}CH_4$ are shown in Fig. 22.

The transient curves for $C^{16}O_2$, $C^{16}O^{18}O$ and $C^{18}O_2$ as shown in Fig. 21C indicate that along the oxygen pathway of the reaction CO_2 remains long enough on the surface to lead to statistical mixing of the oxygen isotopes. The surface residence times obtained from the transient measurements show that the surface serves not only to generate methyl radicals with subsequent reaction of the radicals in the gas phase, but that the surface lifetimes of the intermediates are clearly different and also that readsorption, in particular of CO_2, but also of CO, takes place. In fact these data show that sites along the carbon pathway involved in the formation of C_2H_6, the selective pathway of the reaction, have a lower activity than those involved in the non-selective formation of CO and CO_2.

These results also show unequivocally that oxygen transport through the oxide has a significant contribution to the CH_4 oxidation reaction. Also the fact that CO lags the CO_2-transient indicates the presence of a multi-step surface oxidation pathway.

Lunsford et al. [146] using in situ Raman spectroscopy observed the presence of peroxide ions on Ba/MgO catalysts. This supports the calculations by Islam et al. [60] presented in Section 5.4. In the presence of CO_2 the O_2^{2-}-ions react to form surface carbonates at temperatures above 500°C, which is in agreement with the poisoning effect of CO_2 in the catalytic experiments.

Anshits et al. [147] and Kondratenko et al. [148] ascribe the activity of the Li/MgO and also of Li/Bi_2O_3 catalysts mainly to the presence of impurities, in particular Fe^{3+}-ions. However, they also indicate that the sum of the oxygen defects: $[M^+O^-]$, O_3^- and CO_2^- is equal to the amount of Fe^{3+}. In view of the large amount of evidence obtained in the other investigations referred to here, it nevertheless seems that the activity is mainly due to the oxygen defects and that the impurities only play a subsidiary role. An interesting observation of [148] is that the use of N_2O as oxidant leads to less total oxidation. The authors suggest this to be due to the smaller oxidising power of N_2O so that the further oxidation of the C_2-products is decreased strongly.

Recently Goto and Aika [149] investigated the reaction between methane and $O_O^\bullet$-ions formed by reaction with N_2O on MgO. Using FT-IR spectroscopy they observed the formation of methoxide-ions and

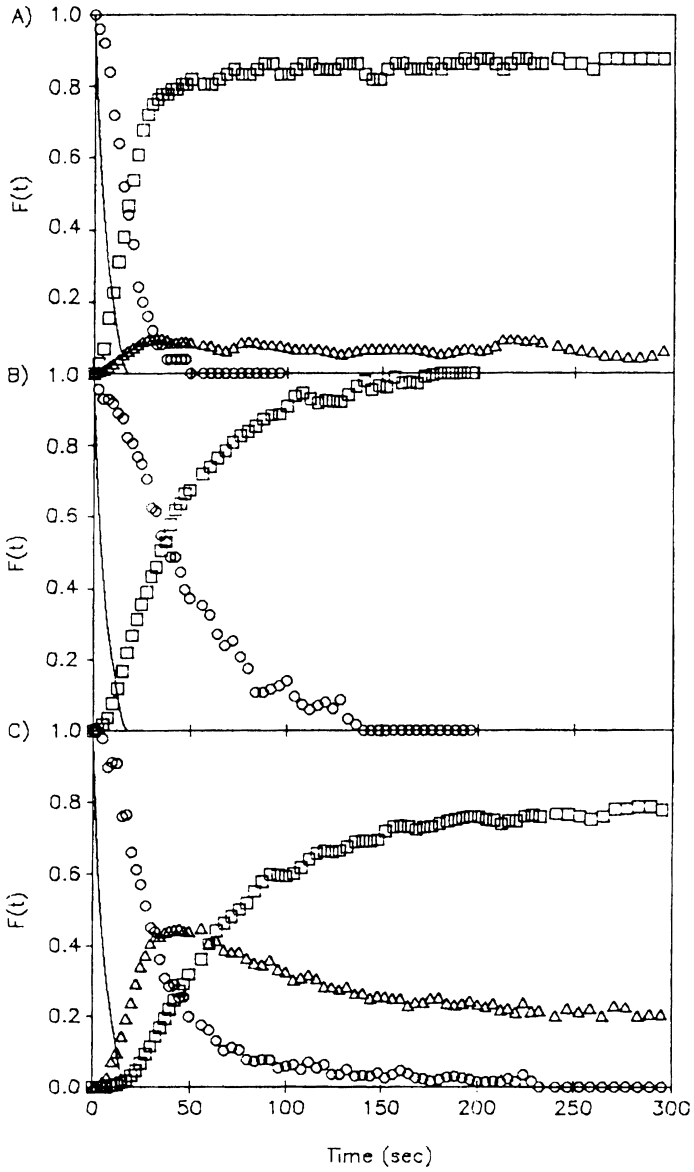

Fig. 21. Molecular oxygen transients during reaction with methane at 645°C over 32.6 mg Li/MgO. (A) O_2-transients, (B) CO-transients, (C) CO_2-transients (reproduced from Fig. 3 of [127], copyright 1991, with permission from Academic Press).

of methanol by reaction with CH_4 at 298 K. The authors propose that the methoxide-ions are formed from the methyl radicals, formed by reaction (22), by the reaction (written here in the Kröger–Vink notation)

$$^{\bullet}CH_3 + O_O{}^{x} \rightarrow OCH_3' + h^{\bullet} \quad (23)$$

The formation of methanol can then occur through one of the following reactions:

$$^{\bullet}CH_3 + OH_O{}^{\bullet} \rightarrow CH_3OH + h^{\bullet} \quad (24)$$

or

$$OCH_3' + OH_O{}^{\bullet} \rightarrow CH_3OH + O_O{}^{x} \quad (25)$$

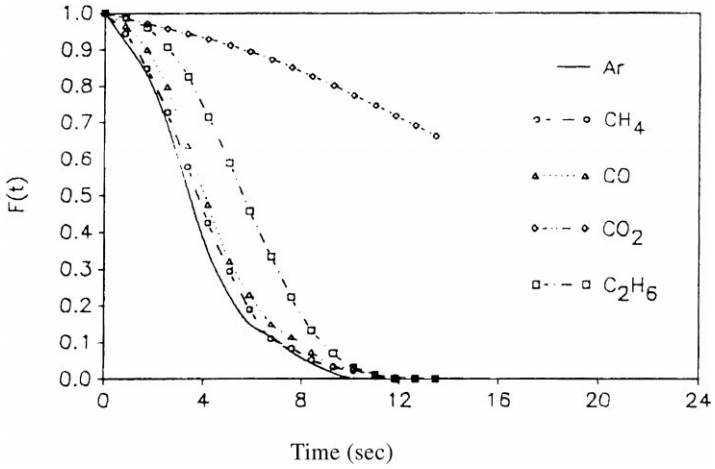

Fig. 22. Carbon transients over 32.6 mg Li/MgO at 645°C (reproduced from Fig. 6 of [127], copyright 1991, with permission from Academic Press).

Desorption of the methanol or methoxide-ions at 773 K leads to their decomposition to CO and H_2.

The effect of SnO_2 addition to Li/MgO was investigated by Nagaoka et al. [150]. The methane conversion increased continuously with the tin content, but the C_2-selectivity showed a sharp maximum of 42% at about 1 mol% Sn, compared with 28% for undoped Li/MgO. This is shown in Fig. 23.

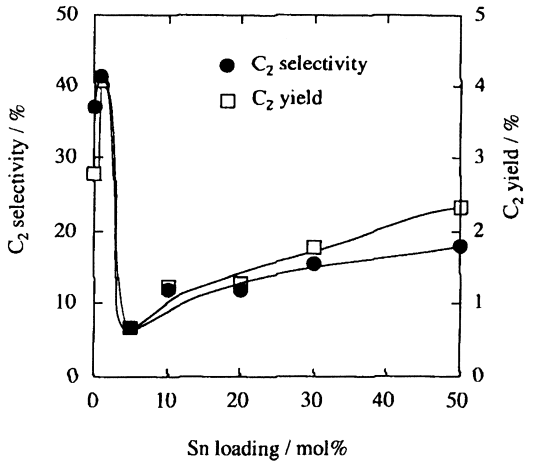

Fig. 23. Dependence of C_2-selectivity and C_2-yield on tin loading of Sn_x–Li/MgO catalysts at 923 K (reproduced from Fig. 2 of [150], copyright 1993, with permission from Academic Press).

From XPS measurements it followed that the concentration of O^- ($O_O^\bullet$) increases up to 1 mol% Sn but decreases again for higher tin contents. The authors propose that for low tin contents the concentration of the active species $[Li^+O^-]=[Li'_{Mg}O_O^\bullet]$ is increased, but that at higher tin contents these are destroyed by reaction with tin leading to the sharp decrease in C_2-selectivity. The relatively small increase in C_2-selectivity above about 5 mol% Sn is ascribed by the authors to the redox cycle Sn^{4+}–Sn^{2+} with participation of O^{2-} ions of a complex tin-containing oxide.

Korf et al. [151] and McNamara et al. [152,153] published a series of papers concerning the influence of dopants on the behaviour of Li/MgO catalysts, but did not try to interpret the results in terms of the defect chemistry and the influence of the dopants thereon.

8.1.2. Lanthanide oxide catalysts

The selective oxidation over doped and undoped rare earth oxides was studied by Korf et al. [154] and Ross et al. [155] who compared Li/MgO, Sm_2O_3 and La_2O_3 catalysts, but did not connect the results with the defect chemistry of the catalysts.

Borchert and Baerns [156] have studied the effect of doping of La_2O_3 with various metal ions (Sr^{2+}, Zn^{2+}, Ti^{4+} and Nb^{5+}) on the C_2-selectivity. Doping with the lower-valent ions caused an increase in the oxygen ion conductivity, corresponding with an increase in

oxygen vacancy concentration, while the higher-valent ions have the opposite effect. Increasing the oxygen partial pressure leads to an increase in the total conductivity due to increasing p-type conductivity, which is explained by the reaction of oxygen with the oxygen vacancies according to the reaction mentioned earlier:

$$V_O^{\bullet\bullet} + \tfrac{1}{2}O_2 \rightarrow O_O^{x} + 2h^{\bullet} \quad (26)$$

The C_2-selectivity is significantly increased by doping of La_2O_3 with Sr^{2+} and Zn^{2+}, while doping with Ti^{4+} and Nb^{5+} leads to a decrease in C_2-selectivity and these effects are thus correlated with the oxygen ion conductivity. The authors suggest that the positive effect of increasing oxygen ion conductivity is due to the corresponding increase in oxygen vacancy concentration which favours the adsorption of gaseous oxygen and its transformation into lattice oxygen, which is also correlated with the increase of p-type conductivity due to the increase in hole concentration according to Eq. (26). As a consequence the surface concentration of weakly adsorbed oxygen species, which are responsible for the non-selective oxidation reactions is decreased with increased Sr^{2+}-content. Doping with Sr^{2+} shows a maximum C_2-selectivity at about 1 at.% Sr^{2+} while the oxygen ion conductivity increases up to 3 at.% Sr^{2+}. The discrepancy between these two effects is explained by segregation of Sr^{2+} to the surface of the La_2O_3 eventually leading to a SrO-like outer layer. The small decrease in selectivity above 1 at.% Sr^{2+} is proposed to be due to the decrease in surface concentration of oxygen vacancies, leading to a slight increase in weakly adsorbed oxygen species.

A similar investigation, now of the influence of doping of Nd_2O_3 with SrO has been reported by Gayko et al. [125]. In Section 3.3 their results of the increase of the conductivity upon doping were already discussed and attention was paid to their measurements of oxygen exchange in Section 7. In this investigation also the contact potential difference (CPD) between the catalyst surface and a reference electrode was measured as a function of the oxygen partial pressure and the temperature. Just as in the investigation of La_2O_3 discussed above, the C_2-selectivity is at all temperatures and oxygen conversions significantly higher for the 1 at.% Sr^{2+}-doped Nd_2O_3 meaning that the consecutive oxidation of C_2-products is diminished by doping with Sr^{2+}. When the catalysts are submitted to successive increases of the partial oxygen pressure the CPD

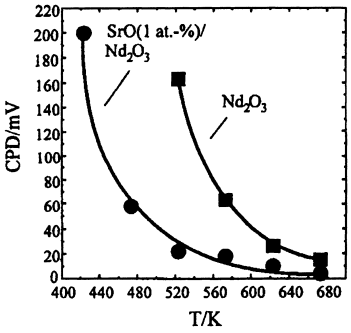

Fig. 24. Comparison of change in CPD as a function of temperature for Nd_2O_3 and 1% SrO/Nd_2O_3 for a change in oxygen partial pressure from 1.0×10^{-3} to 2.0×10^{-3} Pa (reproduced from Fig. 6 of [125], copyright 1998, with permission from Academic Press).

increases stepwise and this increase is much smaller for the Sr^{2+}-doped Nd_2O_3 than for the undoped material as shown in Fig. 24.

When the adsorption equilibrium can be represented by the equation

$$O_{2,g} \Leftrightarrow \frac{2}{m}O_{m,ads}{}^{n-} + \frac{2n}{m}h^{\bullet} \quad (27)$$

then the contact potential difference is given by

$$\mathrm{CPD} = \frac{2n}{m}\frac{RT}{F}\ln(p_{O_2}) + \mathrm{const.} \quad (28)$$

In Table 11 some experimental results of Gayko et al. [125] are given and it is clear that the value of $2n/m$ is significantly smaller for the Sr^{2+}-doped Nd_2O_3. This means that the average charge of the adsorbed oxygen species increases with doping and also with temperature. The interpretation suggested by the authors is that originally adsorbed, neutral oxygen molecules are successively transformed to $O_3{}^-$,

Table 11
Value of $2n/m$ for Nd_2O_3 and 1 at.% SrO/Nd_2O_3 as a function of temperature (taken from Gayko et al. [125])

T (K)	$(2n/m)$ Nd_2O_3	$(2n/m)$ 1 at.% SrO/Nd_2O_3
473	–	1.1±0.36
523	0.31±0.01[a], 0.22±0.01[b]	4.97±0.1[a], 1.52±0.05[b]
573	0.62±0.04[c]	1.91±0.12
623	1.26±0.09[b]	3.08±0.08

[a] 2.0×10^{-4} Pa$<p_{O_2}<1.0\times10^{-3}$ Pa.
[b] $p_{O_2}\geq1.0\times10^{-3}$ Pa.
[c] $p_{O_2}\geq5.0\times10^{-4}$ Pa.

O_2^-, O_2^{2-}, O^- and O^{2-}. Doping with Sr^{2+} shifts the equilibrium between these oxygen species towards the right.

Even though the CPD measurements were performed under reduced pressure the authors suggest that also under reaction conditions weakly bound oxygen species are transformed much faster into lattice oxygen for doped than for pure Nd_2O_3. This explains the increase of the C_2-selectivity upon doping because then the surface concentration of oxygen surface species responsible for total oxidation is decreased.

Computational modelling of this type of reaction by Islam et al. [60] is discussed in Section 5.4. A discussion about the relation between oxygen exchange on these types of catalyst has been presented in Section 7.

LeVan et al. [157] suggest that the favourable influence of SrO on the C_2-selectivity of La_2O_3 is caused by the thermostabilisation of the platelet morphology of La_2O_3, which means that it can be used at higher temperatures, where the selectivity is higher, than without SrO. But no clear explanation is given of the reason why this type of morphology is more favourable. Although it is certainly possible that the morphological influence also contributes to the better performance of La_2O_3, the experimental evidence put forward in [125,156] strongly supports the idea that the main influence of doping with SrO is due to solid state effects and not to the morphology of the catalyst.

An investigation of the oxygen species present on the surface of La_2O_3/CaO has been reported by Yang et al. [158]. EPR measurements of oxygen adsorbed on this catalyst showed the presence of O_2^--ions which desorb on heating in vacuum to 472 K. Adsorption of CO_2 at room temperature leads to the formation of unidentate carbonate ions as shown by IR spectroscopy. When CO_2 and O_2 are co-adsorbed a weaker O_2^{2-} EPR signal is observed. When CO_2 is adsorbed first the adsorption of O_2 as O_2^- is completely inhibited. As it is probably that O_2 adsorbs on oxygen vacancies at the surface this means that CO_2 is not only adsorbed on lattice oxygen ions, but also on oxygen vacancies. Admitting oxygen to the catalyst, outgassed at 1053 K, at the same temperature showed after quenching the presence of O_2^- also. When at 1053 K a methane–oxygen mixture was admitted to the catalyst after adsorbing oxygen at that temperature this led to the gradual disappearance of the O_2^- EPR signal as detected upon quenching after increasing time intervals. Although the presence of O_2^--ions at high temperature on the catalyst surface could not be excluded the authors state that these ions might also be the precursor of, e.g., O_2^{2-}- or O^--ions as the active species for the oxidative coupling of methane.

A special case of oxidative coupling of methane is given by the study of [159] on oxidative coupling with CO_2 on La_2O_3/ZnO catalysts. This was observed to have a high C_2-selectivity of about 90%, much higher than on La_2O_3 or ZnO separately, and also much higher than on Y_2O_3/ZnO and Sm_2O_3/ZnO. The authors suggest a mechanism where a reactive oxygen surface species produces methyl radicals and from methane producing an oxygen-deficient site on the surface. Reoxidation of these oxygen-deficient sites then occurs through reaction with CO_2, using the Kröger–Vink notation the reaction equations then read

$$2CH_4 + 2O_O^{\bullet} \rightarrow 2^{\bullet}CH_3 + 2(OH)_O^{\bullet} \quad (29)$$

$$2(OH)_O^{\bullet} \rightarrow O_O{}^{x} + H_2O(gas) + V_O^{\bullet\bullet} \quad (30)$$

$$V_O^{\bullet\bullet} + 2CO_2(gas) \rightarrow 2O_O^{\bullet} + 2CO(gas) \quad (31)$$

However, it is not clear what the roles of the La_2O_3 and the ZnO in the combined catalyst are and how these oxides co-operate to produce the high C_2-selectivity. Also the difference between the combination of ZnO with the different lanthanide oxides remains unexplained.

Buyevskaya et al. [129] studied oxygen exchange in the presence of methane over Sm_2O_3, Sm_2O_3/MgO and MgO. The presence of methane led to a strong decrease of the amounts of $^{18}O^{16}O$ and $^{16}O_2$ both for exchange on Sm_2O_3 and on Sm_2O_3/MgO. Only when methane is pulsed simultaneously with or after oxygen oxidation, products of methane are formed. This probably means that adsorbed methane species have too short a lifetime so that they already have disappeared when oxygen is pulsed after methane. It also means that oxygen species are consumed faster by reaction with methane than they can recombine. The conclusion is that the activation of oxygen is faster than that of methane. With larger amounts of oxygen present on the surface, i.e. with larger oxygen pulses, the product distribution shift from C_2-hydrocarbons and CO to CO_2, i.e. to a smaller C_2-selectivity. Two possible explanations are presented by the authors: (1) at higher surface concentrations of oxygen the probability of a methane reacting with two or more oxygen

sites leading to total oxidation is higher; (2) at higher surface concentrations of oxygen another type of oxygen species is formed which is more weakly bound to the surface and favours the non-selective oxidation of methane. On the basis of the available experimental data it is not possible to choose between these possibilities.

Yu et al. [160] studied the gas phase oxidation of ethene in the oxidative conversion of methane over CaO (C), La_2O_3/CaO (LC) and SrO–La_2O_3/CaO (SLC) catalysts. The C_2-yield increases in the order C<LC<SLC, in agreement with other results discussed earlier. As the authors expected the ethene oxidation to have a significant influence on the C_2-selectivity this reaction was studied separately. They observed that the gas phase oxidation of ethene is inhibited by these catalysts, compared with that in the absence of a catalyst, in the order C<LC<SLC. It is proposed that this order is related to the increase of the basicity in this series and that the improvement in C_2-selectivity with increasing basicity of the methane coupling reaction is more due to the decrease in ethene oxidation than to an improvement in the methane activation. The chemistry of the inhibition, which is probably connected with chain-carrier trapping by the solid catalyst, has not yet been elucidated.

Lacombe et al. [161,162] performed a detailed study of the mechanism of the oxidative coupling of methane on lanthana catalysts using a variety of transient kinetic techniques including steady-state isotopic transient kinetics (SSITK), a temporal analysis of products (TAP) reactor and steady-state isotopic exchange reactions. For the detailed results of the different experiments we refer to the original papers. Some of the most important conclusions are: (1) basic sites associated with oxygen vacancies dissociate oxygen molecules, forming active species able to activate methane molecules; (2) on localised low-co-ordinate oxygen atoms methyl radicals are adsorbed forming methoxide radical which are then oxidised further to CO_2. This is thus essentially different from the gas phase oxidation proposed by Lin et al. [145] in the case of Li/MgO catalysts, which also implicitly assumed by Yu et al. [160]. These co-ordinatively unsaturated oxygen atoms are similar to the oxygen atoms marked 1 in Fig. 6 and the differing numbers of lattice steps on the outside of the lanthana crystals, due to different thermal treatment, explain the structure sensitivity of the oxidative coupling reaction. The authors also propose a detailed mechanism of the total reaction. This starts (using the Kröger–Vink notation instead of the non-standard notation used by Lacombe et al.) with the activation of oxygen according to

$$\tfrac{1}{2}O_2 + \{O_O{}^x + V_O{}^{\bullet\bullet}\} \rightarrow 2O_O{}^{\bullet} \quad (32)$$

which is followed by the activation of methane forming methyl radicals:

$$CH_4 + O_O{}^{\bullet} \rightarrow {}^{\bullet}CH_3 + (OH)_O{}^{\bullet} \quad (33)$$

The methyl radicals can either associate to ethane or react further with co-ordinatively unsaturated oxygen, denoted by $O_{CUS}{}^x$, at the steps on the surface

$${}^{\bullet}CH_3 + \{O_{CUS}{}^x + V_O{}^{\bullet\bullet}\} \rightarrow ({}^{\bullet}CH_3O)_O{}^{\bullet} + V_O{}^{\bullet} \quad (34)$$

or

$${}^{\bullet}CH_3 + O_{CUS}{}^x + h^{\bullet} \rightarrow ({}^{\bullet}CH_3O)_O{}^{\bullet}$$

where in the second reaction it has been supposed that La_2O_3 is a p-type semi-conductor. The further oxidation then proceeds following the reactions:

$$({}^{\bullet}CH_3O)_O{}^{\bullet} + 4O_O{}^{\bullet} \rightarrow (CO_3)_O{}^x + (OH)_O{}^{\bullet} + (H_2O)_O{}^{\bullet\bullet} + 2V_O{}^{\bullet} \quad (35)$$

$$(CO_3)_O{}^x \rightarrow CO_2(g) + O_O{}^x$$

$$(H_2O)_O{}^{\bullet\bullet} \rightarrow H_2O(g) + V_O{}^{\bullet\bullet}$$

$$2(OH)_O{}^{\bullet} \rightarrow H_2O(g) + V_O{}^{\bullet\bullet} + O_O{}^x$$

Finally the singly charged oxygen vacancies can also react with oxygen to give the active oxygen species

$$\tfrac{1}{2}O_2 + V_O{}^{\bullet} \rightarrow O_O{}^{\bullet} \quad (36)$$

thus closing the complete catalytic cycle both for the selective and the non-selective oxidation of the methane. Of course some of the oxygen vacancies have to be formed on the co-ordinatively unsaturated sites, but this has not been indicated in these reaction equations.

8.1.3. Other oxide systems

Lin and Zeng [163] performed an investigation of the perovskites $La_{0.2}Sr_{0.8}CoO_3$ (LSC) and $SrCo_{0.8}Fe_{0.2}O_3$ as (SCF) catalysts for the oxidative

coupling of methane and compared their catalytic behaviour with that of 5 wt.% Li/MgO. The main conclusions are that both LSC and Li/MgO are good catalysts with a good C_2-selectivity, but that SCF is less useful. An important point for the use of these materials in membrane reactors is that the permeation rate of oxygen must be high enough to prevent too far reduction of the perovskite on the methane side, which leads to a decreased C_2-selectivity as shown by pulse experiments.

Zeng and Lin [164,165] studied the properties of yttria-doped bismuth oxide with the δ-Bi_2O_3 fluorite structure as catalyst for the oxidative methane coupling reaction. When this oxide is brought into contact with methane at high temperatures the methane is initially oxidised with a C_2-selectivity of at least 90%. If this oxide is subsequently reoxidised with oxygen this can be repeated indefinitely. After a contact time of more than about 5 min the reduction of the oxide goes too far and reoxidation to obtain the fluorite structure is not possible any more. According to the authors this means that this material is suitable for use as a membrane, where continuous reoxidation takes place by an oxygen flux through the oxide from the oxygen-rich to the methane-rich side. These authors also studied methane coupling by comparing 30 mol% Y_2O_3 doped Bi_2O_3 with 5 wt.% Li/MgO. The C_2-yield and C_2-selectivity were similar but the space–time yield was much larger for the bismuth-oxide catalyst. The sharp increase of C_2-selectivity and -yield at temperatures above about 800°C is in agreement with the strong increase in ionic conductivity around this temperature. The main effect of yttrium is increasing the activity, while bismuth improves the C_2-selectivity.

Oxidative coupling of methane over CaO–CeO_2 catalysts was studied by Zhang and Baerns [166]. With increasing doping of CeO_2 with CaO the concentration of oxygen vacancies and thus of the oxygen ion conductivity increases strongly through the substitution reaction where Ca^{2+}-ions are placed on Ce^{4+}-sites under formation of Ca''_{Ce}-ions, with charge compensation by oxygen vacancies. As shown in Fig. 25 there is a close parallel between the C_2-selectivity and the conductivity of the CaO–CeO_2 solid solutions, which show a solubility limit close to 25% CaO. Although this does not directly prove the intrinsic connection between oxygen ion conductivity or oxygen vacancy concentration with the C_2-selectivity, it is highly probable that the more reactive adsorbed oxygen species which are responsible for non-selective oxidation of methane are more rapidly converted into lattice oxygen, which is supposed to be responsible for the selective oxidation, when the concentration of oxygen vacancies and/or when the oxygen ion mobility is increased.

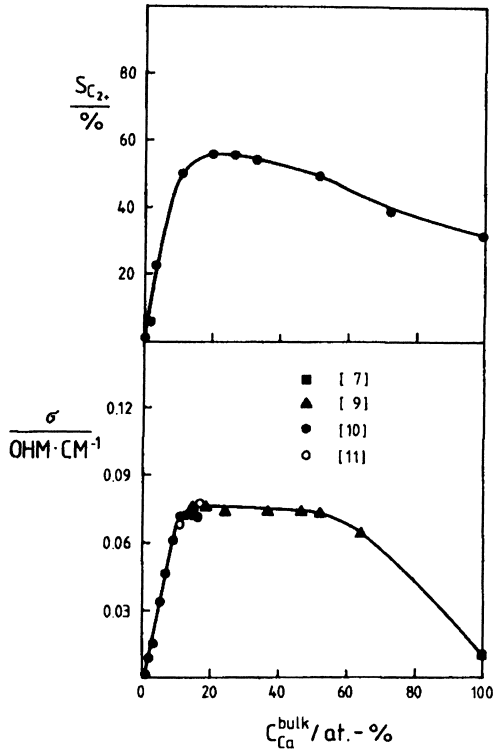

Fig. 25. Dependence of C_2-selectivity and oxygen ion conductivity on Ca-content of CaO–CeO_2 catalysts, reaction conditions: T=1013 K, p_{O_2} = 7 kPa, p_{tot}=0.1 MPa, p_{CH_4} = 93 kPa (reproduced from Fig. 1 of [166], copyright 1992, with permission from Academic Press).

Lehmann and Baerns [167] performed kinetic studies of the oxidative coupling of methane over a NaOH/MgO catalyst. The first order in methane of the reaction rate is in agreement with the formation of methyl radicals from methane is one of the rate determining steps, as found by several other authors mentioned above. The formation of carbon oxides is thought to be due to weakly adsorbed, electrophilic forms of oxygen. The dissociative adsorption of oxygen to the active form needed for the

proton-abstraction is proposed to be responsible for the half order found in the oxygen partial pressure. Although no details of the defects involved are given, the general trend is that the same types of defects are responsible as found for other oxide systems, but with some differences in detail which could not yet be resolved.

On the basis of their classification of oxides suitable for the oxidative coupling of methane mentioned earlier [136] Dubois et al. [168] performed an investigation of thoria based catalysts as ThO_2 is a well-known p-type conducting oxide. By doping with alkaline earth metals and lanthanum they obtained active and selective catalysts. By using these dopants which have a charge lower than thorium oxygen vacancies are introduced leading to an increased activity. Also the existence of stable carbonates of most of these dopants is proposed to increase the selectivity, in agreement with their previous suggestion (see Section 4 and [59]), by lowering the surface concentration of the superoxide ion.

Using steady-state tracing kinetic analysis Efstathiou et al. [169] studied the oxidative coupling of methane over Li^+-doped TiO_2. It was concluded that the amount of reversibly adsorbed methane on this catalyst at 800°C was nearly immeasurable, but there was a large amount of carbon-containing species which probably mainly consist of lithium carbonate. From the transient kinetic results it is concluded further that the steady-state coverage of carbon-containing intermediate species, which are responsible for CO_2 formation, are derived from methane and that the C_2-hydrocarbons only contribute little to the rate of CO_2 formation in the steady-state.

8.2. Partial oxidation of methane to synthesis gas and oxygen containing products

Tsang et al. [170] recently presented a review of the conversion of methane to synthesis gas in which they considered methane steam reforming

$$CH_4 + H_2O \rightarrow CO + 3H_2 \quad (37)$$

dry reforming of methane with carbon dioxide

$$CH_4 + CO_2 \rightarrow 2CO + 2H_2 \quad (38)$$

and partial oxidation of methane with air or oxygen:

$$CH_4 + \tfrac{1}{2}O_2 \rightarrow CO + 2H_2 \quad (39)$$

of which the first two are strongly endothermic, while the third is exothermic. Referring to Hickmann and Schmidt [171] and Hickmann et al. [172], Tsang et al. pointed out that the direct partial oxidation route could be performed over metal coated monolith catalysts under adiabatic conditions at short residence times, but no oxide catalysts were mentioned for this reaction. Indirect dry reforming of methane with CeO_2 as catalyst was described by Otsuka [173]. In this two step reaction CeO_2 is first reduced with methane under the formation of synthesis gas, followed by reoxidation of the reduced catalyst with CO_2.

Steghuis et al. [174] and Steghuis [175] investigated the partial oxidation of methane to C_1-products using titania and yttria/zirconia catalysts. Although the authors mainly concentrated their investigation to selectivity, activity and product analysis, one of their conclusions is that the active site for the catalytic reaction is $O_{(s)}^-$. This can probably also be written as $O_{(s)}^\bullet$ pointing to the involvement of oxygen defects in this reaction too. Further work is needed to find a closer connection with the defect properties of the used catalysts.

As pointed out by Sokolovskii et al. [176] it is difficult to obtain formaldehyde or methanol with high yields by partial oxidation of methane. On the usual catalysts the selectivity is low because total oxidation takes place. These authors proposed the use of special modes of reactor operation but did not mention the influence of the properties of the catalyst itself.

8.3. Methane combustion

Saracco et al. [177] studied methane combustion on Mg-doped $LaCrO_3$ perovskite catalysts. Magnesium oxide, formed as a separate phase during the synthesis of the catalysts, has a favourable influence because it decreases the rate of sintering of the perovskite at high temperatures. But the magnesium present in the perovskite structure also leads to a significant increase of the catalytic activity. This is ascribed to the formation of active sites for the hydrogen abstraction from methane, which is supposed to be the rate determining step in the oxidation process. The authors

propose that magnesium, is present on the chromium site of the perovskite as Mg'_{Cr} which is accompanied by charge compensation by an increase in the charge of the chromium ions, which are then present as $Cr_{Cr}^{\bullet}$. Because the Mg^{2+}-ion is larger than the Cr^{3+}-ion and $Cr_{Cr}^{\bullet}$ smaller this explains the absence of any change in the lattice parameter with increasing magnesium content. But it cannot be excluded that part of the charge compensation can also occur via formation of oxygen vacancies. It is proposed that the increase in the catalytic activity is explained by higher oxygen-reactivity near the $Cr_{Cr}^{\bullet}$-defects, leading to the formation of Cr_{Cr}^{x} and an oxygen vacancy. Fresh oxygen adsorbs on the generated oxygen vacancies, restoring the original situation. The kinetics suggest that, at least with doping percentages above 20 dissociative oxygen adsorption plays an important role. Because the values of the heats of adsorption and of the activation energies are practically unchanged after doping the increase in the reaction rate is proposed to be due to an increase in the number of active sites and thus in a larger pre-exponential factor, rather than in an increase in the activity of the separate sites.

Similar conclusions were drawn by Marchetti and Forni [178] for perovskites of the form $La_{1-x}A_xMnO_3$ with A=Sr (x=0.2, 0.4), Eu (x=0.1) and Ce (x=0.1). $LaMnO_3$ is non-stoichiometric with part of the Mn^{3+}-ions oxidised to Mn^{4+} and charge compensation by the presence of metal ion vacancies. This means that substituting La^{3+} with a bivalent metal (Sr, Eu) leads to a decrease of the metal ion vacancy concentration (and perhaps even to the formation of oxygen vacancies) while the reverse occurs for doping with a fourvalent metal (Ce). They observe that the catalysts most active for oxygen exchange at low temperature, e.g., with x_{Sr}=0.4, are least active for methane combustion at higher temperatures. This indicates that the activation of methane is the most difficult step which becomes easier when more oxygen is available which is the case when there is an oxygen excess in the compound, i.e. with increasing amount of metal ion vacancies, e.g., due to doping with Ce.

Ferri and Forni [179] perovskites of the form $La_{1-x}A_xBO_3$ with A=Sr (x=0.0, 0.2, 0.4), Eu (x=0.1) and Ce (x=0.1) for B=Co and A=Sr (x=0.0, 0.2) for B=Ni and Fe. $LaCoO_3$ has oxygen vacancies and Co^{4+}-ions as majority defects. Substitution with a bivalent metal (Sr, Eu) increases, but with a fourvalent metal (Ce) decreases the concentration of oxygen vacancies, so that the effect on the methane combustion activity is just the opposite as for $LaMnO_3$.

A different oxide which has been considered for methane combustion, a.o. by Kundakovic and Flytzani-Stephanopoulos [180] is ceria. This oxide has active sites for methane oxidation, but sintering leads to loss of activity. Doping with oxides of metals such as La and Zr causes a decrease of crystal size and prevents sintering at high temperatures and at the same time increases both the surface and bulk reducibility, both effects leading to higher methane oxidation activity. The doping with La^{3+} moreover introduces extra oxygen vacancies which further increases the catalytic activity. The addition of transition metals like Ag and Cu leads to a further improvement by an increase of the reducibility and a larger oxygen uptake. Unfortunately details of the interaction between ceria and the transition metals are not given.

Barium hexaferrite $BaFe_{12}O_{19}$ in which 1 and 5 wt.% iridium was introduced was studied by Favre et al. [181]. The parent compound is an efficient methane combustion catalyst, but its properties remain nearly unchanged with iridium-doping, even though the high activity of iridium was expected to lead to an increase of the activity. However, the iridium is probably located inside the spinel blocks of the hexaferrite structure and is thus not easily accessible to the gas phase. Furthermore the substitution of iron by iridium appears to be very limited, probably due to the difficulty of charge compensation of the Ir^{4+}-ions.

Cho et al. [182] investigated La–Cr–O catalysts for the combustion of methane. Their catalysts consisted of a mixture of the perovskites $LaCrO_3$ and $LaCr_{1.01}O_{3-\delta}$ and the catalytic activity was ascribed to oxygen-deficient sites, but these were neither further identified, nor was it clear which of the two components was the active one.

Unfortunately, in the papers discussed in this section, although the contribution of (surface) defects is mentioned, the correlation between catalytic behaviour and the defect structure is not really worked out.

8.4. Selective oxidation and ammoxidation of hydrocarbons

Recently the advances and some future trends in selective oxidation and ammoxidation of hydrocarbons have been reviewed by Grasselli [183]. Apart from kinetic investigations the main emphasis of the study of the catalysts, which are usually multi-metal oxides often containing vanadium or molybdenum as one of the active constituents, has been on the structure of the catalysts and its relation with the reaction mechanism. The selective oxidation can occur either with insertion of oxygen, such as in the formation of acrolein from propane, or without insertion oxidation, i.e. the case of oxidative dehydrogenation, e.g., the formation of *iso*-butene from *iso*-butane.

Important contributions to the structural approach use the "crystallochemical model of active sites" introduced by Ziolkowski and used in many publications. For example the oxidation of butane and butene on different faces of $(VO)_2P_2O_7$ has been treated in [184,185]. Courtine and Bordes [186] reviewed much of the work performed in this field and state in conclusion that, although a classification of monophasic or multi-phasic selective oxidation catalysts is starting to emerge a full understanding of the surface and interfacial phenomena occurring in catalytic oxidation reactions is not yet available. An extensive review of the surface reactivity of oxides based on these principles has recently been given by Bordes [187]. The conclusion that in particular the (1 0 0) plane of $(VO)_2P_2O_7$ is important for the selective oxidation of butane to maleic anhydride is supported by a recent report of [188]. They show that the properties of the catalyst are highly influenced by the way the catalyst is prepared. The best catalysts are obtained with a precipitation technique in which catalysts with a high crystalline disorder are prepared such that they consist of very thin plates, mainly consisting of the (1 0 0) plane.

The structure of the vanadium phosphate catalyst $(VO)_2P_2O_7$ for butane oxidation was investigated by Nguyen et al. [189]. These authors showed that in this catalyst, depending on the way of preparation, extended defects which can be modelled as stacking faults perpendicular to the *a* and *c* axes are present. One of these defects can explain the presence of some V^{5+} in the material and this was confirmed by titration and ^{31}P NMR experiments. These defects are most prominent in samples prepared to be optimum catalysts for the oxidation of *n*-butane to maleic anhydride. These results also give an explanation for the influence of the method of preparation on the catalytic properties of these vanadyl-phosphate catalysts.

However, even if the structural requirements are certainly important other factors clearly also play a great role. For the oxidation of *n*-butane on VPO catalysts this has been shown, e.g., by Zhang-Lin et al. [190,191] who conclude that this reaction implies the participation of a limited number of superficial layers of the catalyst and that it depends strongly on the redox properties of V^{5+}-ensembles on the $(VO)_2P_2O_7$ matrix. In particular the V^{5+}/V^{4+} redox couple is very important.

Védrine et al. [192,193] show that many oxidation reactions in heterogeneous catalysis show a Mars–van Krevelen mechanism. As this includes activation of the molecule to be oxidised by a metal ion, insertion of oxygen from the lattice and the transfer of one or more electrons this means that both acid–base and redox properties of the catalyst are important. It also means that the requirements on the catalyst depend on the type of molecule to be oxidised: normal or *iso*-alkane, alkene, aromatic hydrocarbon, etc. But the type of oxidation leads to different requirements too, e.g., in the differences between oxidative dehydrogenation, oxidative coupling and reactions in which oxygenated products are formed. A very important point, which is often overlooked, is their conclusion that oxidation catalysis must be viewed as a dynamic process in which different partial reactions may have very different time constants as stated, e.g., by Mirodatos [194].

An interesting observation concerning the selective oxidation of *n*-butane, but-1-ene and but-1,3-diene with $(VO)_2P_2O_7$ as catalyst was reported by Taufiq-Yap et al. [195,196]. In an investigation of the selective oxidation of these compounds temperature programmed desorption (TPD) and anaerobic temperature programmed oxidation (TPO) were applied. In the TPD experiments an oxygen evolution peak was observed with a shoulder at 998 K and a maximum at 1020 K. Selective oxidation of all substrates occurred at 965–990 K and the total amount of oxygen reacting was equal to that evolved in TPD. This shows that, for a not yet elucidated reason, the oxygen evolving from the catalyst is uniquely selective in the oxidation

of butane and butenes. When CO is submitted to TPO it shows three oxidation peaks of which the low temperature one coincides with the selective oxidation peak of butane and the butenes. It is proposed that the oxygen involved in the higher temperature oxidation peaks either has a larger activation energy of diffusion through the lattice or for the CO/O(surf) reaction and that this explains the high selectivity of the butane to maleic anhydride oxidation. As the reaction is industrially carried out at much lower temperatures the selective pathway, due to its lower activation energy, is favoured over the non-selective pathway. It is also suggested that the oxygen evolution occurs by the formation of extended defects, producing glide planes on the surface as shown by high resolution electron microscopy by Gai and Kourtakis [197], which might also be the same as those mentioned by Nguyen et al. [189]. This is one of the few examples of the study of a non-steady-state use of a catalyst.

In the ammoxidation reaction a hydrocarbon is oxidised in the presence of ammonia:

$$C_nH_{2n+2} + NH_3 + \tfrac{3}{2}O_2 \rightarrow C_{n-1}H_{2n-1}CN + 3H_2O \quad (40)$$

written for the case of a saturated alkane with nitrile as product, but similar reactions occur for aromatic hydrocarbons, e.g., toluene giving benzonitrile.

Andersson et al. [198] studied this reaction for propane and toluene using vanadium antimonate catalysts with Sb:V ratios of 1–5. They observed that vanadium sites are responsible both for the activation of the hydrocarbon and for the insertion of nitrogen, but that the antimony performs no specific role in the catalytic reaction. Free vanadia on the surface of the catalyst promotes the conversion of ammonia to nitrogen, which causes a decrease in the selectivity of the nitrile formation, due to the smaller amount of available ammonia. This is in particular the case for propane because the ammoxidation of propane needs a higher temperature (500°C) than that of toluene (370°C). At larger Sb:V ratios the amount of free vanadia on the surface is diminished and thus an increased selectivity results.

Nilsson et al. [199,200] studied propane ammoxidation with Al–Sb–V-oxides as catalyst and the results support those of Andersson et al. [198]. They propose the active site to be of the type sketched in Fig. 26.

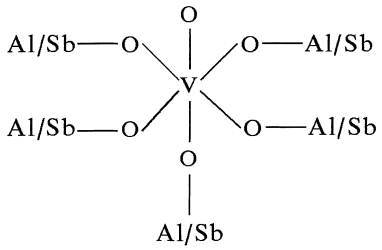

Fig. 26. Active site in Al–Sb–V-oxide catalyst (reproduced from Scheme 1 of [199], copyright 1996, with permission from Academic Press).

These results form an example of the validity of the site isolation theory originally proposed by Callahan and Grasselli [201].

Partial oxidation of *iso*-butane to methacrolein and ammoxidation to methacrylonitrile over bismuth–molybdate catalysts with Nb_2O_5 has been studied by Matsuura et al. [202]. These authors propose that the reaction starts with the abstraction of a hydrogen atom form *iso*-butane, under formation of an *iso*-butyl radical by an O^--ion which is formed on Nb_2O_5 by thermal activation:

$$Nb_{Nb}{}^{x} + O_O{}^{x} \rightarrow Nb'_{Nb} + O_O{}^{\bullet} \quad (41)$$

$$C_4H_{10} + O_O{}^{\bullet} \rightarrow {}^{\bullet}C_4H_9 + (OH)_O{}^{\bullet}$$

This radical is subsequently transformed to an *iso*-butoxide ion on the bismuth–molybdate surface using an electron trapped at an oxide vacancy on the surface

$${}^{\bullet}C_4H_9 + V_O{}^{\bullet} + O_O{}^{x} \rightarrow (OC_4H_9)_{ads}{}^{-} + V_O{}^{\bullet\bullet} \quad (42)$$

where evidently the *iso*-butoxide ion occupies an oxygen site at the surface. However, it might well be that the *iso*-butoxide ion is formed by reaction of the radical with a lattice oxygen, analogous to the ideas of Lacombe et al. [161,162] as shown in the second Eq. (34)

$${}^{\bullet}C_4H_9 + O_O{}^{x} + h^{\bullet} \rightarrow ({}^{\bullet}C_4H_9O)_O{}^{\bullet} \quad (43)$$

where the plus one effective charge of course corresponds with a real charge of minus one.

As the two reactions occur on different phases the course of the regeneration of the catalyst is not quite

clear. A reaction which might occur on the Nb_2O_5 particles might be

$$Nb'_{Nb} + 2(OH)_O^{\bullet} \rightarrow Nb_{Nb}{}^{x} + O_O^{\bullet} + H_2O(gas) \quad (44)$$

Unfortunately the authors, even if they indicate the involvement of defects, do not present any further considerations concerning details of the defect structure of the two catalyst components.

The *iso*-butoxide formed in reaction (42) reacts further under the formation of methacrolein and some *iso*-butene, while the methacrolein reacts further with ammonia and oxygen on the bismuth–molybdate catalyst to methacrylonitrile

$$\begin{aligned} CH_2 &= C(CH_3)CHO + NH_3 + \tfrac{1}{2}O_2 \\ &\rightarrow CH_2{=}C(CH)_3C{\equiv}N + 2H_2O \end{aligned} \quad (45)$$

The oxydehydrogenation of propane over Mg–V–Sb-oxide catalysts has been studied by Michaels et al. [203,204]. These authors conclude that the selective oxidative dehydrogenation of propane to propene and the formation of CO and CO_2 are at least partly parallel reactions, the first being zero order in oxygen and the second being half order. This means that the selective oxidation is probably by reaction with lattice oxygen, while the total oxidation occurs with the participation of dissociatively adsorbed oxygen. The experimental evidence suggests that V–O radicals are responsible for the activation of propane. If these centres are structurally isolated from each other, e.g., in an antimony matrix they are selective for partial oxidation to propene. However, if there are adjacent active sites these react with the adsorbed hydrocarbon and lead to total oxidation. This indicates, in agreement with the experimental results, that lowering the vanadium content improves the selectivity by reducing the number of neighbouring vanadium sites.

Agaskar et al. [205] have investigated *n*-butane oxidation to maleic anhydride over vanadyl pyrophosphate. In this case, aside from the structural features which are similar to the previously discussed reactions in this section, a crucial feature is the occurrence of a "pseudo-ozonide" species formed by the interaction of adsorbed oxygen molecules with an adjacent metal-oxo group. It would be very interesting indeed if computational modelling would be applied to the different surface states considered in this model in order to confirm the present speculations based on the kinetic features of this reaction.

An interesting proposal to use perovskite-type chloro-oxides with the formula $SrFeO_{3-\delta}Cl_{\sigma}$ for the oxidative dehydrogenation was done by Dai et al. [206]. The idea was to influence the defect concentrations, in particular the oxygen vacancy concentration by the doping with chlorine, which simultaneously leads to a change in the Fe^{4+}/Fe^{3+}-ratio. The central point of the idea is that the chlorine-ions are inserted into oxygen vacancies. Unfortunately, however, the composition of their chlorine-containing catalyst $SrFeO_{3-0.382}Cl_{0.443}$ is not in agreement with the proposed model. The defect formation equation reads

$$\begin{aligned} \text{“}SrFeO_3\text{”} + \frac{\sigma}{2}Cl_2 \rightarrow \text{“}SrFeO_{3-\delta-\sigma}Cl_{\sigma}\text{”} + \frac{\delta}{2}O_2 \\ + \delta V_O^{\bullet\bullet} + \sigma Cl_O^{\bullet} + (2\delta + \sigma)Fe'_{Fe} \end{aligned} \quad (46)$$

where for clarity the oxygen missing due to the formation of oxygen vacancies and that due to doping with chlorine have been indicated separately. The concentrations have to be calculated using the electroneutrality condition

$$2[V_O^{\bullet\bullet}] + [Cl_O^{\bullet}] = [Fe'_{Fe}] \quad (47)$$

and the site conservation condition

$$[O_O{}^{x}] + [V_O^{\bullet\bullet}] + [Cl_O^{\bullet}] = 3 \quad (48)$$

showing that $\delta+\sigma \geq \sigma$, i.e. the number of missing oxygen ions must be larger than the number of chlorine-ions inserted, in contrast to the composition given by Dai et al. As the formation of interstitial chlorine-ions is highly improbable there is no direct explanation for the experimentally found composition. This means that the conclusions can unfortunately not be accepted, but it is to be hoped that this line of thinking is pursued further for in principle it is an interesting possibility to influence the defect structure in this way.

Zanthoff and Buchholz [207] investigated the reaction mechanism of the ammoxidation over VSb_xO_y (x=1, 2 and 5) and $(VO)_2P_2O_7$. The insertion of nitrogen is clearly different: short-lived surface forms of adsorbed nitrogen compounds play the main role on the V–Sb–O catalysts, but long-lived NH_x-species participate in the reaction over $(VO)_2P_2O_7$. Furthermore only lattice oxygen plays a role in the oxidation

step over V–Sb–O catalysts whereas adsorbed oxygen lead to total oxidation over $(VO)_2P_2O_7$.

For most of the reactions treated in this section up to this point there have as yet been no studies on the effect of the conducting or defect properties of the catalysts on their catalytic behaviour. Only recently applications of computational modelling studies to these catalysts have been performed by Witko [99].

Sokolovskii et al. [208,209] discussed the selective oxidation and ammoxidation of paraffins. For the formation of unsaturated nitriles, such as acrylonitrile from propane the hydrocarbon activation seems to be the important step which proceeds at rather high temperatures. The activation occurs via heterolytic C–H bond dissociation by interaction with acid–base sites of the catalyst under formation of a carbanion. This releases a hydride ion giving propylene which is subsequently activated on the basic sites of the catalyst forming an allyl-type intermediate, which reacts with oxygen and ammonia giving acrylonitrile. However, for ethane these authors showed that the reaction has to be performed at a relatively low temperature to prevent further oxidation of the, rather unstable, intermediate product acetaldehyde. But lattice oxygen is not active enough at these low temperatures so that adsorbed oxygen species are necessary to activate the hydrocarbon. But these oxygen species are also active for total oxidation, causing rather low selectivities. Unfortunately these authors do not consider the possibility to change the catalyst properties along the lines discussed above (see, e.g., Section 8.1) to improve the hydrocarbon activation rate, without leading to total oxidation.

Al'kaeva et al. [210] explain the non-linearity of the temperature dependence of the formation of acrolein and acrylic acid from propene by the contribution of lattice oxygen mobility to the reoxidation of the catalyst. In order to prevent reaction limitation by reoxidation the bulk oxygen transport must be high enough, which according to the authors is possible by using higher temperatures. The possibility to increase the bulk oxygen transport, e.g., by doping the catalyst is not mentioned.

The oxidative dehydrogenation of propane on vanadium oxide/magnesium oxide (VMgO) catalysts was investigated with a variety of transient kinetic techniques by Pantazadis et al. [51,211,212], Burrows et al. [213] and Creaser et al. [214]. The VMgO catalysts investigated had varying vanadium contents from 0 to 45 wt.% and showed maximum propene yields around 14 wt.% vanadium. This correlates well with the acid–base properties of the catalysts as determined from NH_3 and SO_2 adsorption. Too high basicity but also the absence of basicity favour the unselective route above the selective one, as observed experimentally for low or high vanadium content, respectively. The electrical conductivity of all samples varied with p_{O_2} to the power $1/n$ with values of n ranging from 4 to 6, indicating these materials to be n-type semi-conductors with anionic vacancies. Surprisingly the highest conductivity was found for MgO, which according to expectation should be a nearly perfect insulator. The authors propose as an explanation that the conduction is mainly along the surface due to the presence of hydroxyl- and carbonate-groups. However, this is not fully consistent with the p_{O_2}-dependence and this discrepancy is not explained.

Conductivity measurements of the catalysts showed that under reaction conditions there was a strong increase in conduction which disappeared completely upon exposing the catalyst to oxygen alone. Introducing propane again caused an increase in conduction. The authors propose this to be due to the reduction of V^{5+} to V^{4+} or V^{3+} and formation of anionic vacancies which are needed to accommodate the electrons causing the increased conductivity. However, this conductivity could also be explained as a hopping conductivity between differently charged vanadium ions (small polaron conductivity) without the involvement of vacancies. In fact their reaction scheme can be written, using the Kröger–Vink-notation as

oxidation of propane:

$$C_3H_8(g) + 2V_V^{x} + 2O_O^{x} \rightarrow C_3H_8(g) + 2V_V' + 2(OH)_O^{\bullet} \quad (49)$$

$$2(OH)_O^{\bullet} \rightarrow H_2O(g) + O_O^{x} + V_O^{\bullet\bullet}$$

reoxidation of catalyst:

$$V_O^{\bullet\bullet} + 2V_V' + \tfrac{1}{2}O_2(g) \rightarrow O_O^{x} + 2V_V^{x} \quad (50)$$

and the hopping conductivity can schematically be written, without involving any vacancies, as

$$^1V_V' + {}^2V_V^{x} \rightarrow {}^1V_V^{x} + {}^2V_V' \quad (51)$$

In these equations V_V is of course a vanadium ion on a vanadium site, while V_O represents an oxygen vacancy.

Using a temporal-analysis-of-products (TAP) reactor it was shown that the oxidative dehydrogenation of propane follows a Mars–van Krevelen mechanism with fast oxygen migration through the oxide lattice. Oxygen labelling showed that there was no gaseous oxygen exchange: oxygen can only be consumed irreversibly by reoxidation of the reduced catalyst. An important feature observed was also that a reversible surface reconstruction occurred during the reaction which is assumed to determine the elementary steps of the overall oxidative dehydrogenation process.

8.5. Oxidation and reduction of nitrogen oxides

The reduction of NO_x under lean conditions, i.e. with hydrocarbons and oxygen present using metal oxides has been reported by Bethke et al. [215] and Kung and Kung [216]. In most cases the catalysts contain oxide supported metal particles, but they also find that Li/MgO and in particular La_2O_3 are active catalysts for this process, while at the same time having a good selectivity, meaning that the hydrocarbons are (practically) only oxidised by nitrogen oxides and not by the free O_2 present. In analogy with their activity for oxidative coupling of methane (see Section 8.1) it is suggested that their activity for lean NO_x-reduction is due to their ability to form $^{\bullet}CH_3$-radicals. It would be very interesting to know whether the modification of this type of catalyst, as discussed in Section 8.1 would have similar effects on lean NO_x-reduction as on the oxidative coupling of methane, but no investigations of this type have yet been reported.

9. Membrane processes

9.1. Introduction

Porous oxide membranes, both of non-conducting oxides and of ionic or mixed conducting oxides can be used in ceramic membrane reactors. Fully dense sintered ionic and mixed conducting oxides can also be used as a separating membrane in a ceramic membrane reactor. An important advantage is the possibility of a controlled supply (or removal) of oxygen to (or from) the side where the catalyst and the reactants are located. Another promising feature of this approach is that the oxygen flux may alter the relative amounts of different oxide species (such as O_2 (adsorbed molecule), O (adsorbed neutral atom), O_2^- (superoxide), O_2^{2-} (peroxide), O_3^- (ozonide), O^-, etc.) on the catalyst surface. In this way it is possible to supply species having a strong influence on the selectivity of partial oxidation and oxidative conversion reactions. A special point of interest is also that the oxidising species and the reactants to be converted can be fed to different sides of the membrane. In the latter case the membrane acts as a separation membrane. Oxygen separation by mixed conducting membranes has recently been reviewed by Bouwmeester and Burggraaf [217]. Of course oxides showing proton conduction can also be used as membrane materials. A recent review of the application of proton conducting oxides has been published by Iwahara [218].

Eng and Stoukides [139] reviewed the different ways to work with dense solid electrolyte membranes onto which porous electrodes are attached on both surfaces. This is shown schematically in Fig. 27.

Solid oxide potentiometry is a valuable technique enabling, among others, continuous measurement of the (thermodynamic) activity of oxygen on the surface of a catalyst, which is present as a layer on the membrane. In conjunction with kinetic measurements it can be used to study the mechanism of catalytic reactions on metals, but also on oxides [219]. See also the reviews by Vayenas [220] and Stoukides [221].

A general review of present experience with and future opportunities of catalytic inorganic membrane reactors has recently been presented by Saracco and Specchia [222]. They treat the membranes and their properties themselves, the reactor systems in which they can be used and also engineering and operating issues of membrane reactors.

In the next two parts of this section the different types of membrane and of the type of operation are treated separately.

9.2. Porous membranes

Lafarga et al. [223] studied the application of porous ceramic membrane reactors to the oxidative

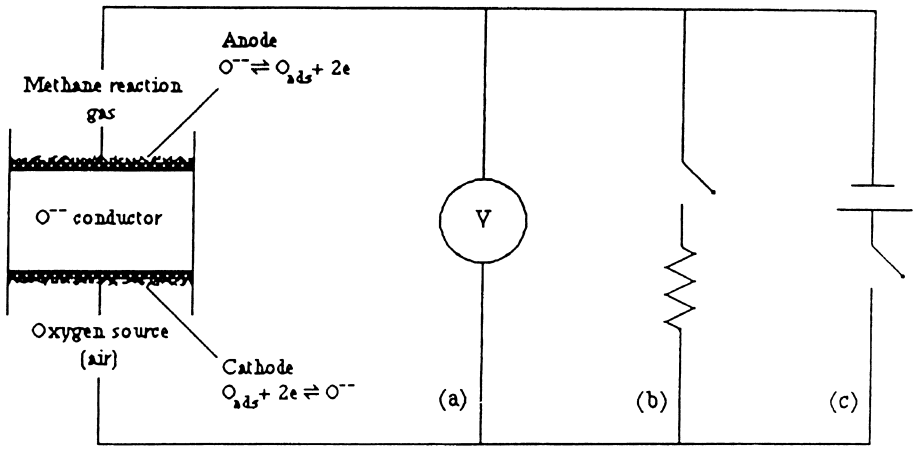

Fig. 27. Schematic diagram of solid electrolyte membrane cell with applications: (a) open-circuit solid electrolyte potentiometry; (b) solid oxide fuel cell; (c) electrochemical oxygen pump (reproduced from Fig. 1 of [139], copyright 1991, with permission from Marcel Dekker).

coupling of methane. These have as one advantage over dense membranes that higher oxygen fluxes can usually be obtained. By modifying alumina microfiltration membranes by partial plugging of the pores with silica these authors were able to lower the oxygen permeation flux sufficiently to keep the oxygen partial pressure low enough to optimise the C_2-selectivity. Coronas et al. [224] subsequently studied the reaction aspects of such a membrane reactor. Different reactor set-ups are shown schematically in Fig. 28.

It was found that all types of membrane reactors gave a considerably higher C_2-selectivity, especially at low and moderate methane and oxygen conversions. The selectivity was not as high as expected due to the unfavourable permeation pattern of oxygen: more oxygen permeated near the end of the permeation zone. To obtain a better oxygen distribution along the bed the ceramic membrane must be modified such that the permeability decreases as the reactor exit is approached. Moreover modification of the catalytic properties of

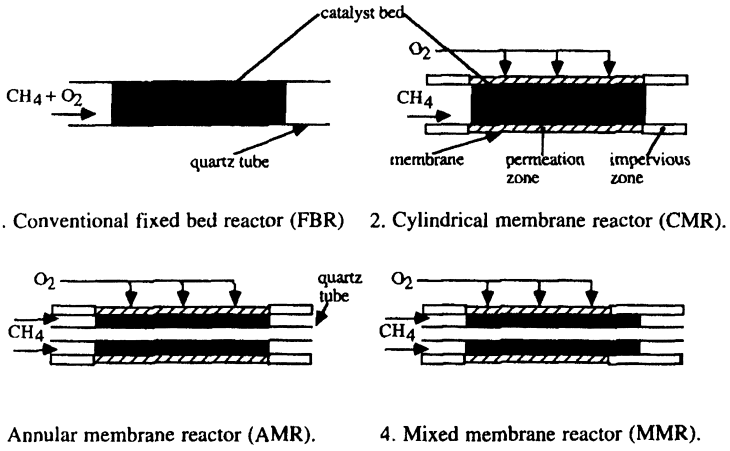

Fig. 28. Scheme of different types of reactor configuration. Hatched=porous membrane, black=Li/MgO catalyst (reproduced from Fig. 1b of [224], copyright 1994 with permission from Elsevier Science).

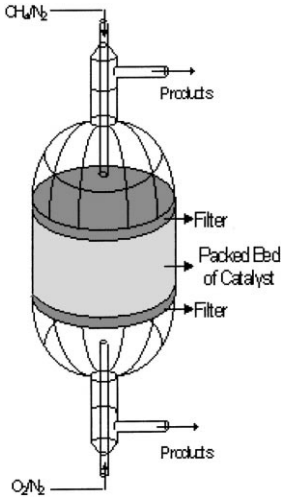

Fig. 29. Schematic cross-section of fixed bed barrier reactor (reproduced with permission from Fig. 6 of Chapter 5 of [225]).

the membrane itself is also highly desirable in order for the membrane to give a positive contribution to the hydrocarbon yield.

Neomagus [225] studied porous alumina membranes for use in oxidation reactors. He observed that it was difficult to obtain reproducible and controllable impregnation of the membrane with respect to homogeneity of the catalyst. In the partial oxidation of *iso*-butene it was found that there was an extensive slip of the *iso*-butene through the membrane due to its too low catalytic activity which made it impossible to make use of the attractive mode of operation with separate feed of reactant and oxygen. As an alternative reactor set-up the *fixed bed barrier reactor* as shown in Fig. 29 was used.

This reactor consists of a fixed bed of dried phosphomolybdic acid catalyst particles pressed between two filter disks with feed of the *iso*-butene to one side and oxygen to the other. In agreement with the reaction model for this reactor it was observed that the methacrolein selectivity increased with an increase of the pressure difference over the bed. Similarly such a reactor was also applied to the partial oxidation of methane to synthesis gas and the results were compared with those obtained for a conventional fixed bed reactor, both using a Pt on γ-Al_2O_3 catalyst. The selectivity was higher for the barrier reactor and also (initially) increased with the pressure difference over the fixed bed in the barrier reactor.

9.3. Dense membranes

9.3.1. Introduction

We must here distinguish between membranes where oxygen ions (or vacancies) and those where protons or hydroxyl-groups are the majority moving atomic species. Besides ionic conduction these compounds may also be electron or electron hole conductors so that we then have mixed conducting membranes. In the next section the membranes with oxygen ion conduction or mixed oxygen ion and electron conduction are discussed, followed by a section considering proton or proton and electron mixed conduction. An interesting group of materials which have been proposed for use as membranes is based on $Bi_4V_2O_{11}$ doped with different metals such as Cu, Ni, Co and Zn and studied by Abraham et al. [226], Abraham and co-workers [227], Boivin et al. [228] and Boivin and Mairesse [229]. These materials are collectively designated as BIMEVOX materials and have very high oxygen conductivity, which is appreciable even at temperatures as low as 400–500°C. As far as could be ascertained these compounds have not yet been studied as oxidation catalysts, but it seems probable that they have very interesting possibilities in that field also.

9.3.2. Oxygen ion conducting membranes

A review of methane oxidation with solid oxide membranes showing oxygen ion conduction has been recently been published by Eng and Stoukides [139].

Early experiments on the oxidative coupling of methane using membrane reactors were described by Nozaki et al. [230,231]. In the first paper the use of lead oxide, modified by alkali-metal additions, was used as membrane. In the second paper thin membranes of doped Bi_2O_3 on porous supports are described which showed good C_2-selectivity but at rather low yields. Dense membranes of doped zirconia, covered with a PbO/K_2O layer gave reasonable C_2-yields for calcium- and magnesium-doped zirconia where the rate was limited by oxygen transport through the membrane, while on yttrium-doped zirconia the rate was limited by the surface reaction on the catalyst layer. Dense membranes of $CaCo_{0.8}Fe_{0.2}O_3$ and

$SrCe_{0.95}Yb_{0.05}O_3$ gave much smaller C_2-selectivities, which could be improved by the application of a PbO/K_2O layer.

Oxygen transport through $La_{1-x}Sr_xFeO_{3-\delta}$ membranes, with x between 0.1 and 0.4, has been studied by ten Elshof et al. [232,233], first in air/He gradients and subsequently in air/CO,CO_2 gradients. In air/He gradients the oxygen flux could be described by bulk diffusion-limited permeation behaviour. However, in air/CO,CO_2 gradients a different behaviour was observed. Here the oxygen fluxes were linearly dependent on the CO partial pressure and on the strontium content. This led to the conclusion that now the oxygen flux is limited by the surface reaction. Two models, one based on an Eley–Rideal mechanism, the second based on a Langmuir–Hinshelwood mechanism, both lead to a kinetic expression which agrees with the experimental results. In both models the oxygen vacancies, present at the surface, play a definite role, in agreement with the dependence of the flux on the strontium content.

In another investigation ten Elshof et al. [234] studied the oxidative coupling of methane in a membrane reactor with a mixed conducting perovskite membrane having the composition: $La_{0.6}Sr_{0.4}Co_{0.8}Fe_{0.2}O_3$. With partial oxygen pressures between 0.01 and 1 bar at the high oxygen side of the membrane and helium as sweep gas at the permeate side it was found that the flux is close to $1\,mmol\,m^{-2}\,s^{-1}$ at 1173 K. The activation energy of the oxygen permeation was 130–140 $kJ\,mol^{-1}$. The oxygen flux was limited by a surface process at the permeate side of the membrane. When methane was added to the helium at the permeate side the oxygen flux was only slightly increased. Methane was converted to ethane and ethene with selectivities up to 70%, but at low conversions of only about 1–3%. The authors conclude that it is important for methane coupling purposes that the oxygen flux is limited by surface exchange kinetics, because otherwise reduction of the membrane surface would occur which would cause a decrease of C_2-selectivity. Also substantial improvement of methane conversion and C_2-selectivity is expected by modifying the surface of the membrane, e.g., by applying methane coupling catalysts such as Li/MgO or Sr/La_2O_3.

Hibino et al. [235] studied oxidative coupling of methane in a membrane reactor with $BaCe_{0.8}Gd_{0.2}O_{3-\delta}$, which is a mixed oxide ion–electron hole conductor. In the oxidative coupling experiments one side of the membrane was in contact with methane (10% in Ar), the other side with different amounts of O_2, also mixed with Ar. The effect of the p_{O_2} on the rates of formation of the different products are shown in Fig. 30.

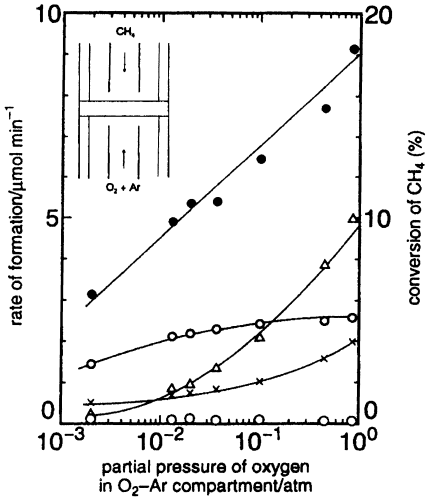

Fig. 30. Effect of oxygen partial pressure in O_2–Ar mixture on formation rates and conversion of methane at 1173 K: ○: C_2H_4, O: C_2H_6, Δ: CO, ×: CO_2, ●: CH_4-conversion (reproduced from Fig. 3 of [235], copyright 1997, with permission from the Royal Society of Chemistry).

In this way reasonable conversions of methane could be obtained with much higher selectivities than when the methane and oxygen were fed to the same side of the membrane (co-feed mode). This shows that the oxygen species released from the membrane at the CH_4-side is more active for C_2-formation than gaseous oxygen or oxygen adsorbed directly from the gas phase. However, it was not possible in this study to identify unequivocally the exact type of oxygen species responsible for the better results of the methane coupling.

In separate experiments a number of $BaCe_{1-x}Gd_xO_{3-\delta}$-powders were also tested as catalysts for the oxidative coupling of methane and some results are shown in Fig. 31.

Maximum selectivity for C_2H_4 was observed at 20% Gd, and at that point the CO_2-selectivity had a minimum. The activity and selectivity of this material correlated well with the conductivity as a

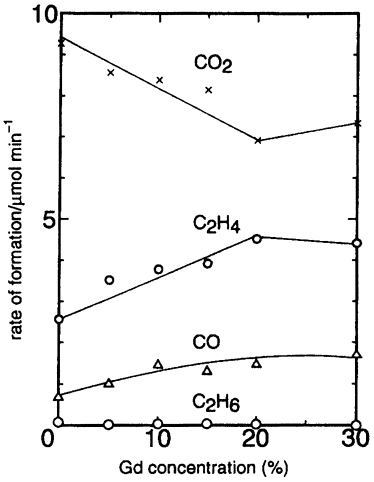

Fig. 31. Rates of formation of oxidation products of methane over $BaCe_{1-x}Gd_xO_{3-\delta}$-powders at 1173 K as a function of Gd^{3+}-content (reproduced from Fig. 7 of [235], copyright 1995, with permission from the Royal Society of Chemistry).

function of Gd-content. C_2H_6 was not formed at all. It is clear that here also the C_2-selectivity was significantly lower than in the case of the membrane reactor.

Lin et al. [236] developed equations for the transport of oxygen through thin mixed conducting membranes. In these equations both the surface reactions on the membrane–gas interface and the diffusion of the different charged species in the solid are taken into account. In general the results obtained in this way are complex, implicit equations correlating the oxygen permeation flux to the driving force, the membrane thickness and the rate constants of all separate steps. For special cases it is possible to derive simpler equations. An analysis of the oxidative coupling of methane in a dense oxide membrane reactor was performed by Wang and Lin [237]. Calculations show that using an impervious but highly oxygen permeable ceramic membrane with a surface which is catalytically active for the oxidative coupling reaction gives the possibility to achieve much higher C_2-yields than with a conventional packed bed reactor. The high C_2-yield can only be achieved under conditions such that the oxygen flux, the methane flow rate and the intrinsic reaction rate match each other.

Xu and Thomson [238] investigated oxidative coupling in membrane reactors using an ion-conducting perovskites of the form $La_{1-x}A_xCo_{0.2}FeO_{0.8}O_{3-\delta}$ with x=0.4 (LSCF-4628), 0.6 (LSCF-6428) for A=Sr and x=0.8 for A=Ba (LBCF-2828). The materials with $Sr_{0.6}$ and $Ba_{0.8}$ showed the highest oxygen fluxes and gave C_2-selectivities of about 50% at 1098 K.

At the surface of the membrane on the methane side of the reactor oxygen ions are consumed by two competing reactions

$$2CH_4(g)+O_O{}^x+2h^\bullet \rightarrow 2^\bullet CH_3 + H_2O(g) + V_O{}^{\bullet\bullet} \quad (52)$$

$$2O_O{}^x + 4h^\bullet \rightarrow O_2(g) + 2V_O{}^{\bullet\bullet}$$

or, writing holes as small polarons in the form $O_O{}^\bullet$

$$2CH_4(g) + 2O_O{}^\bullet \rightarrow 2^\bullet CH_3 + H_2O(g) + V_O{}^{\bullet\bullet} + O_O{}^x \quad (53)$$

$$4O_O{}^\bullet \rightarrow O_2(g) + 2O_O{}^x + 2V_O{}^{\bullet\bullet}$$

namely hydrogen abstraction from methane and recombination with formation of molecular oxygen. Because the oxygen formed in the second of these reactions can cause oxidation in the gas phase a high oxygen flux does not necessarily lead to an increase in the C_2-selectivity. The response of the methane coupling reaction to p_{CH_4} is shown in Fig. 32.

The data in Fig. 32a show that in LBCF-2828 and LSCF-4628 the C_2-selectivity is about 50%, thus being much higher than the 18% observed for the same material in a packed bed reactor [239]. The rates of C_2-production were also higher by a factor of 7 than those in the packed bed reactor. Fig. 32c shows that the amount of oxygen formed on the methane side of the membrane reactor decreases strongly with increasing p_{CH_4}. This indicates that oxygen ion recombination, the second reaction of Eq. (52) or Eq. (53), occurs simultaneously with the first reaction. This accounts for the low selectivities at low p_{CH_4}, because then gaseous oxygen is formed causing combustion of C_2-products. The total oxygen flux increases by a factor of 3–5 when nitrogen is replaced by methane on the low oxygen side of the membrane. Thus the oxidative coupling reaction increases the rate of reaction of the oxygen ions arriving at that surface. This indicates that the limiting step is not the diffusion through the membrane, but the surface reactions of Eq. (52) or Eq. (53), in agreement with the conclusions of ten Elshof et al. [232–234]. Increasing the partial pressure

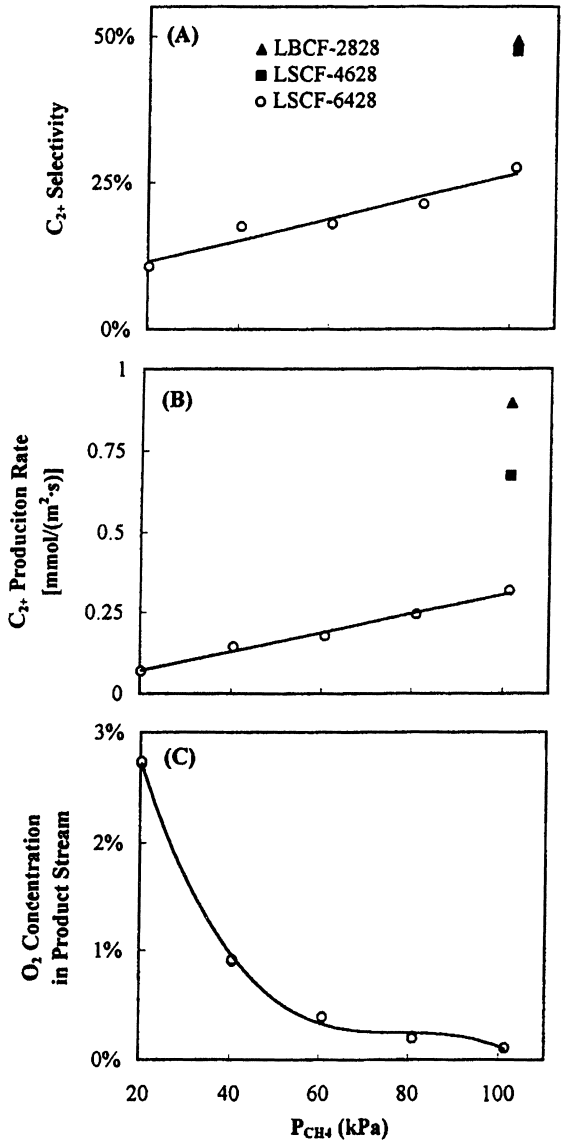

Fig. 32. Effect of p_{CH_4} on methane coupling in a membrane reactor, T=1098 K, p_{O_2}=101 kPa (reproduced from Fig. 3 of [238], copyright 1997, with permission from the American Institute of Chemical Engineers, all rights reserved).

of oxygen at the high oxygen side leads to an increase in the oxygen flux, but the C_2-selectivity remains the same. This means that the oxygen ion recombination rate is too high and competes successfully with the oxidative coupling reaction. Also it can be concluded that for materials of this type to be of practical use the oxidative coupling activity should be increased, without at the same time increasing the oxygen recombination rate.

Membrane reactors have also been studied for the partial oxidation of methane to syngas. Balachandran et al. [240] studied membranes made of a perovskite with the composition $La_{0.2}Sr_{0.8}Fe_{0.6}Co_{0.4}O_{3-\delta}$ in tubular form. On the inside of the tube, the methane side, a rhodium-based reforming catalyst was applied to the surface of the membrane. At 750°C methane conversion (80% CH_4 in Ar, 1 bar) was >98% with a CO-selectivity of about 90% and an hydrogen yield which is about 2 times the CO-yield. As this type of perovskite is a good catalyst for methane combustion, see, e.g., the work by Ferri and Forni mentioned earlier [179], the reaction might proceed in such a way that first total combustion of methane occurs, followed by a reforming reaction leading to syngas, according to the reaction equations:

$$\begin{aligned} &CH_4 + 2O_2 \rightarrow CO_2 + 2H_2O \\ &CH_4 + 3CO_2 \rightarrow 4CO + 2H_2O \\ &\underline{8CH_4 + 8H_2O \rightarrow 8CO + 24H_2} \\ &12CH_4 + 6O_2 \rightarrow 12CO_2 + 24H_2 \end{aligned} \quad (54)$$

where the second and third reactions are catalysed by the rhodium reforming catalyst.

Another interesting group of materials investigated by Balachandran and co-workers [241–244] is based on a composition in the region $Sr_4(Fe_{6-x}Co_x)O_{13+\delta}$, one of which can also be written as $SrFeCo_{0.5}O_x$. These compounds are not simple perovskites because the B/A ratio (when writing a perovskite as ABO_3) is larger than 1. They have a layer structure, consisting of perovskite layers alternating with $(Fe,Co)_2O_{2.5}$ layers. These compounds combine high electronic/ionic conductivity with an appreciable oxygen permeability. Dense membranes of these materials can be used to separate high-purity oxygen from air and also to partially oxidise methane to synthesis gas, without the need for external electrical circuit. The oxidation of methane to synthesis gas using a $SrFeCo_{0.5}O_x$ membrane [245] could be performed at a methane conversion of 99% with a selectivity to CO of higher than 95% and a H_2/CO ratio of nearly 2.

Tsai et al. [246] investigated perovskites of the form $La_{1-x}A_xFe_{0.8}Co_{0.2}O_{3-\delta}$ with A=Ba (x=0.6 and 0.8), A=Ca (x=0.6) and A=Sr (x=0.6). Several configurations were tested and in one of these a 5% Ni on

Al_2O_3 reforming catalyst was packed on top of the membrane. The CH_4 conversion and the oxygen flux increased during the first 500 h of reactor operation. After that time steady values were obtained with a CH_4 conversion of about 80% and a CO-selectivity of nearly 100%. The increase in oxygen flux was proposed to be due to superficial reduction of the perovskite leading to an increased oxygen gradient. After about 500 h a stable membrane structure was obtained giving much better results than the original membrane. Just as in the case mentioned above for the work of [240] here also we might have complete oxidation of CH_4 followed by a reforming reaction.

Azgui et al. [247] studied the oxidative dimerisation of propene, to hexadiene and benzene, using a disk of bismuth oxide-lanthanum oxide $(Bi_2O_3)_{0.85}(La_2O_3)_{0.15}$ catalyst as membrane at a temperature of 500°C. Propene conversions of around 40% and C_6-selectivities of 70–80% were obtained. A study of the used membrane showed the presence of metallic bismuth which means that the oxygen transport through the oxide itself is not sufficient to keep all bismuth in the oxidised state. Furthermore cracks were also observed in the membrane after use. This leads to the conclusion that at least part of the oxygen has diffused through these cracks, but as no oxygen or carbon dioxide were observed on the hydrocarbon side this probably means that on that side the oxygen is incorporated in the oxide as lattice ions and is thus not available for non-selective oxidation.

9.3.3. Proton conducting membranes

Already in 1981 Iwahara et al. [248] discussed the application to steam electrolysis to produce hydrogen gas by sintered oxides based on $SrCeO_3$, which exhibit proton conduction when exposed to a hydrogen containing atmosphere at high temperature. Important advantages mentioned for the use of these materials as the electrolyte in electrochemical reactors were the prevention of dilution of hydrogen with water and the fact that fuel circulation is unnecessary when the reactor is used in the fuel cell mode. On the other hand the current efficiency was below 100% due to the mixed conductivity of these materials and also rather high voltages were needed due to the relatively low conductivity of the membranes. Using $SrCe_{0.95}Yb_{0.05}O_{3-\alpha}$ as a solid membrane Iwahara et al. [249] showed the possibility to use the cell as hydrogen extractor from $CO+H_2O$, steam or ethane. Also pure hydrogen gas could be obtained by steam electrolysis. The energy efficiency was low but was expected to be increased by using a thinner electrolyte tube.

In a later study Iwahara et al. [250] investigated $BaCeO_3$ doped with Nd^{3+}, La^{3+}, Y^{3+} and Ca^{2+}. In particular the neodymium doped material shows a significantly higher proton conduction in wet air than $SrCeO_3$. This material was used as solid electrolyte in a steam electrolyser producing hydrogen and in a hydrogen/air fuel cell. Here again the resistance of the solid electrolyte was the main factor limiting cell performance but it was significantly better than that of the $SrCeO_3$ used in the previous study [248].

Hamakawa et al. [251,252] investigated methane coupling using $SrCe_{0.95}Yb_{0.05}O_{3-\alpha}$ (SCYO) as solid electrolyte in an electrochemical cell. This is in effect a dehydrogenation reaction and because of the absence of O_2, which is responsible for non-selective total oxidation, this may lead to a much better C_2-selectivity than can be obtained with the conventional catalytic processes. A schematic view of the configuration used for these investigations is shown in Fig. 33. When a current is impressed hydrogen is pumped electrochemically from anode to cathode, enhancing the formation of C_2-compounds at the anode. If the electrolyte is not a pure proton conductor but a mixed proton–electron

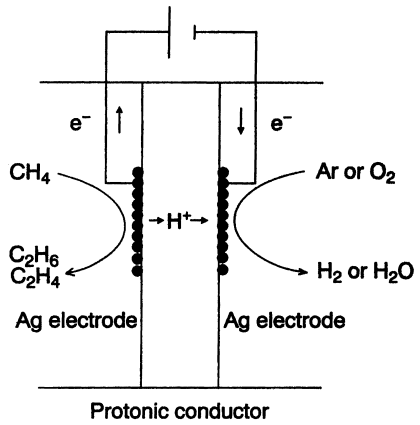

Fig. 33. Two compartment cell for the dehydrogenative dimerisation of CH_4 using Ag-electrodes and $SrCe_{0.95}Yb_{0.05}O_{3-\alpha}$ as a solid electrolyte (reproduced from Fig. 1 of [251], copyright 1993, with permission from the The Electrochemical Society).

hole conductor the cell is self-short-circuited and reaction occurs even without external current.

When on the left side a 1% H_2 in helium gas mixture is introduced and an O_2–Ar mixture on the right-hand side then at very low p_{O_2} hydrogen is evolved on the right-hand side upon passing a current and the amount of hydrogen is proportional to the current. Also the amount of H_2 formed is nearly equal to that calculated from Faraday's law. With increasing p_{O_2} on the right-hand side water is formed instead of hydrogen and the amount is smaller than that corresponding to Faraday's law. This indicates the contribution of electron hole conduction with increasing p_{O_2}. Separate conduction experiments have shown that besides proton conduction electron hole conduction predominates over electron conduction.

The defect equilibria in $SrCe_{0.95}Yb_{0.05}O_{3-\alpha}$ are

$$\tfrac{1}{2}O_2 + V_O^{\bullet\bullet} \rightarrow O_O^{x} + 2h^{\bullet} \quad (55)$$

$$H_2O(g) + V_O^{\bullet\bullet} = 2H^{\bullet} + O_O^{x}$$

or

$$H_2O(g) + O_O^{x} + V_O^{\bullet\bullet} = 2OH_O^{\bullet}$$

These two equilibria are dependent: increasing p_{O_2} shifts reaction (55) to the right, thus diminishing the concentration of oxygen vacancies and increasing the concentration of electron holes. As a consequence the equilibrium reactions (56) shift towards the left. The overall effect is an increase in electron hole and a decrease in proton conduction. Consequently in experiments with a hydrogen containing gas mixture on the left-hand side and oxygen containing gas on the right-hand side water is formed on the right-hand side, even without an externally applied current.

When a CH_4/Ar mixture is introduced on both sides of the cell there is no hydrogen transport and only about 1% conversion of CH_4 to C_2-products is observed, while the stable cell voltage is 0.47 V. When O_2 is admitted on the right-hand side water vapour starts to be developed while the cell voltage decreases to 0.24 V and the rate of formation of C_2-products increase, without the formation of any CO or CO_2. When a current is impressed the rate of formation of C_2-products is increased even more. However, the hydrogen evolution is increased substantially more which is ascribed by the authors to carbon formation at the anode according to:

$$CH_4 \rightarrow C + 2H_2 \quad (57)$$

Chiang et al. [253] also investigated the dehydrogenative dimerisation of methane using proton conducting $SrCe_{0.95}Yb_{0.05}O_{3-\alpha}$ as solid electrolyte. Based on their experimental results they propose that the rate determining step is the formation of a methyl radical by proton-abstraction. In a paper by Marnellos et al. [254] a study of different reactor types for this reaction is presented. The results indicate that in all cases the $SrCe_{0.95}Yb_{0.05}O_{3-\alpha}$-membrane reactors give substantially larger yield than the corresponding conventional catalytic reactors. Experimental results show that the real reactor behaviour is more complicated than indicated by the calculations. But the results clearly show that the equilibrium conversion of a hydro or dehydrogenation reaction can be dramatically changed by using a proton conducting membrane in an electrochemical reactor-cell.

A careful and extensive investigation of oxidative coupling of methane using a high-temperature proton conducting membrane has recently been reported by Langguth et al. [255] who studied the same material SCYO as investigated by Hamakawa et al. [251,252] discussed above and used a cell similar to the one shown in Fig. 33. Even when no oxygen was present, with pure methane on one side and helium on the other side both CO_2 and CO were formed. The authors showed that the first is probably formed from a small, residual impurity of oxygen in the methane. The second is probably formed by a slight reduction of the solid electrolyte. When air was admitted to the opposite side of the methane the conversion changed drastically but the selectivity slowly decreased with time. The latter was ascribed to the presence of significant oxygen ion conduction occurring simultaneously with proton conduction. Furthermore, as also proposed by Hamakawa et al. [251,252], they observed coke formation leading to decreased conversion and C_2-selectivity.

Addition of water to the air side leads to a decrease in CO_2 and CO formation and practically no change in the rate of formation of C_2-products. In particular the former is in agreement with a decrease in oxygen ion conduction due to the decrease in oxygen vacancy concentration by absorption of water. When

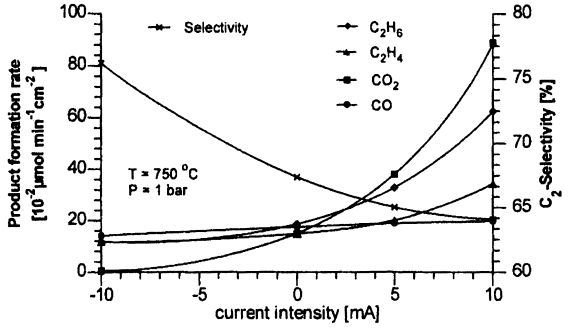

Fig. 34. Effect of external current on the product formation rate and C_2-selectivity in methane coupling in a membrane cell with SCYO as solid electrolyte (reproduced from Fig. 11 of [255], copyright 1997, with permission from Elsevier Science).

water is added to the hydrocarbon side CO formation is considerably increased while CO_2 formation also increases but much less. Simultaneously the formation of C_2-products is suppressed. These results indicate that under these circumstances steam reforming of methane occurs.

Finally some of the experiments were performed using an impressed external current from which pure hydrogen gas could be obtained. In Fig. 34 the effect of the externally applied current is shown.

A positive current corresponds with increased oxygen and proton conduction. It is clear that the increased conduction, as expected, leads to increased reaction rates. But also it is observed that the formation of non-selective products is increased more than that of the C_2-products, leading to a decrease in C_2-selectivity.

This investigation indicates that this complicated system has to be studied further because it is not yet possible to give an unequivocal explanation of all observations. However, it can be stated that under the conditions used in this investigation the SCYO-membrane simultaneously exhibits oxygen ion conduction, proton conduction and electronic conduction, the relative contributions of which depends in different ways on the experimental conditions.

9.3.4. Electrocatalysis: electrically driven membrane reactors

In solid electrolyte electrochemical cells the essential steps all involve electrocatalytic reactions, i.e. reactions with charge transfer to or from an electrode. These take place primarily at the three-phase boundary (tpb) solid electrolyte/electrode/gas phase. Moreover there may also be catalytic reactions, without charge transfer, occurring on the electrode surface exposed to the gas phase. An important feature is the improvement and control of catalytic properties of metals and metal oxides using the effect of non-faradaic electrochemical modification of catalytic activity (NEMCA). For a general review of these types of processes we refer to the survey of this field by Vayenas et al. [256]. For electrolyte cells in which energy generation and conversion of chemical compounds take place simultaneously, see Section 9.3.5 on solid oxide fuel cells in this review.

Eng and Stoukides [257] investigated the methane coupling reaction in a cell with yttria-stabilised zirconia as solid electrolyte and platinum as catalyst/electrodes. They performed both solid electrolyte potentiometry, during reaction and electrochemical oxygen pumping. They conclude that CH_4 is first adsorbed on the platinum where hydrogen abstraction under formation of methyl radicals occurs. The C_2-selectivity reached 15% at 900°C with a C_2-yield of 4%. Electrochemical oxygen pumping had only a very small effect which the authors ascribe to the fact that an important part of the reaction proceeds in the gas phase.

A recent example of an electrocatalytic reaction is the synthesis of ammonia at atmospheric pressure as described by Marnellos and Stoukides [258]. In this case a proton conducting oxide of the strontia–ceria–ytterbia type ($SrCe_{0.95}Yb_{0.05}O_3$) is used. In this way complete conversion of the hydrogen transported through the electrolyte at a rate $I/2F$, where I is the current and F the Faraday, is obtained and in fact this is the limiting step of the reaction. In order to obtain greater amounts of product it is necessary to develop proton conducting solid electrolytes with a higher conductivity than those available at the moment.

9.3.5. Catalysis aspects of solid oxide fuel cells

The study of solid oxide fuel cells, i.e. of fuel cells with a solid compound, usually an oxide, as electrolyte is primarily directed at the generation of electricity and from this point of view are described in a recent review by Hammou and Guindet [259]. However,

they also get attention from investigators who try to combine the generation of electricity with the conversion of the fuel (e.g., methane) into other, more useful and valuable products, such as reviewed by Kuchynka et al. [260]. But in both applications the electrode reactions should have high rates at small overvoltages in order to minimise energy losses. This means that the catalytic properties of the electrodes are extremely important for the development of viable fuel cells. At the anode, where the fuel compound is oxidised, the reactivity should be high and, in the case where the fuel is to be partially oxidised to useful products, it should also show a sufficiently high selectivity for the desired products. At the cathode, where oxygen reduction takes place, only the activity is of interest for which the essential step in most solid oxygen fuel cells is:

$$\tfrac{1}{2}O_2 + 2e^- = O^{2-} \tag{58}$$

Normally each of the three reactants is in one phase: O_2 in the gas phase, electrons in the electrode and oxygen ions in the solid electrolyte. A similar case is hydrogen oxidation at the anode:

$$\tfrac{1}{2}H_2 + O^{2-} = H_2O + 2e^- \tag{59}$$

where H_2 and H_2O are in the gas phase, electrons in the electrode and oxygen ions again in the electrolyte.

When metal or semi-conductor electrodes are used the rate determining step is usually assumed to be the charge transfer at the three-phase-boundary: electrolyte–electrode–gas. This was shown to be the case for hydrogen oxidation at nickel electrodes by de Boer [261]. However when the electrode is an oxide semi-conductor which also shows oxygen ion conduction, such as, e.g., substituted lanthanum–transition metal perovskites, there is another possibility, namely that the reaction (58) also takes place on the surface of the electrode material. Then oxygen absorption and transport in the bulk of the mixed conducting electrode may have an important influence in determining the electrode polarisation.

To investigate this point, the mechanism and kinetics of oxygen reduction on porous $La_{1-x}Sr_xCoO_{3-\delta}$ electrodes has recently been studied by Adler [262]. A schematic cross-section of the electrode model is shown in Fig. 35a. In this model the overall electrode reaction (58) is assumed to occur as a homogeneous

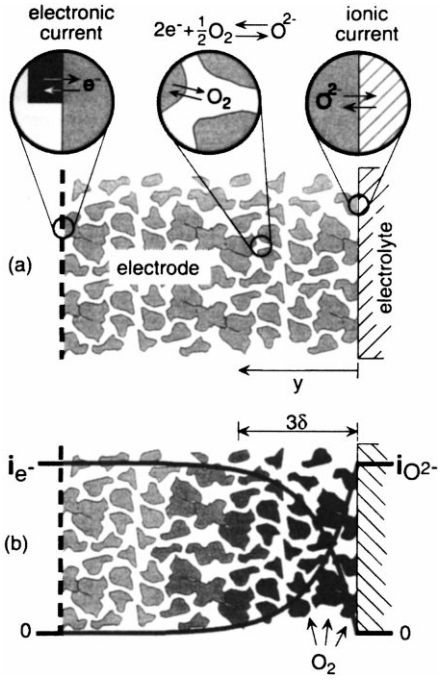

Fig. 35. (a) Schematic of the electrode reaction model; (b) schematic of the steady-state electronic and ionic currents in the mixed conducting electrode (reproduced from Fig. 1 of [262], copyright 1998, with permission from Elsevier Science).

reaction over the internal surface of the electrode. Because of the finite ionic (and electronic) conductivity it is expected that the contribution of absorption of molecular oxygen by the mixed conducting electrode and the conversion of electronic to ionic current occurs over a finite region, with thickness δ, of the electrode as shown schematically in Fig. 35b.

Using this model the characteristic length δ, shown in Fig. 35b, is given by

$$\delta = \sqrt{\frac{c_v D_v (1-\varepsilon)}{r_0(\alpha_f + \alpha_r) a \tau}} \tag{60}$$

where c_v is the vacancy concentration and D_v the vacancy diffusion co-efficient in the electrode material, ε the porosity, a the surface area, τ the tortuosity of the porous electrode, r_0 the exchange neutral flux density, which is proportional to the surface reaction rate of the oxygen reduction and α_f and α_r are the kinetic constants of order 1.

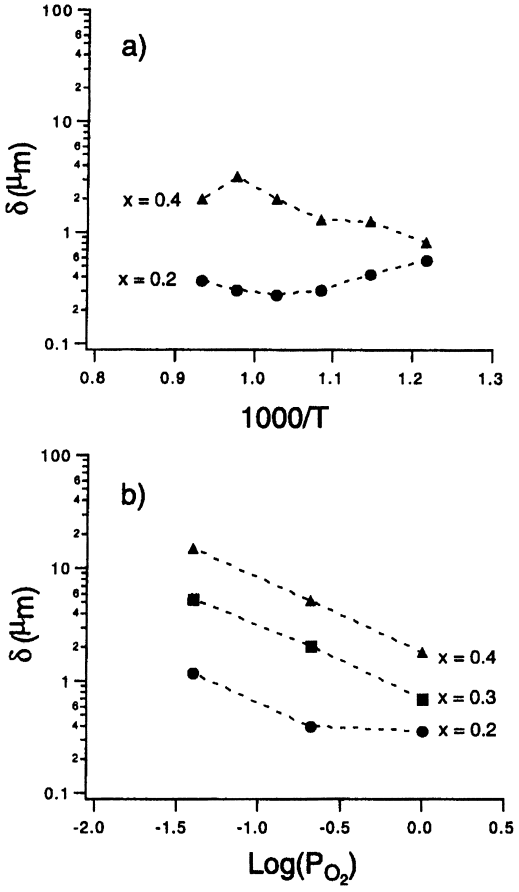

Fig. 36. Size of the active region δ, as a function of x, T and p_{O_2}. Circles, triangles and squares indicate x=0.2, 0.3, 0.4, respectively (reproduced from Fig. 8 of [262], copyright 1998, with permission from Elsevier Science).

On the three types of electrode material with x=0.2, 0.3 and 0.4 both d.c. and a.c. polarisation measurements were performed and the results obtained indicate that O_2-reduction on these materials is limited primarily by surface chemical exchange and solid state diffusion in the electrode material. When the parameters calculated from the polarisation results are substituted into Eq. (58) the thickness δ of the active region can be calculated and the results are shown in Fig. 36.

As expected the size of the active region increases with x and with decreasing p_{O_2}, i.e. with increasing oxygen vacancy concentration in the mixed conducting electrode, in agreement with the prediction of Eq. (58). The thickness of the active region is of the same order of magnitude as the thickness, about 15 μm, of the electrode itself.

10. Concluding remarks

Major advances have been booked in the computational modelling of defect structure and behaviour of catalysts. But this work has mainly been limited to the properties of the catalyst and less to those of the reacting molecules and thus present only half the story. In the field of the reactions considered here the computational study of the reacting molecule in interaction with the catalyst, e.g., using the cluster approach as used by van Santen [92], Ackermann et al. [115], Witko et al. [96] and reviewed recently by Hutchings et al. [263], has hardly begun yet. However, for the further development of this field it is to be hoped that these methods are going to be applied more extensively to the catalytic reactions considered here.

At the moment this work is mainly limited to trying to find explanations for the course of reactions and the influence of the catalyst thereon. Even there only a beginning has been made. As remarked by Courtine and Bordes [186] about selective oxidation catalysts: “a full understanding of the surface and interfacial phenomena occurring in these reactions is not yet straightforward”. The design of catalysts using the ideas presented is just starting, but as yet limited to special systems like zeolites as recently reviewed by Thomas [264].

For many reactions considered here there have as yet been no studies on the effect of the conducting or defect properties of the catalysts on their catalytic behaviour. The number of applications of computational modelling studies is still rather limited. In a number of papers the contribution of (surface) defects is mentioned, but the correlation between catalytic behaviour and the defect structure is not really worked out. As indicated above there is also a need for a better definition of surface structures and surface defects. In fact it is suggested that the Kröger–Vink-notation for bulk defects has to be extended before it is fully applicable to surface defects too. Furthermore much additional work is needed to find a closer connection between the defect properties of the used catalysts and their catalytic properties. Another important point that has not yet had much emphasis is the dynamics of defect

processes and it is to be hoped that the application of transient kinetic techniques, such as used by the group of Mirodatos (see, e.g. [161,162]) is going to become more widespread.

The technological challenges presented by Iwahara [265] for the application of proton conducting ceramics are still valid and are analogously applicable to the use of oxygen conducting membrane materials. Some criteria for the application of high-temperature proton conductors in solid oxygen fuel cell applications have been discussed by Schober et al. [266] and may point to obtaining even better materials than those available now. The possibilities of the application of these very interesting materials seem very promising, e.g., for dehydrogenation reactions by the equilibrium shift possible due to the separation of reactants or products from hydrogen. However, practical applications have not yet been possible and further work is certainly necessary before they are realised.

References

[1] P.J. Gellings, H.J.M. Bouwmeester, Catal. Today 12 (1992) 1–105.
[2] P.J. Gellings, H.J.M. Bouwmeester (Eds.), The CRC Handbook of Solid State Electrochemistry, CRC Press, Boca Raton, 1997.
[3] R.K. Grasselli, J.F. Brazdil (Eds.), Solid State Chemistry in Catalysis, ACS Symposium Series No. 279, American Chemical Society, Washington, DC, 1985.
[4] F.F. Volkenshtein, The Electronic Theory of Catalysis on Semiconductors, Pergamon Press, Oxford, 1963.
[5] K. Hauffe, T. Wolkenstein, Proceedings of the Symposium on Electronic Phenomena in Chemisorption and Catalysis on Semiconductors, Moscow, 1968, Walter de Gruyter, Berlin, 1969.
[6] B. Delmon, Solid State Ionics 101–103 (1997) 655–660.
[7] I. Abrahams, P. Bruce, Solid state background, in: P.J. Gellings, H.J.M. Bouwmeester (Eds.), The CRC Handbook of Solid State Electrochemistry, CRC Press, Boca Raton, 1997, pp. 76–119.
[8] R.W.G. Wyckoff, Crystal Structures, Vol. 2. Inorganic Compounds RX_n, R_nMX_2, R_nMX_3, Interscience, New York, 1964.
[9] P.E. Caro, J. Less Common Met. 16 (1968) 376.
[10] F.A. Kröger, H.J. Vink, Solid State Phys. 3 (1956) 307.
[11] H. Arzoumanian, Oral comment during Fourth Sabatier Conference on Catalysis, Strasbourg, 5–9 July 1999.
[12] H. Iwahara, Solid State Ionics 53–56 (1992) 575.
[13] C.R.A. Catlow, P.S. Baram, S.C. Parker, J. Purton, K.V. Wright, Philos. Trans. Roy. Soc. London A 350 (1995) 265–276.
[14] K.V. Wright, R. Freer, C.R.A. Catlow, Phys. Chem. Minerals 20 (1994) 500–503.
[15] K.V. Wright, C.R.A. Catlow, Phys. Chem. Minerals 20 (1994) 515–518.
[16] K.V. Wright, C.R.A. Catlow, Phys. Chem. Minerals 23 (1996) 38–41.
[17] P.S. Baram, S.C. Parker, Philos. Mag. B 73 (1996) 49–58.
[18] T. Schober, W. Schilling, H. Wenzl, Solid State Ionics 86/88 (1996) 653–658.
[19] G. Brouwer, Philips Res. Rep. 9 (1954) 366.
[20] F.A. Kröger, The Chemistry of Imperfect Crystals, 2nd Edition, North-Holland, Amsterdam, 1974.
[21] D.A. Stevenson, N. Jiang, R.M. Buchanan, F.E.G. Henn, Solid State Ionics 62 (1993) 279–285.
[22] T. Schober, J. Friedrich, J.B. Condon, Solid State Ionics 77 (1995) 175–179.
[23] H. Iwahara, T. Yajima, T. Hibino, K. Ozaki, H. Suzuki, Solid State Ionics 61 (1993) 65–69.
[24] J.A. Labrincha, J.R. Frade, F.M.B. Marques, Solid State Ionics 61 (1993) 71–75.
[25] K.C. Liang, Y. Du, A.S. Nowick, Solid State Ionics 69 (1994) 117–120.
[26] H. Iwahara, H. Uchida, K. Ono, K. Ogaki, J. Electrochem. Soc. 135 (1988) 529–533.
[27] W. Münch, G. Seifert, K.-D. Kreuer, J. Maier, Solid State Ionics 86/88 (1996) 647–652.
[28] Th. Matzke, U. Stimming, Ch. Karmonik, M. Soetramo, R. Hempelmann, F. Güthoff, Solid State Ionics 86/88 (1996) 621–628.
[29] K.-D. Kreuer, Th. Dippel, Yu.M. Baikov, J. Maier, Solid State Ionics 86/88 (1996) 613–620.
[30] F. Krug, T. Schober, T. Springer, Solid State Ionics 81 (1995) 111–118.
[31] F. Freund, H. Wengeler, J. Phys. Chem. Solids 43 (1982) 129–145.
[32] M.S. Islam, M. Cherry, Solid State Ionics 97 (1997) 33–37.
[33] K.D. Kreuer, E. Schönherr, J. Maier, Solid State Ionics 70/71 (1994) 278.
[34] T. Norby, O. Dyrlie, P. Kofstad, J. Am. Chem. Soc. 75 (1992) 1176.
[35] K.-D. Kreuer, A. Fuchs, J. Maier, Solid State Ionics 77 (1995) 157–162.
[36] A.S. Nowick, A.V. Vaysleyb, Solid State Ionics 97 (1997) 17–26.
[37] E. Matsushita, A. Tanase, Solid State Ionics 97 (1997) 45–50.
[38] J.B. Condon, T. Schober, Solid State Ionics 97 (1997) 51–58.
[39] K.-D. Kreuer, Solid State Ionics 97 (1997) 1–15.
[40] T. Kudo, Survey of types of solid electrolytes, in: P.J. Gellings, H.J.M. Bouwmeester (Eds.), The CRC Handbook of Solid State Electrochemistry, CRC Press, Boca Raton, 1997, pp. 195–22.
[41] I. Riess, Electrochemistry of mixed ionic–electronic conductors, in: P.J. Gellings, H.J.M. Bouwmeester (Eds.), The CRC Handbook of Solid State Electrochemistry, CRC Press, Boca Raton, 1997, pp. 223–268.
[42] M.H.R. Lankhorst, H.J.M. Bouwmeester, H. Verweij, J. Am. Ceram. Soc. 80 (1997) 2175–2198.

[43] T. Norby, A.G. Andersen, Appl. Catal. 71 (1991) 89–102.
[44] I. Balint, K.-I. Aika, J. Chem. Soc., Faraday Trans. 91 (1995) 1805–1811.
[45] I. Balint, K.-I. Aika, J. Chem. Soc., Faraday Trans. 93 (1997) 1797–1801.
[46] S. Sunde, K. Nisancioglu, T.M. Gür, J. Electrochem. Soc. 143 (1996) 3497–3504.
[47] H. Yokokawa, N. Sakai, T. Kawada, M. Dokiya, Solid State Ionics 52 (1992) 43–56.
[48] J.A. Duffy, Geochim. Cosmochim. Acta 57 (1993) 3961–3970.
[49] J. Portier, G. Campet, J. Etourneau, B. Tanguy, J. Alloys Compounds 209 (1994) 285–289.
[50] A. Lebouteiller, P. Courtine, J. Solid State Chem. 137 (1998) 94–103.
[51] A. Pantazidis, A. Auroux, J.-M. Hermann, C. Mirodatos, Catal. Today 32 (1996) 81–88.
[52] J. Nowotny, Interface electrical phenomena in ionic solids, in: P.J. Gellings, H.J.M. Bouwmeester (Eds.), The CRC Handbook of Solid State Electrochemistry, CRC Press, Boca Raton, 1997, pp. 121–160.
[53] D.C. Sayle, S.C. Parker, J.H. Harding, Philos. Mag. A 69 (1994) 787–792.
[54] P.J. Scanlon, R.A.M. Bink, F.P.F. van Berkel, G.M. Christie, L.J. van Ijzendoorn, H.H. Brongersma, R.G. van Welzenis, Solid State Ionics 112 (1998) 123–130.
[55] T.X.T. Sayle, S.C. Parker, C.R.A. Catlow, J. Phys. Chem. 98 (1994) 13625–13630.
[56] V.D. Sokolovskii, F. Arena, S. Coluccia, A. Parmaliana, J. Catal. 173 (1998) 238–242.
[57] A. Bielanski, J. Haber, Catal. Rev. Sci. Eng. 19 (1979) 1–41.
[58] C. Louis, T.L. Chang, M. Kermarec, T. LeVan, J.M. Tatibouët, M. Che, Catal. Today 13 (1992) 283–289.
[59] J.-L. Dubois, M. Bisiaux, H. Mimoun, C.J. Cameron, Chem. Lett. (1990) 967.
[60] M.S. Islam, J.H. Ilett, S.C. Parker, J. Phys. Chem. 98 (1994) 9637–9641.
[61] H. Kathrein, F. Freund, J. Nagy, J. Phys. Chem. Solids 45 (1984) 1155–1163.
[62] J. Wang, L. Chen, C. Li, J. Mol. Catal. A 139 (1999) 315–323.
[63] C.R.A. Catlow, L. Ackermann, R.G. Bell, D.H. Gay, S. Holt, D.W. Lewis, M.A. Nygren, G. Sastre, D.C. Sayle, P.E. Sinclair, in: R.C. Tennyson, E.V. Kiv (Eds.), Computer Modelling of Electronic and Atomic Processes in Solids, NATO ASI Series 3, Vol. 22, Kluwer Academic Publishers, Dordrecht, 1997, pp. 5–29.
[64] C.R.A. Catlow, L. Ackermann, R.G. Bell, D.H. Gay, S. Holt, D.Q.W. Lewis, M.A. Nygren, G. Sastre, D.C. Sayle, P.E. Sinclair, J. Mol. Catal. A 115 (1997) 431–448.
[65] C.R.A. Catlow, L. Ackermann, R.G. Bell, F. Cora, D.H. Gay, M.A. Nygren, J.C. Pereira, G. Sastre, B. Slater, P.E. Sinclair, Faraday Discuss. 106 (1997) 1–40.
[66] A.B. Lidiard, J. Chem. Soc., Faraday Trans. 2 85 (1989) 341–349.
[67] W.C. Mackrodt, J. Chem. Soc., Faraday Trans. 2 85 (1989) 541–554.
[68] J.H. Harding, Defects, surfaces and interfaces, in: C.R.A. Catlow (Ed.), Computer Modelling in Inorganic Crystallography, Academic Press, New York, 1997, pp. 185–199.
[69] S.C. Parker, E.T. Kelsey, P.M. Oliver, J.O. Titiloye, Faraday Discuss. 95 (1993) 75–84.
[70] P.M. Oliver, G.W. Watson, E.T. Kelsey, S.C. Parker, J. Mater. Chem. 7 (1997) 563–568.
[71] P.R. Kenway, S.C. Parker, W.C. Mackrodt, Surf. Sci. 326 (1995) 301–310.
[72] M.J. Davies, S.C. Parker, G.W. Watson, J. Mater. Chem. 4 (1994) 813–816.
[73] C.R.A. Catlow, R.A. Jackson, J.M. Thomas, J. Phys. Chem. 94 (1990) 7889–7893.
[74] C.R.A. Catlow, D.H. Gay, A.L. Rohl, D.C. Sayle, Topics Catal. 3 (1996) 135–167.
[75] R. Gorman, Computer simulation of the structure and reactivity of catalytic metal oxides, Ph.D. Thesis, University of Keele, 1992.
[76] J. Purton, D.W. Bullett, P.M. Oliver, S.C. Parker, Surf. Sci. 336 (1995) 166–180.
[77] T.X.T. Sayle, S.C. Parker, C.R.A. Catlow, Surf. Sci. 316 (1994) 329–336.
[78] T.X.T. Sayle, S.C. Parker, C.R.A. Catlow, J. Chem. Soc., Chem. Commun. (1992) 977–978.
[79] G. Balducci, J. Kaspar, P. Fornasiero, M. Graziani, M.S. Islam, J.D. Gale, J. Phys. Chem. B 101 (1997) 1750–1753.
[80] G. Balducci, J. Kaspar, P. Fornasiero, M. Graziani, M.S. Islam, J. Phys. Chem. B 102 (1998) 557–561.
[81] P. Fornasiero, G. Balducci, R. Di Monte, J. Kaspar, V. Sergo, G. Gubitosa, A. Ferrero, M. Graziani, J. Catal. 164 (1996) 173–183.
[82] H. Cordatos, D. Ford, R.J. Gorte, J. Phys. Chem. 100 (1996) 18128–18132.
[83] A. Dietrich, C.R.A. Catlow, B. Maigret, Mol. Simulation 11 (1993) 251–265.
[84] D.C. Sayle, D.H. Gay, A.L. Rohl, C.R.A. Catlow, J.H. Harding, M.A. Perrin, P. Nortier, J. Mater. Chem. 6 (1996) 653–660.
[85] D.C. Sayle, C.R.A. Catlow, M.-A. Perrin, P. Nortier, J. Phys. Chem. 100 (1996) 8940–8945.
[86] D.C. Sayle, C.R.A. Catlow, M.-A. Perrin, P. Nortier, Catal. Lett. 38 (1996) 203–208.
[87] D.C. Sayle, T.X.T. Sayle, S.C. Parker, J.H. Harding, C.R.A. Catlow, Surf. Sci. 334 (1995) 170–178.
[88] D.C. Sayle, T.X.T. Sayle, S.C. Parker, C.R.A. Catlow, J.H. Harding, Phys. Rev. B 50 (1994) 14505–14998.
[89] H. Kuhlenbeck, G. Odörfer, R. Jaeger, G. Illing, M. Menges, Th. Mull, H.-J. Freund, M. Pöhlchen, V. Staemmler, S. Witzel, C. Scarfschwerdt, K. Wennemann, T. Liedtke, M. Neumann, Phys. Rev. B 43 (1991) 1969–1986.
[90] M. Pöhlchen, Ph.D. Thesis, Ruhr-Universität Bochum, Bochum, Germany, 1992.
[91] M. Pöhlchen, V. Staemmler, J. Chem. Phys. 97 (1992) 2583–2592.
[92] R.A. van Santen, J. Mol. Catal. A 115 (1997) 405–419.
[93] L. Ackermann, J.D. Gale, C.R.A. Catlow, J. Phys. Chem. B 101 (1997) 10028–10034.

[94] M. Witko, Catal. Today 32 (1994) 89–95.
[95] J. Haber, M. Witko, R. Tokarz, Appl. Catal. 157 (1997) 3–22.
[96] M. Witko, R. Tokarz, K. Hermann, Polish J. Chem. 72 (1998) 1565–1583.
[97] J. Haber, M. Witko, R. Tokarz, Appl. Catal. A 157 (1997) 3–22.
[98] M. Witko, R. Tokarz, J. Haber, Appl. Catal. A 157 (1997) 23–44.
[99] M. Witko, Electronic properties of surface oxygen centres in V–O containing systems, Presented orally during Fourth Sabatier Conference on Catalysis, 5–9 July 1999, Strasbourg.
[100] K. Hermann, M. Witko, R. Druzinic, A. Chakrabarti, B. Tepper, M. Elsner, A. Gorschlüter, H. Kuhlenbeck, H.J. Freund, J. Electr. Spectrosc. Related Phenom. 98–99 (1999) 245–256.
[101] N.U. Zhanpeisov, T. Bredow, K. Jug, Catal. Lett. 39 (1996) 111–118.
[102] R.W. Grimes, C.R.A. Catlow, J. Am. Ceram. Soc. 73 (1990) 3251–3256.
[103] S.B. Adler, J.W. Smith, J. Chem. Soc., Faraday Trans. 89 (1993) 3123–3128.
[104] A. Dwivedi, A.N. Cormack, Philos. Mag. A 61 (1990) 1–22.
[105] H.W. Brinkman, W.J. Briels, H. Verweij, Chem. Phys. Lett. 247 (1995) 386–390.
[106] M. Cherry, M.S. Islam, C.R.A. Catlow, J. Sol. State Chem. 118 (1995) 125–132.
[107] M.S. Islam, M. Cherry, C.R.A. Catlow, J. Sol. State Chem. 124 (1996) 230–237.
[108] H. Yamashita, Y. Machida, A. Tomita, Appl. Catal. A 79 (1991) 203.
[109] D. Dissanayake, J.H. Lunsford, M.P. Rosynek, J. Catal. 143 (1993) 286–298.
[110] Z. Kalenik, E.E. Wolf, Catal. Lett. 9 (1991) 441–450.
[111] Z. Kalenik, E.E. Wolf, Catal. Lett. 11 (1991) 309–318.
[112] Z. Kalenik, E.E. Wolf, Catal. Today 13 (1992) 255–264.
[113] A.G. Anshits, E.N. Voskresenskaya, L.I. Kurteeva, Catal. Lett. 6 (1990) 67.
[114] J.D. Foot, E.A. Colbourn, C.R.A. Catlow, J. Phys. Chem. Solids 49 (1988) 1225–1232.
[115] L. Ackermann, J.D. Gale, C.R.A. Catlow, J. Phys. Chem. B 101 (1997) 10028–10034.
[116] G. Ertl, Angew. Chem., Int. Ed. Engl. 29 (1990) 1219.
[117] G. Ertl, H.-J. Freund, Phys. Today (1999) 32–38.
[118] H.-J. Freund, Angew. Chem., Int. Ed. Engl. 36 (1997) 452–475.
[119] V.E. Henrich, P.A. Cox, The Surface Science of Metal Oxides, Cambridge University Press, Cambridge, 1994.
[120] C. Noguera, Physics and Chemistry at Oxide Surfaces, Cambridge University Press, Cambridge, 1996.
[121] R. Wichtendahl, M. Rodriguez-Rodrigo, U. Härtel, H. Kuhlenbeck, H.-J. Freund, Surf. Sci. 423 (1999) 90–98.
[122] B. Baumeister, H.-J. Freund, J. Phys. Chem. 98 (1994) 11962–11968.
[123] T. Klüner, H.-J. Freund, J. Freitag, V. Staemmler, J. Chem. Phys. 104 (1996) 10030–10040.
[124] T. Klüner, H.-J. Freund, V. Staemmler, R. Kosloff, Phys. Rev. Lett. 80 (1998) 5208–5211.
[125] G. Gayko, D. Wolf, E.V. Kondratenko, M. Baerns, J. Catal. 178 (1998) 441–449.
[126] K.P. Peil, J.G. Goodwin Jr., G. Marcelin, J. Phys. Chem. 93 (1989) 5977–5979.
[127] K.P. Peil, J.G. Goodwin Jr., G. Marcelin, J. Catal. 131 (1991) 143–155.
[128] T. Karasuda, K.-I. Aika, J. Catal. 171 (1997) 439–448.
[129] O.V. Buyevskaya, H. Rothaemel, H.W. Zanthoff, M. Baerns, J. Catal. 150 (1994) 71–80.
[130] J.E. ten Elshof, M.H.R. Lankhorst, H.J.M. Bouwmeester, J. Electrochem. Soc. 144 (1997) 1060–1067.
[131] J.E. ten Elshof, M.H.R. Lankhorst, H.J.M. Bouwmeester, Solid State Ionics 99 (1997) 15–22.
[132] P. Mars, D.W. van Krevelen, Chem. Eng. Sci. 3 (Suppl.) (1954) 41.
[133] Y. Jiang, I.V. Yentekakis, C.G. Vayenas, Science 264 (1994) 1563–1566.
[134] Z. Zhang, X.E. Verykios, M. Baerns, Catal. Rev. Sci. Eng. 36 (1994) 507–556.
[135] E.N. Voskresenskaya, V.G. Roguleva, A.G. Anshits, Catal. Rev. Sci. Eng. 37 (1995) 101–143.
[136] J.-L. Dubois, Ch.J. Cameron, Appl. Catal. 67 (1990) 49–71.
[137] E.E. Wolff (Ed.), Methane Conversion by Oxidative Processes, Catalysis Series, Van Nostrand Reinhold, New York, 1992.
[138] G.A. Martin, C. Mirodatos, Fuel Process. Technol. 42 (1995) 179–215.
[139] D. Eng, M. Stoukides, Catal. Rev. Sci. Eng. 33 (1991) 375–412.
[140] J.H. Lunsford, Catal. Today 6 (1990) 235.
[141] J.A. Lercher, A.G. Bitter, A.G. Steghuis, J.G. van Ommen, K. Seshan, NIOK Book, 1998.
[142] D.J. Driscoll, W. Martir, J.-X. Wang, J.H. Lunsford, J. Am. Chem. Soc. 107 (1985) 58–63.
[143] T. Ito, J.-X. Wang, C.-H. Lin, J.H. Lunsford, J. Am. Chem. Soc. 107 (1985) 5062–5068.
[144] J.-X. Wang, J.H. Lunsford, J. Phys. Chem. 90 (1986) 5883–5887.
[145] C.-H. Lin, J.-X. Wang, J.H. Lunsford, J. Catal. 111 (1988) 302–316.
[146] J.H. Lunsford, X. Yang, K. Haller, J. Laane, J. Phys. Chem. 97 (1993) 13810–13813.
[147] A.G. Anshits, E.N. Voskresenskaya, E.V. Kondratenko, N.G. Maksimov, Catal. Today 24 (1995) 217–223.
[148] E.V. Kondratenko, N.G. Maksimov, A.G. Anshits, Kinet. Catal. 36 (1995) 716–720.
[149] A. Goto, K.-I. Aika, Bull. Chem. Soc. Jpn. 71 (1998) 95–98.
[150] K. Nagaoka, T. Karasuda, K.-I. Aika, J. Catal. 181 (1999) 160–164.
[151] S.J. Korf, J.A. Roos, L.J. Veltman, J.G. van Ommen, J.R.H. Ross, Appl. Catal. 56 (1989) 119–135.
[152] D.J. McNamara, S.J. Korf, K. Seshan, J.G. van Ommen, J.R.H. Ross, Catal. Sci. Technol. 1 (1991) 243–248.
[153] D.J. McNamara, S.J. Korf, K. Seshan, J.G. van Ommen, J.R.H. Ross, Can. J. Chem. Eng. 69 (1991) 883–890.
[154] S.J. Korf, J.A. Roos, J.M. Diphoorn, R.H.J. Veehof, J.G. van Ommen, J.R.H. Ross, Catal. Today 4 (1989) 279–292.

[155] J.R.H. Ross, J.G. van Ommen, S.J. Korf, in: A. Holmen et al. (Eds.), Natural Gas Conversion, Elsevier, Amsterdam, 1991, pp. 213–221.
[156] H. Borchert, M. Baerns, J. Catal. 168 (1997) 315–320.
[157] T. LeVan, M. Che, J.-M. Tatibouët, Catal. Lett. 14 (1992) 321–329.
[158] T. Yang, L. Feng, S. Shen, J. Catal. 145 (1994) 384–389.
[159] C. Chen, Y. Xu, G. Li, X. Guo, Catal. Lett. 42 (1996) 149–153.
[160] L. Yu, W. Li, V. Ducarme, C. Mirodatos, G.A. Martin, Appl. Catal. A 175 (1998) 173–179.
[161] S. Lacombe, C. Geantet, C. Mirodatos, J. Catal. 151 (1995) 439–452.
[162] S. Lacombe, H. Zanthoff, C. Mirodatos, J. Catal. 155 (1995) 106–116.
[163] Y.S. Lin, Y. Zeng, J. Catal. 164 (1996) 220–231.
[164] Y. Zeng, Y.S. Lin, Ind. Eng. Chem. Res. 36 (1997) 277–283.
[165] Y. Zeng, Y.S. Lin, J. Catal. 182 (1999) 30–36.
[166] Z. Zhang, M. Baerns, J. Catal. 135 (1992) 317–320.
[167] L. Lehmann, M. Baerns, J. Catal. 135 (1992) 467–480.
[168] J.-L. Dubois, B. Rebours, Ch.J. Cameron, Appl. Catal. 67 (1990) 73–79.
[169] A.M. Efstathiou, S. Lacombe, C. Mirodatos, X.E. Verykios, J. Catal. 148 (1994) 639–647.
[170] S.C. Tsang, J.B. Claridge, M.L.H. Green, Catal. Today 23 (1995) 3–15.
[171] D.A. Hickmann, L.D. Schmidt, Science 259 (1993) 343.
[172] D.A. Hickmann, E.A. Haupfear, L.D. Schmidt, Catal. Lett. 17 (1993) 223.
[173] K. Otsuka, T. Ushiyama, I. Yamanaka, Chem. Lett. (1993) 1517.
[174] A.G. Steghuis, J.G. van Ommen, J.A. Lercher, Stud. Surf. Sci. Catal. 119 (1998) 831–836.
[175] A.G. Steghuis, Catalysed partial oxidation of methane to synthesis gas, 1998, Ph.D. Thesis, University of Twente, Enschede, The Netherlands.
[176] V.D. Sokolovskii, N.J. Coville, A. Parmaliana, I. Eskendirov, M. Makoa, Catal. Today 42 (1998) 191–195.
[177] G. Saracco, G. Scibilia, A. Iannibello, G. Baldi, Appl. Catal. B 8 (1996) 229–244.
[178] L. Marchetti, L. Forni, Appl. Catal. B 15 (1998) 179–187.
[179] D. Ferri, L. Forni, Appl. Catal. B 16 (1998) 119–126.
[180] L. Kundakovic, M. Flytzani-Stephanopoulos, J. Catal. 179 (1998) 203–221.
[181] A. Favre, N. Guilhaume, J.M.M. Millet, M. Primet, Catal. Lett. 49 (1997) 207–211.
[182] S.J. Cho, K.S. Song, I.S. Ryu, Y.S. Seo, M.W. Ryoo, S.K. Kang, Catal. Lett. 58 (1999) 63–66.
[183] R.K. Grasselli, Catal. Today 49 (1999) 141–143.
[184] J. Ziolkowski, E. Bordes, P. Courtine, J. Catal. 122 (1990) 126–150.
[185] J. Ziolkowski, E. Bordes, P. Courtine, J. Mol. Catal. 84 (1993) 307–326.
[186] P. Courtine, E. Bordes, Appl. Catal. A 157 (1997) 45–65.
[187] E. Bordes, in: R.W. Joyner, R.A. van Santen (Eds.), Elementary Reaction Steps in Heterogeneous Catalysis, Vol. 398, NATO Advanced Study Institute, 1993, pp. 137–153.
[188] H. Horowitz, R.M. Contractor, Influencing redox properties of VPO catalysts for selective butane oxidation in a circulating solids reactor, Presented orally during Fourth Sabatier Conference on Catalysis, Strasbourg, 5–9 July 1999.
[189] P.T. Nguyen, A.W. Sleight, N. Roberts, W.W. Warren, J. Solid State Chem. 122 (1996) 259–265.
[190] Y. Zhang-Lin, M. Forissier, R.P. Sneeden, J.C. Védrine, J.C. Volta, J. Catal. 145 (1994) 256–266.
[191] Y. Zhang-Lin, M. Forissier, J.C. Védrine, J.C. Volta, J. Catal. 145 (1994) 267–275.
[192] J.C. Védrine, J.M.M. Millet, J.C. Volta, Catal. Today 32 (1996) 115–123.
[193] J.C. Védrine, G. Coudurier, J.M.M. Millet, Catal. Today 33 (1997) 3–13.
[194] C. Mirodatos, Dynamics of oxygen species in oxidation processes investigated by transient kinetic techniques, Presented orally during Fourth Sabatier Conference on Catalysis, 5–9 July 1999, Strasbourg.
[195] Y.H. Taufiq-Yap, B.H. Sakakini, K.C. Waugh, Catal. Lett. 46 (1997) 273–277.
[196] Y.H. Taufiq-Yap, B.H. Sakakini, K.C. Waugh, Catal. Lett. 48 (1997) 105–110.
[197] L.P. Gai, K. Kourtakis, Science 67 (1995) 661.
[198] A. Andersson, S.L.T. Andersson, G. Centi, R.K. Grasselli, M. Sanati, F. Trifirò, Appl. Catal. A 113 (1994) 43–57.
[199] J. Nilsson, A.R. Landa-Canovas, S. Hansen, A. Andersson, J. Catal. 160 (1996) 244–260.
[200] J. Nilsson, A.R. Landa-Canovas, S. Hansen, A. Andersson, Catal. Today 33 (1997) 97–108.
[201] J.L. Callahan, R.K. Grasselli, Am. Inst. Chem. Eng. J. 9 (1963) 755.
[202] I. Matsuura, H. Oda, K. Oshida, Catal. Today 16 (1993) 547–554.
[203] J.N. Michaels, D.L. Stern, R.K. Grasselli, Catal. Lett. 42 (1996) 135–137.
[204] J.N. Michaels, D.L. Stern, R.K. Grasselli, Catal. Lett. 42 (1996) 139–148.
[205] P.A. Agaskar, L. DeCaul, R.K. Grasselli, Catal. Lett. 23 (1994) 339–351.
[206] H.X. Dai, C.F. Ng, C.T. Au, Catal. Lett. 57 (1999) 115–120.
[207] H.-W. Zanthoff, S.A. Buchholz, Catal. Lett. 49 (1997) 213–217.
[208] V.D. Sokolovskii, A.A. Davydov, O.Yu. Ovsitser, Catal. Rev. Sci. Eng. 37 (1995) 425–459.
[209] V.D. Sokolovskii, Catal. Today 24 (1995) 377–381.
[210] E.M. Al'kaeva, T.V. Andrushkevich, O.Yu. Ovsitser, V.D. Sokolovskii, Catal. Today 24 (1995) 357–359.
[211] A. Pantazidis, S.A. Bucholz, H.W. Zanthoff, Y. Schuurman, C. Mirodatos, Catal. Today 40 (1998) 207–214.
[212] A. Pantazidis, A. Burrows, C.J. Kiely, C. Mirodatos, J. Catal. 177 (1998) 325–334.
[213] A. Burrows, A. Pantazidis, C. Mirodatos, C.J. Kiely, Inst. Phys. Conf. Ser. 153 (1997) 379–382.
[214] D. Creaser, B. Andersson, R.R. Hudgins, P.L. Silveston, J. Catal. 182 (1999) 264–269.
[215] K.A. Bethke, M.C. Kung, B. Yang, M. Shah, D. Alt, C. Li, H.H. Kung, Catal. Today 26 (1995) 169–183.

[216] H.H. Kung, M.C. Kung, Catal. Today 30 (1996) 5–14.
[217] H.J.M. Bouwmeester, A.J. Burggraaf, Dense ceramic membranes for oxygen separation, in: P.J. Gellings, H.J.M. Bouwmeester (Eds.), The CRC Handbook of Solid State Electrochemistry, CRC Press, Boca Raton, 1997, pp. 481–553.
[218] H. Iwahara, Solid State Ionics 86/88 (1996) 9–15.
[219] P.J. Gellings, H.J.A. Koopmans, A.J. Burggraaf, Appl. Catal. 39 (1988) 1–24.
[220] C.G. Vayenas, Solid State Ionics 28–30 (1988) 1521.
[221] M. Stoukides, Ind. Eng. Chem. Res. 27 (1988) 1745.
[222] G. Saracco, V. Specchia, Catal. Rev. Sci. Eng. 36 (1994) 305–384.
[223] D. Lafarga, J. Santamaria, M. Menéndez, Chem. Eng. Sci. 49 (1994) 2005–2013.
[224] J. Coronas, M. Menéndez, J. Santamaria, Chem. Eng. Sci. 49 (1994) 2015–2025.
[225] H.W.J.P. Neomagus, A catalytic membrane reactor for partial oxidation reactions, Ph.D. Thesis, University of Twente, Enschede, The Netherlands, 1999.
[226] F. Abraham, J.C. Boivin, G. Mairesse, G. Nowogrocki, Solid State Ionics 40/41 (1990) 934–937.
[227] E. Pernot, M. Anne, M. Bacmann, P. Strobel, J. Fouletier, R.N. Bannier, F. Abrahem, G. Mairesse, G. Nowogrocki, Solid State Ionics 70/71 (1994) 259–263.
[228] J.C. Boivin, C. Pirovano, G. Nowogrocki, G. Mairesse, Ph. Labrune, G. Lagrange, Solid State Ionics 113/115 (1998) 639–651.
[229] J.C. Boivin, G. Mairesse, Chem. Mater. 10 (1998) 2870–2888.
[230] T. Nozaki, S. Hashimoto, K. Omata, K. Fujimoto, Ind. Eng. Chem. Res. 32 (1993) 1174–1179.
[231] T. Nozaki, O. Yamazaki, K. Omata, K. Fujimoto, Chem. Eng. Sci. 47 (1992) 2945–2950.
[232] J.E. ten Elshof, H.J.M. Bouwmeester, H. Verweij, Solid State Ionics. 81 (1995) 97–109.
[233] J.E. ten Elshof, H.J.M. Bouwmeester, H. Verweij, Solid State Ionics. 89 (1996) 81–92.
[234] J.E. ten Elshof, H.J.M. Bouwmeester, H. Verweij, Appl. Catal. A. 130 (1995) 195–212.
[235] T. Hibino, T. Sato, K. Ushiki, Y. Kuwahara, J. Chem. Soc., Faraday Trans. 91 (1995) 4419–4422.
[236] Y.S. Lin, W. Wang, J. Han, AIChE J. 40 (1994) 786–798.
[237] W. Wang, Y.S. Lin, J. Membr. Sci. 103 (1995) 219–233.
[238] S.J. Xu, W.J. Thomson, Special ceramics processing issue., AIChE J. 43 (11A) (1997) 2731–2740.
[239] S.J. Xu, Catalysts for the oxidative coupling of methane, MS Thesis, Washington State University, Pullman, 1994.
[240] U. Balachandran, J.T. Dusek, S.M. Sweeney, R.B. Poeppel, R.L. Mieville, P.S. Maiya, M.S. Kleefisch, S. Pei, T.P. Kobylinski, C.A. Udovich, A.C. Bose, Am. Ceram. Soc. Bull. 75 (1995) 71–75.
[241] B. Ma, U. Balachandran, J.-H. Park, S.U. Segre, Solid State Ionics 83 (1996) 65–71.
[242] B. Ma, U. Balachandran, J.-H. Park, J. Electrochem. Soc. 143 (1996) 1736–1744.
[243] B. Ma, U. Balachandran, Solid State Ionics 100 (1997) 53–62.
[244] B. Ma, J.P. Hodges, J.D. Jorgensen, D.J. Miller, J.W. Richardson Jr., U. Balachandran, J. Solid State Chem. 141 (1998) 576–586.
[245] U. Balachandran, P.S. Maiya, B. Ma, J.T. Dusek, R.L. Mieville, J.J. Picciolo, Proceedings of the Fourth Workshop on Optimisation of Catalytic Membrane Reactor Systems, Oslo, Ceramics Group, 30–31 May 1997, pp. 15–26.
[246] C.-Y. Tsai, A.G. Dixon, W.R. Moser, Y.H. Ma, AIChE J. Ceram. Process. 43 (1997) 2741–2759.
[247] S. Azgui, F. Guillaume, B. Taouk, E. Bordes, Catal. Today 25 (1995) 391–396.
[248] H. Iwahara, T. Esaka, H. Uchida, N. Maeda, Solid State Ionics 3/4 (1981) 359–363.
[249] H. Iwahara, T. Esaka, H. Uchida, K. Ogaki, Solid State Ionics 18/19 (1986) 1003–1007.
[250] H. Iwahara, H. Uchida, K. Ono, K. Ogaki, J. Electrochem. Soc. 135 (1988) 529–533.
[251] S. Hamakawa, T. Hibino, H. Iwahara, J. Electrochem. Soc. 140 (1993) 459–462.
[252] S. Hamakawa, T. Hibino, H. Iwahara, J. Electrochem. Soc. 141 (1994) 1720–1725.
[253] P.-H. Chiang, D. Eng, P. Tsiakaras, M. Stoukides, Solid State Ionics 77 (1995) 305–310.
[254] G. Marnellos, O. Sanopoulou, A. Rizou, M. Stoukides, Solid State Ionics 97 (1997) 375–383.
[255] J. Langguth, R. Dittmeyer, H. Hofmann, G. Tomandl, Appl. Catal. A 158 (1997) 287–305.
[256] C.G. Vayenas, S.I. Bebelis, I.V. Yentekakis, S.N. Neophytides, Electrocatalysis and electrochemical reactors, in: P.J. Gellings, H.J.M. Bouwmeester (Eds.), The CRC Handbook of Solid State Electrochemistry, CRC Press, Boca Raton, 1997, pp. 445–480.
[257] D. Eng, M. Stoukides, J. Catal. 130 (1991) 306–309.
[258] G. Marnellos, M. Stoukides, Science 282 (1998) 98–100.
[259] A. Hammou, J. Guindet, Solid oxide fuel cells, in: P.J. Gellings, H.J.M. Bouwmeester (Eds.), The CRC Handbook of Solid State Electrochemistry, CRC Press, Boca Raton, 1997, pp. 407–443.
[260] D.J. Kuchynka, R.L. Cook, A.F. Sammelis, J. Electrochem. Soc. 138 (1991) 1284–1299.
[261] B. de Boer, SOFC Anode-hydrogen oxidation at porous nickel and nickel/yttria-stabilised zirconia cermet electrodes, 1998, Ph.D. Thesis, University of Twente, Enschede, The Netherlands.
[262] S.B. Adler, Solid State Ionics 111 (1998) 125–134.
[263] G.J. Hutchings, G.W. Watson, D.J. Willock, Chem. Ind. (1997) 603–607.
[264] J.M. Thomas, Designing new inorganic catalysts., J. Mol. Catal. A 115 (1997) 371–377.
[265] H. Iwahara, Solid State Ionics 77 (1995) 289–298.
[266] T. Schober, F. Krug, W. Schilling, Solid State Ionics 97 (1997) 369–373.